The University of Nottingham
School of Mechanical, Materials and Manufacturing Engineering

Breeding a better stove: the use of Computational Fluid Dynamics and Genetic Algorithms to optimise a wood burning stove for Eritrea

Hugh Burnham-Slipper BEng, MPhil

Thesis submitted to the University of Nottingham for the degree of Doctor of Philosophy

December 2008

ABSTRACT

Improved cooking stoves can bring significant benefits to women and children in rural African situations, due to reduced fuel consumption and improved indoor air quality. This investigation focuses on the use of Computational Fluid Dynamics (CFD) and Genetic Algorithms (GAs) to optimise a stove for Eritrea.

Initial work focussed on developing a model of wood combustion in a fixed bed. An experimental investigation was carried out on regular wood cribs to determine the burn rate and temperature field above a wood fire. The experimental data was used to develop a numerical model using CFD software Fluent 6.2 and user-defined functions for the fixed bed of fuel. The model assumed that pyrolysis was limited by heat transfer through the fuel, and that char combustion was limited by oxygen diffusion to the fuel surface. Simulation results yielded a mean and maximum error of 16% and 42% respectively in fuel burn rate.

In the second phase of the investigation, the numerical model of wood combustion was used as part of a larger CFD model to capture the behaviour of a complete stove. The model was compared with experimental data for rocket type stoves with different geometries. The model correctly identified the trends of fuel burn rate and heat transfer in the experimental data, though agreement with experimental values was poor and the model exhibited significant errors when altering stove height and diameter.

In the final phase of the investigation, the stove model was used in conjunction with a genetic algorithm to optimise the stove shape. Two methods of genetic coding were investigated. The resulting stove is expected to half fuel consumption compared to the classic mogogo stove, though this remains to be experimentally verified.

ACKNOWLEDGEMENTS

Thanks are given to all those who have helped during the course this work. Mike Clifford and Steve Pickering gave me the opportunity to study and provided clear and timely supervision. Don Giddings advised and has become a close friend. Pat Harrison built all hardware and helped arrange experimental work. The Eritrean Diaspora of Nottingham participated in experimental work and taught me to cook ingera. Colleagues in the Windowless Mezzanine of Hell shared the joy and the pain. Last but not least Sarah, Rowan and Marcus loved me throughout.

Bzaba zemowata assa, men yegedesen,
bzayke gfafa assa,
n callo assawi seb?

Who cares about the dead fish,
except fishermen,
and other fish-oriented people?

Elabered proverb

TABLE OF CONTENTS

NOMENCLATURE

a	crib volume-specific area [m^2/m^3]
a_l	local absorption coefficient [m^{-1}]
c	specific heat capacity
C	constant
C_1	constant in k-ε model
C_2	constant in k-ε model
$C_{3\varepsilon}$	constant in k-ε model
CCF	cooking cycle fuel
CCT	cooking cycle time
C_μ	constant in k-ε model
d	nozzle diameter
D	diffusivity [m^2/s]
E	energy [J]
F_0	buoyancy produced per unit time at the source (Appendix B)
g	gravitational constant [m/s2]
G_b	rate of turbulence kinetic energy formation due to buoyancy [$kg/m.s^3$]
G_k	rate of turbulence kinetic energy formation due to shear [$kg/m.s^3$]
h	heat transfer coefficient
H	enthalpy [J/kg]
h_m	mass transfer coefficient [m/s]
I	radiation intensity [W/m^2]
k	turbulent kinetic energy [m^2/s^2]
k_0	chemical kinetic reaction rate

k_m	mass transfer constant [$m^{0.5}/s^{0.5}$]
l	fuel block length [m]
m	mass
m'	volumetric mass rate [kg/m^3s]
n	number of fuel blocks per crib layer [-]
n^l	local refractive index [-]
Nu_0	Nusselt number for stagnation point
Nu_{exp}	Nusselt number from experiment
Nu_{fc}	Nusselt number correct for natural convection
Nu_p	Nusselt number corrected for edge effects
p	crib porosity (void fraction) [-]
Pr	Prandtl number
r	radius [m]
R	radius [m]
Ra	Rayleigh number
Re	Reynolds number
S	surface area
SFC	specific fuel consumption
S_ε	source of dissipation of turbulent kinetic energy
t	time
T	temperature [K]
u_i	velocity in direction i [m/s]
V	crib volume [m^3]
w	fuel block width [m]
x	direction vector
Y	species mass fraction [-]
z	height [m]
α	Reynolds number exponent
β	Prandtl number exponent
γ	(*z/d*) exponent
ε	emissivity
ε	rate of dissipation of turbulent kinetic energy [m^2/s^3]
λ	thermal conductivity [W/m.K]

μ	dynamic viscosity [Pa.s]
v	kinematic viscosity [m^2/s]
ρ	density [kg/m3]
σ	Stefan-Boltzmann constant
$\hat{\sigma}$	standard deviation
Σ	sensitivity[-]
σ_k	turbulent Prandtl number [-]
Ψ	lumpiness function [-]
ω	lumpiness frequency [m-1]

Subscript

0	initial condition
∞	free-stream
$CO2$	carbon dioxide
$evap$	evaporation
gel	gelatinisation
i	direction vector index
j	direction vector other index
m	molecular
m	mass
$O2$	oxygen
p	pyrolysis
s	surface
t	turbulent

CHAPTER 1: INTRODUCTION

Eritrea is a country of approximately 4 million inhabitants, comprising the seaboard and northern highlands of the empire formerly known as Abyssinia (Figure 1.1). The population is predominantly Tigrinya, a Coptic Christian ethnic group who populate the fertile highlands and who share many points of culture and language with the Ethiopian Tigray. Despite these similarities their recent history has been dominated by internecine fighting, resulting in Eritrea's independence in 1991. A fragile peace exists between the two sides. During The Struggle the Ethiopians systematically deforested the Eritrean countryside in a bid to remove cover for guerrilla fighters. The 1984 Ethiopian famine highlighted by Band Aid was experienced equally by Eritreans. Eritrea has also been touched by the African AIDS pandemic and the country currently lies 153rd of 171 in the Human Development Index (UNDP, 2004).

The staple food of both the Tigrigna and the Tigray (as well as other ethnic groups in Eritrea and southern Sudan) is a large pancake called ingera or taita (Figure 1.2). It is prepared from fermented batter and cooked on a mogogo stove. The traditional mogogo consists of a griddle plate of sun-dried "black" clay (approximate dimensions: 20mm thick; 500mm diameter; Figure 1.3), set in a base of stone and clay. The base typically has a large opening at the front for fuel and a smaller opening at the back for ventilation. Mogogo stoves are built and used almost exclusively by women. The mogogo plate typically costs 100 Nakfa (US$ 4 in 2004, compare to US$ 1000 per capita GDP; CIA, 2005); other materials are found and therefore nominally free.

Figure 1.1. Eritrea and Ethiopia

Figure 1.2. A lavish plate of ingera

There have been two notable mogogo optimisation projects. In Ethiopia the German non-governmental organisation GTZ Household Energy promoted the "mirt" stove (GTZ, 2005). It consists of six cast concrete sections and the mogogo plate, and incorporates a seat for a saucepan heated by the flue gases. There is no grate, chimney or special insulation around the combustion chamber. The stove retails for 40-60 Birr (US$ 4-6), and is manufactured by artisans in around 60 locations across the country as part of the GTZ project (HEDON, 2008).

In Eritrea an optimised stove was promoted by the Energy Research and Training Centre (ERTC, an arm of the Eritrean Ministry of Energy), and won the 2003 Ashden Award (van Buskirk, no date). The ERTC mogogo features a fired clay grate, a chimney of cast concrete tubes and specially designed curved bricks with cavities to act as insulation around the combustion chamber. The stove is manufactured by a single enterprise in the capital city, Asmara, and costs US$ 40, though this price is subsidised by a carbon credit scheme (van Buskirk, no date). The project has focused heavily on installing ERTC stoves in refugee camps. While stoves have also been installed in civilian settings, stove owners are marked as government lackeys in a regime that has significantly eroded personal freedoms, and has not had a wide uptake.

Though these two projects have resulted in improved stoves and they have met with some success, they both have significant political barriers to universal adoption as an improved stove in Eritrea. In the following sections we will examine the principal methods used to develop a novel improved stove for Eritrea, which aims to be better placed than previous stoves, and over-step them in the degree of improvement and optimisation.

Figure 1.3. Traditional mogogo.

Figure 1.4. GTZ improved mogogo.

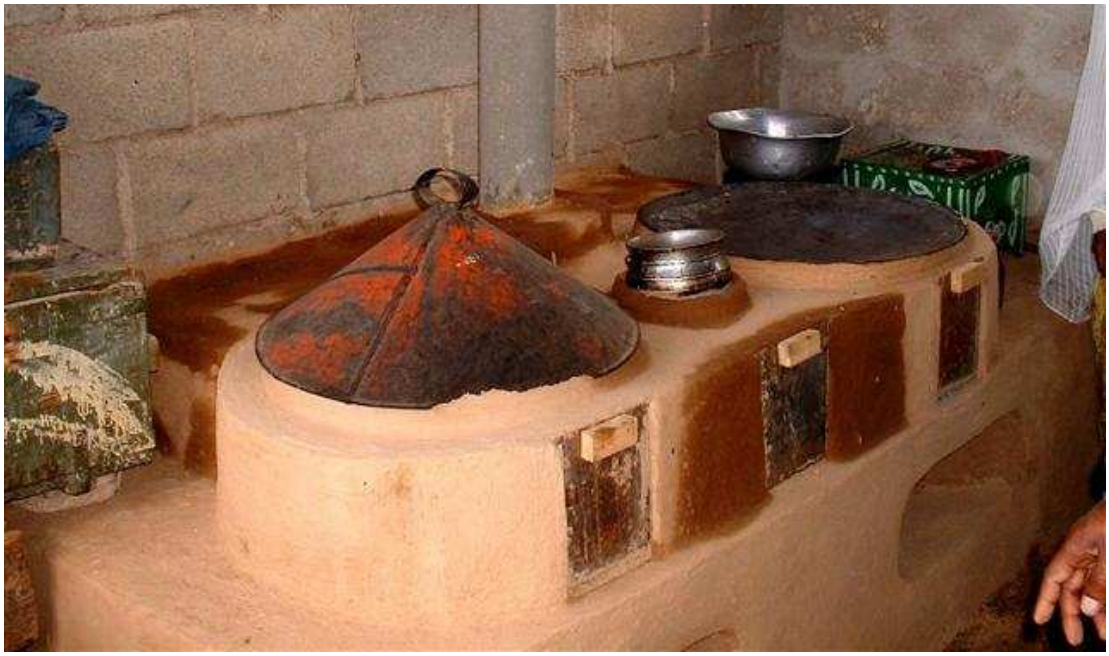

Figure 1.5. ERTC improved mogogo.

1.1 APPROPRIATE AND INTERMEDIATE TECHNOLOGY

The terms 'appropriate technology' and 'intermediate technology' are often used interchangeably though they do have distinct definitions. They are also commonly confounded with 'low technology' as opposed to 'high technology'.

Appropriate technology is a design or procurement philosophy which attempts to match a product with the locally available resources, including raw materials and the knowledge and skills required for manufacture and maintenance. The decision to use 'appropriate' technology is a fundamental part of the design process, both in the industrialised world and the developing world. However, in the industrialised world it is commonly overlooked because almost all technologies

are appropriate. The only candidates for inappropriate technology in the West are technologies that have been superseded, such as clockwork, VHS and coracles. On the other hand, in the developing world, expertise and resources are often absent or prohibitively expensive, so the issue of appropriate or inappropriate technology is more acutely felt.

Meanwhile, intermediate technology is a concept introduced in *Small is Beautiful* (Schumaker, 1973). The text states that work should be (a) dignified and meaningful above all else, (b) efficient, (c) in harmony with nature and (d) decentralised, operating in small units. As the name implies, intermediate technology is therefore a halfway house between aboriginal and high technologies. The espousal of manpower in artisan employment rather than mechanisation plays to the strengths of many areas in the developing world, making 'intermediate technology' an appropriate choice for those regions.

The intermediate technology movement is commonly concerned with raising the standard of living for the poor in developing nations by addressing day-to-day problems: food production, potable water, shelter, cooking and household energy. Practical Action (formerly ITDG, Rugby, UK; founded by Schumaker in 1966) and Aprovecho (Oregan, USA; founded c. 1980) are two of the most prominent intermediate technology organisations, and it is to Aprovecho we now turn for a key development in stove optimisation: the rocket elbow.

The rocket elbow has become widely recognised as a world leader in high efficiency, intermediate technology stoves (Scott, 2006). The upright section is the combustion chamber, insulated to improve efficiency, and tall enough to induce a draft, drawing air in to improve combustion. The horizontal section is the fuel magazine. A shelf in the magazine supports the fuel, allowing air to pass from underneath without the need for an expensive grate. The small aperture for fuel promotes the use of small twigs and sticks with two advantages: first small sticks are easier to find and second they have a larger specific surface area, improving combustion. The pot sits atop the stove, and a skirt guides hot flue gases across the bottom and up the side of the pot to ensure maximum heat transfer. The rocket elbow was first introduced in Central America, but versions are now in use in Sub-Saharan Africa and Asia (Scott, 2006; Aprovecho, 2007). To date most rocket stoves have been developed to cook food in pots, different versions being adapted to locally available materials. None has so far been developed for cooking ingera or similar pancakes.

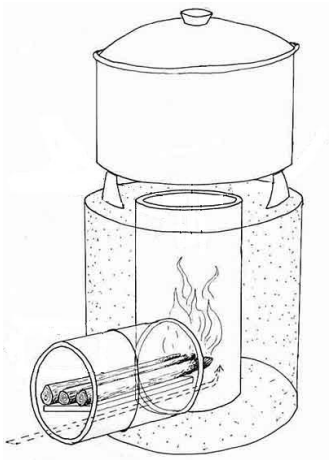

Figure 1.6. The rocket elbow (Aprovecho, 2005)

1.2 COMPUTATIONAL FLUID DYNAMICS

Computational Fluid Dynamics (CFD) is a technique to predict fluid flow by finding the numerical solution to a set of partial differential equations governing the continuity of mass, momentum and energy in the flow field. This set of equations (the Navier-Stokes Equations) is highly coupled and non-linear, and has no analytical solution for all but the most simple of cases. Consequently the problem domain must be discretised (typically using the finite volume method) and a solution found through numerical methods. The finite volume method is able to cope with an unstructured mesh, allowing complicated geometry to be modelled.

Turbulence is a significant complication to the problem of modelling most engineering flows and several strategies have been developed to account for it. At one end of the spectrum is the attempt to resolve even the smallest of turbulent structures (Direct Numerical Simulation), which requires immensely fine meshes with cells as small as fractions of a millimetre. This is clearly computationally very expensive, and not a particularly practical solution to engineering problems which have scales of meters or tens or hundreds of meters. At the other end of the spectrum is the attempt to model the turbulence by artificially increasing the viscosity of the fluid, thereby increasing the rate of mixing and the resistance to flow (Reynolds Averaged Navier-Stokes, or RANS models). The question of where to increase the viscosity and by how much is governed by additional conservation equations for turbulent kinetic energy and rate of dissipation of turbulent kinetic energy. While no single RANS model can accurately predict all flow regimes, they are all considerably cheaper than DNS simulations, and the k-ε model in particular has become the work-horse of industrial CFD simulations. RANS models incur the additional complication of correctly modelling the turbulent and laminar regions of the boundary layer near non-slip surfaces in the domain. Again two principal

methods exist for overcoming this problem: either a very coarse mesh is used and the model includes assumptions about the thickness of the laminar sub-layer (the wall-function approach), or a finer mesh is used and the flow is resolved well into the laminar region (the enhanced wall-function approach). Both are well accepted methods.

Mixing of different materials can be modelled by adding further continuity equations to those listed above, either for fuel mixture fraction (in the case of combustion) or for individual chemical species. Reactions are affected by adding sink and source terms in the equations for reactants and products (where the rate of reaction is limited either by mixing or chemical kinetics), and appropriate sources in the energy equation to account for endothermic and exothermic reactions. A more detailed review of CFD is given by Versteeg and Malalasekera (2007).

Several commercial CFD software packages are available: STAR-CD is one part of an engineering software suit developed by cd-adapco and is well supported; OpenFOAM is an open-source CFD package with the advantage that additional models are easily added to the original code; Fluent and CFX are both owned by the ANSYS group and very well supported; Fluent has the added advantage that it can easily incorporate user-defined functions, allowing it to be tailored to the needs of the individual user. While a strong case could be made for using any of these (or indeed any other code), the rest of this project was carried out using Fluent 6.2 for the simple reason that it was extremely well supported in the University of Nottingham and progress could be made quickly.

1.3 OPTIMISATION ALGORITHMS

Engineering is awash with efforts to optimise a design before committing to manufacture. This requires that a function be formulated that gives the quality of a candidate solution in terms of a set of input parameters. Several strategies exist for finding the set of parameters that gives the optimum solution (let us assume by maximising a function).

In the simplest case it is sufficient to set the differential of the function to zero and find the corresponding set of parameters. While this method ensures finding all maxima, including the global maximum, it is intractable for all but the simplest of problems. An alternative is to evaluate the function for all combinations of input parameters, and chose the parameter set with the optimum output value. This method immediately runs into problems for functions with continuous input parameters, where it is necessary only to evaluate the function at discrete points. An additional (and perhaps more pressing) difficulty is that the number of

potential solutions increases exponentially with the number input parameters, and the solution space becomes prohibitively large to investigate. It is therefore appropriate to only evaluate a subset of all solutions, and the task of efficiently identifying which subset falls to optimisation algorithms. The taxonomy of optimisation algorithms may be broadly split into deterministic and probabilistic algorithms.

Deterministic algorithms are characterised by having a unique path from the initial solution to the optimum. In the hill-climbing algorithm the solution proceeds though the solution space by the path of steepest ascent. In the divide and conquer algorithm the solution space is successively halved, and at each step the two halves are compared to ascertain which contains the optimal solution (for example, to find the word 'syzygy' in the dictionary without a priori knowledge, it is most efficient open the book at M, evaluate that the target word lies in the second half of the solution space, then sub-divide M-Z at R, and so on until you arrive at the page containing 'syncretic', 'syrup', 'syzygy' and 'tabernacle'). Such methods are ideal for very smooth search spaces, but run the risk of premature convergence (that is arriving at a local rather than global maximum).

Probabilistic algorithms on the other hand contain a random element, leading to faster run times but running the risk of missing the very peak of the global optimum. Methods include simulated annealing, genetic algorithms and a family of techniques related to swarm behaviour. In these last methods, a population of agents move around the search space following rules mimicking the behaviour of groups of ants or fish. Arrival at the optimum is achieved by the flow of information between agents, and the behaviour of the swarm, not the individual. In the simulated annealing algorithm a single solution is proposed. This solution is compared with a randomly selected neighbour (created by changing one parameter by an index of one), and the new solution is either accepted or rejected as a replacement of the existing solution. The probability of acceptance is related to the relative qualities of the two candidates, the better solution is not always accepted, and the algorithm is less likely to converge prematurely. Genetic algorithms mimic the process of natural selection and survival of the fittest: the solution space is populated by a set of randomly generated solutions, which are free to mate and recombine their parameters to create new solutions. The probability of being selected for a mating event increases with the quality of the solution, with the result that the mean quality of the population increases with time. Parameters in the solutions are also subject to random mutations, which allow convergent solutions to jump to new areas of the solution space and void premature convergence. The use of recombination and random mutations

means that genetic algorithms are very well suited to evaluating non-linear search spaces.

1.4 THESIS AIMS AND OVERVIEW

The existing improved stoves for cooking ingera are both inappropriate to Eritrea: one is associated with Ethiopia, and the other is associated with the government of a hated regime. Both rely on centralised manufacture. It is therefore the aim of the work in this thesis to develop an improved cooking stove for the preparation of ingera in Eritrea, based on appropriate intermediate technology. The reviews in Chapter 2 demonstrate that there are many aspects to stove improvement, including efficiency, emissions, manufacture and longevity, and it would be desirable to examine all of these aspects, however the work presented in this thesis focuses uniquely on improving the efficiency of the mogogo stove while maintaining heat flux at a level suitable for cooking ingera. Furthermore, the principle objective is to use computer-aided design tools to reduce the experimental load and to gain a deeper understanding of the relevant phenomena (specifically fuel devolatalisation, char and volatile combustion, radiation and convection heat transfer). The work in the thesis is broken into the following chapters:

- *Chapter 2: Literature Review.* Details are given of experimental test procedures for thermal and emissions performance of cooking stoves, and modelling techniques for pyrolysis of charring fuels, flaming combustion, radiation and convection heat transfer, as well as a general review of stove modelling studies. It is concluded that while most of the elements are in place to continue with the work of computer-aided stove improvement, the various pyrolysis and char combustion models must be re-parsed to give a computationally cheap model that can be used effectively with a genetic algorithm.
- *Chapter 3: Combustion.* A numerical model of wood burning in a fixed bed is presented. Flow in the fuel bed is resolved by assuming mean values of bed void fraction and fuel specific surface area. Results of simulations with the numerical model were in reasonable agreement with experimental data for the rate of combustion and the temperature profile above the burning fuel. The most significant shortfall of the model was the effect of soot was not included in the radiation sub-model, with the result that flame temperatures were over predicted. Additional inputs for this chapter came from appendices B, C and D.

- *Chapter 4: Convection Heat Transfer.* In order to address the shortfall identified in Chapter 3, an investigation was carried out to determine the level of convection heat transfer from a jet impinging on the bottom of a simulated cooking pot. The investigation yielded an experimental correlation that was in broad agreement with published data, despite a rather crude experimental technique. A CFD model of jet impingement showed a shortfall in the k-ε turbulence model, leading to local errors in heat transfer, though area-averaged behaviour was in reasonable agreement with experimental data.
- *Chapter 5: Stove Performance.* Details are given of an experimental investigation of a modified rocket stove, leading to correlations for fuel burn rate and heat transfer to the pot with stove geometry. Data from Chapter 4 are used to estimate the levels of convection and radiation heat transfer to the pot. A CFD model of the whole stove reproduced the same trends as experimental data, though it did not respond well to changes in stove height.
- *Chapter 6: Stove Optimisation.* Details are given of a genetic algorithm used to improve stove performance. Two methods are compared for genetic coding of the stove. Characteristics of optimised stoves are combined and discussed. Additional experimental investigations for mogogo plate thermal properties and mogogo stove performance are given in appendices E and F. Algorithm code is given in appendix G.
- *Chapter 7: Conclusions and Recommendations.* Conclusions from each chapter all summarised, as well as findings from the project as a whole. Recommendations for further work are also discussed.
- *Appendix A: References.*
- *Appendix B: Turbulent Buoyant Plumes.* The k-ε CFD model was validated against experimental data for the velocity and temperature field in a turbulent buoyant plume above a point heat source, in order to demonstrate that a non-reacting version of the flow regime resolved in Chapter 3 is accurate.
- *Appendix C: Crib Flow Resistance.* Experimental and analytical analyses were conducted of resistance to flow presented by wood cribs with various configurations. Results were used as input parameters for the model of wood crib combustion in Chapter 3.
- *Appendix D: Fuel Characteristics.* Details are given of the proximate analysis of wood used as a fuel in the experimental investigations in

Chapters 3 and 5, as well as calorific value and resistance to flow of a packed bed of char.

- *Appendix E: Mogogo Thermal Properties*. An experiemental investigation was carried out using Lee's discs to estimate the specific heat capacity and thermal conductivity of a mogogo plate. There parameters were used as inputs to the stove model used for optimisation in Chapter 6.
- *Appendix F*: Mogogo Thermal Assessment. A classic mogogo was used to cook ingera in laboratory conditions with two aims: the first was to estimate the thermal efficiency of the mogogo as a baseline for design purposes, the second was to estimate the heat flux required to successfully cook ingera. This was a target parameter for the optimisation algorithm in Chapter 6.
- *Appendix G*: Algorithm Scripts. Code for the fuel devolatalisation UDF developed in Chapter 3, and the various files required for the genetic algorithm presented in Chapter 6.

Work to minimise the emissions of a mogogo stove would be of real benefit, however this would require a significantly more complex numerical model of char combustion, volatile species evolution and soot formation and combustion in order to account for carbon monoxide and soot, commonly held to be the most harmful emissions from cooking fires. The work in this thesis is not intended to significantly extend the frontiers of engineering science in any one field, but to apply a series of engineering techniques to a practical problem. While there are novel aspects to the nature of the engineering techniques as used herein, the main value of the work lies in the application of existing techniques to a novel field.

CHAPTER 2: LITERATURE REVIEW

The review in this chapter is broken into three sections. In the first, experimental techniques are presented for analysing stoves for thermal performance and emissions performance. In the second section a review is made of numerical modelling techniques relating to the key areas of stove operation: the pyrolysis of charring fuels, char combustion, volatile combustion, radiation and convection heat transfer and finally previous models of complete stoves. In the third section, a review is given of engineering optimisation techniques and their application to stoves. Finally, it is concluded that work needs to be done to create a sufficiently cheap model of wood combustion to use in a genetic algorithm, and that the experimental techniques that currently exist for evaluating stove performance are not accurate enough to collect data to back up model development.

2.1 EXPERIMENTAL INVESTIGATIONS

2.1.1 Thermal Performance Test Procedures

Several parameters have been proposed to evaluate and compare the performance of cooking stoves, each requiring different test procedures.
Perhaps the most widely used term is efficiency. There are several definitions of efficiency, relating to different aspects of a stove's operation:

- *Combustion efficiency:* ratio of heat energy released by the flame to chemical energy in the fuel.
- *Heat Transfer efficiency:* ratio of energy entering the pot to energy in the flame.
- *Pot efficiency:* ratio of energy remaining in the pot to energy entering the pot. This metric has been used to discourage evaporation of water as a wasteful process.

- *Overall efficiency:* ratio of energy in the pot to energy in the fuel. This is the product of all the other definitions of efficiency. Many investigators do not recognise pot efficiency, so describe overall efficiency as the product of combustion efficiency and heat transfer efficiency.

Geller (1982) carried out extensive tests on Indian stoves and summarised his findings as 84% combustion efficiency, 17% heat transfer efficiency and 43% pot efficiency. These results highlighted the need to address heat transfer as the critical issue in stove design while combustion efficiency is already at a reasonable level. His results have been broken down further in Figure 2.1.

Cooking Cycle

Geller (1982) measured the efficiency of stoves in the Ungra area of India over a complete cooking cycle. He defined useful energy to be energy used to raise the temperature of the pots, cooking medium and food, and energy to transform the food into its cooked state (i.e. energy required for any chemical reactions in food preparation, such as starch gelatinization when cooking rice). Energy consumed was the energy available in the initial mass of wood, less energy in the remaining charcoal. Stated mathematically:

$$\eta = \frac{(m_p c_p + m_m c_m + m_f c_f)\Delta T + m_f h_f}{m_w h_w - m_c h_c} \qquad (2.1)$$

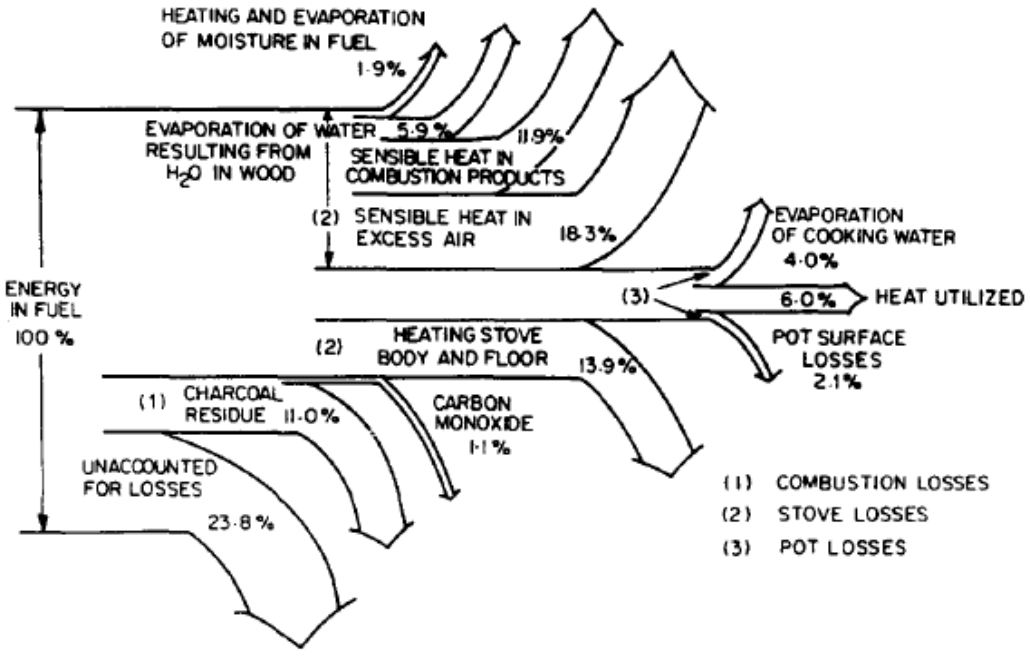

Figure 2.1. Energy balance for cooking (Geller, 1982).

where m is mass, c is specific heat and T is temperature. The subscripts p, m, f, w and c stand for pots, medium, food, wood and charcoal respectively. The energy of chemical reaction of the food is given by h_f, and the calorific values of wood and charcoal are h_w and h_c respectively.

Geller was at pains to point out that the latent heat of evaporation of water was not included in the useful energy. He argued that it would otherwise be possible to improve the efficiency of the stove or cooking procedure by wantonly evaporating water with no effect on the cooking of food. His definition encourages the use of a lid whilst simmering food, though it obviously overlooks cultural preferences for particular tastes in food which cannot be captured in an equation (Similarly, solar cookers have not enjoyed the boom that was expected, partly because of the cultural preference of a smoky flavour to some foods).

Geller's method appears to give a very realistic value of cooking efficiency, but it has several disadvantages. It is very dependant on the cooking style of the individual, meaning that it is not repeatable, and requires a large sample population to be meaningful. The method requires a large amount of specific heat data for all the food types that are being prepared, which is not always commonly available. The method is also requires in situ measurement of every ingredient that is to be cooked, as well as the wood and remaining char. Geller noted that this process is very intrusive and possibly demeaning for the women involved.

Geller's method has not proved popular with other investigators, though he is apparently alone in explicitly taking into account the sensitivities of his target beneficiaries.

Water Boiling Test

The American development agency Volunteers in Technical Assistance (VITA) developed the Water Boiling Test (WBT) which has been widely accepted as the standard efficiency test. The method is simple to implement and requires relatively little measurement or data on material properties. The latest version was published by Bailis et al. (2004):

> *The WBT… consists of three phases:*
>
> *1) The tester begins with the stove at room temperature and uses a pre-weighed bundle of wood to boil a measured quantity of water in a standard pot. The tester then replaces the boiled water with a fresh pot of cold water to perform the second phase of the test.*

2) Water is boiled beginning with a hot stove in order to identify differences in performance between a stove when it is cold and when it is hot.

3) The tester again boils a measured amount of water and then, using a pre-weighed bundle of wood, simmers the water at just below boiling for a measured period of time (45 minutes). The third step simulates the long cooking of legumes or pulses that is common throughout much of the world.

This combination of tests is intended to measure the stove's performance at both high and low power outputs, which are important indicators of the stove's ability to conserve fuel.

The method yields a set of metrics which can be used to evaluate the performance of a stove: efficiency, time to boil, burn rate, firepower, turn-down ratio (ratio of the stove's high power output to its low power output) and specific fuel consumption (ratio of masses wood consumed to food prepared). In this method the latent heat of evaporation of water is included in the useful energy, such that the efficiency is calculated as follows:

$$\eta = \frac{m_w c_{p,w} \Delta T + \Delta m_w h_e}{m_f h_f - m_c h_c} \qquad (2.2)$$

where the subscripts w, e, f and c stand for water, evaporation, fuel and charcoal.

Effectiveness

Bryden et al. (2000) have worked to improve the performance of a plancha or griddle stove for use in Central America, where the pot is not in direct contact with the flames. Instead, the exhaust gases from the combustion chamber are used to heat a metal plate which in turn is used to heat either a kettle, a pot of food or to cook tortillas. These three cooking regimes require quite different temperature distributions over the heated surface, with the result that optimisation of the stove could not be measured as efficiency. Instead they have developed a measure of effectiveness based on the uniformity of the temperature distribution over the heated surface.

Other investigators have developed forms of effectiveness appropriate to their own applications. Geller (1982) made use of the specific fuel consumption, defined as the ratio of mass of wood consumed to mass of food produced. Likewise, van Buskirk (no date) has used the effectiveness measure of mass of wood per item when evaluating stoves used to cook Eritrean ingera.

2.1.2 Emissions Test Procedures

The emissions from stoves has been directly related to a litany of long term health issues such as acute respiratory infections, chronic obstructive pulmonary disease, lung cancer, tuberculosis, low birth weight and perinatal conditions, asthma, cataracts and heart disease (McCracken and Charron, 2003). Additionally, carbon monoxide is known to be a highly toxic gas in the short term. Many investigators have been motivated by these health issues, and as such they have focused on un-vented stoves, which discharge their exhaust gases directly into the kitchen or cooking area. Meanwhile, others have been motivated by the production of gases linked to climate change, and are not concerned about whether the emissions are discharged into a living space as all emissions will eventually make their way into the atmosphere. Either way, it becomes apparent that collecting and measuring the volume and concentration of emissions from an un-vented stove is a very different matter than for a vented stove, where a probe can simply be inserted into the flue to measure concentrations of various species of gas. Two methods have been developed to assess the emissions from un-vented stoves: the hood and chamber methods, or direct and indirect methods.

Hood Method

The hood method was proposed by Butcher (1984). It requires that the stove be placed under a hood connected to an extractor fan. The dilution of exhaust gas and ambient air can be estimated from the ratio of temperatures in the flame and in the duct. The strength of the fan and height of the hood above the stove are set such that the induced air flow is strong enough to collect all of the exhaust gases produced by the stove, but not so strong as to affect combustion conditions. Typical air velocities around the stove are 0.1 m/s, which are not large compared with 0.25 m/s air currents in a closed room (Ballard-Tremeer, 1996). Ballard-Tremeer (1999a) investigated the effect of the induced air flow on the production of carbon monoxide, and found it to be small in comparison to the effect of stove design.

The method is very useful as a laboratory tool, but of limited use for testing stoves in the field, as it requires a large amount of bulky equipment. Many investigators have adopted it, rather than the indirect or chamber method.

Chamber Method

The chamber method was proposed by Ahuja et al. (1987). It requires a room with a steady rate of ventilation. The stove is placed in the room, and acts as a source of pollutants, which are measured by a device which is also in the room. Given the assumptions that the air in the room is well mixed (i.e. there is no

vertical stratification of smoke) and that the rate of production of the pollutant is constant, the following expression describes the evolution of pollutant concentration, c:

$$c(t) = \frac{FE}{VS}(1 - e^{-St}) \qquad (2.3)$$

where F is the fire power, E the emission factor (ratio of masses of pollutant to wood consumed), V the volume of the room and S is the ventilation rate. The stove is used to perform some cooking task and the concentrations of pollutants are monitored continuously. After the task, the stove is extinguished or removed from the room, and the pollutant concentrations monitored until they decay to ambient levels. The second part of the test is used to evaluate the ventilation rate, S, while the first part is used to assess the actual performance of the stove.

The method is useful in that it is easily employed in a remote location since relatively few measurements or equipment are required. As Ballard-Tremeer indicated (1999b), it rests on the assumption that the burn-rate of the stove is constant, which is in direct conflict with the requirements of the water boiling test.

2.1.3 General Findings

It has been noted that increasing the fire power of the stove decreases the efficiency (Joshi et al., 1989; Gupta et al., 1998; Ballard-Tremeer, 1996): a more vigorous fire results in gases moving away from the hot combustion areas quickly, resulting in incomplete combustion and smaller residence times, hence lower efficiencies. Ballard-Tremeer (1996) describes the phenomenon as 'the economy of smallness'.

Comparing designs of stove, the following investigators have found that improved stoves do tend to have improved efficiencies: Ballard-Tremeer and Jewurek, 1996; Joshi et al., 1991; Bhattacharya, Albina and Salam, 2002; Zhang et al., 1999a. They generally credit the improvements in efficiency to insulation around the fire chamber, the use of a fire grate, reduction of thermal inertia and small passages for flue gases to pass by the pot. However they also report that 'improved' stoves often suffer from higher emissions, arguing that the improvement in efficiency has come about by a large increase in heat transfer efficiency coupled with a smaller decrease in combustion efficiency. The result is seen as a net increase in efficiency and an increase in the emissions of products of incomplete combustion (PIC). The decrease in combustion efficiency is associated with a lowering of the pot: the flame is in better contact with the pot, increasing the heat transfer coefficient, but also reducing the likelihood of

complete combustion of volatiles within the flame. Additionally, improved stoves have enclosed fire boxes in an attempt to reduce the amount of excess air, but inadvertently this increases the thermal inertia of the stove. Ballard-Tremeer (1996) also notes that the burn rate of 'improved' or enclosed stoves is much more erratic. He argues that the enclosed flame is more difficult to see and is less likely to be tended to achieve optimal combustion conditions.

The impact of fuel type and conditions has been investigated by several authors: Joshi et al., 1989 and 1991; Bhattacharya, Albina and Khaing, 2002; Gupta, 1998; Venkataraman, 2001; Zhang et al., 1999a and 2000. These studies are somewhat academic, as low income rural families will be restricted to using whatever fuel is to hand, rather than being able to make informed decisions of what fuel type to use depending on efficiency and emissions characteristics. Nonetheless, the findings are instructive.

The concept of a fuel ladder has been used by Zhang et al. (2000), whereby fuels were ranked according to their cleanliness. From dirtiest to cleanest, the ladder is approximately: dung cakes, agricultural residue, brushwood, fuel wood, kerosene and LPG. Fuels higher up the ladder are cleaner burning, but also more expensive. Low grade fuels are often associated with high emissions of PIC and carbon dioxide per unit of useful energy delivered.

Joshi et al. (1989 and 1991) also point out that lower grade fuels not only have a lower calorific value, but also tend to show a lower efficiency: low grade fuels such as dung tend to smoulder rather than flame (due to low volatile content), with two consequences. First hot combustion gases are less likely to impinge on the bottom of the pot, and second there is less radiative heat transfer.

Bhattacharya et al. (2002) studied the effect of fuel wood moisture level as well as size. They concluded that the size of fuel pieces has no direct impact on emissions, though increasing moisture content tends to reduce the efficiency of a stove and increase the emissions of carbon monoxide: energy is consumed in heating and evaporating the water which would otherwise be used to heat the pot and its contents. They also investigated the impact of ignition technique on emissions, finding that lighting a fire from the top and allowing the combustions zone to work down through the bed of fuel was more efficient: volatiles are released straight into the hottest part of the flame thereby ensuring thorough combustion, whereas volatiles released from a bottom-up burning fire are more liable to escape the hot regions which will encourage them to burn.

Investigators are at pains to differentiate between emissions of pollutants and exposure to emissions: emissions are the amount of a pollutant produced, generally measures in grams of pollutant per kilogram of fuel, while exposure to

pollutant indicates the amount of pollutant that an individual will come into contact with, defined in terms of the product of concentration [mg/m^3] and time [h]. While exposure is directly related to the emissions of a stove, it also takes into account the design of the room housing the stove, ventilation conditions, and how much of the day is spent indoors. Zhang et al. (1999b) used pollutant concentrations from a previous study and assumptions of a constant ventilation rate (similar to Ahuja et al., 1987) to predict the exposure rates of household members to carbon monoxide in houses in China where biomass stoves were used. They noted that men suffer lower exposure rates than women as they are often away from the house during cooking times, and that woman and young children suffer exposures higher than the legal maximum set by US health and safety legislation (80 h-mg/m^3 CO exposure).

McCracken and Charron (2003) evaluated the exposure levels of Nicaraguan women to particle matter less that 2.5 μm aerodynamic diameter, in order to assess the effectiveness of the EcoStove in reducing emissions. The study required 60 householders to be equipped with backpacks containing filters and personal air-pumps with flow rates of 4 l/min. The women participating in the study were also asked to fill in a detailed timesheet of activities and environmental parameters which may have affected their exposure to smoke. The study demonstrated that the EcoStove reduced average $PM_{2.5}$ concentrations from 400–600 μg/m^3 with an open fire to approximately 100 μg/m^3 with the EcoStove.

Naeher et al. (2001) also evaluated the exposure of women and children to smoke (TSP or total suspended particulates) in the kitchen whilst cooking with gas, planchas and open fires. At the same time they aimed to assess the accuracy of attempts to use carbon monoxide as a tracer for smoke. Exposure kits, containing air-pumps and filters to measure $PM_{2.5}$ levels and Draeger tubes to measure CO exposure, were attached to the participants of the study and also positioned in the kitchens. They found CO levels up to 10 ppm and $PM_{2.5}$ levels up to 2200 μg/m^3. They found that there was a strong correlation between CO and PM in spaces, but not on people. Correlations were strong for wood smoke, but weak for LPG (for which emissions are substantially lower).

The levels of PM exposure cited here are far in excess of legal values proposed in the developed world, such as 40 μg/m^3 continuous residential level and 100 μg/m^3 one hour limit specified by the Canadian authorities (Health Canada, 1995).

2.2 MODELLING

Many of the phenomena observed in cooking stoves have already been studied and are well understood, including the combustion of charring fuels, combustion in solid and gas phases and radiation and convection heat transfer. Smouldering combustion has also been examined in depth, and reviewed by Ohlermiller (1985), but is not of direct importance to the current investigation. While phenomenological models are important, this review will focus on models that are easily combined with the Navier-Stokes equations and have already been implemented in commercial CFD software.

2.2.1 Devolatalisation and Pyrolysis

The terms 'devolatalisation' and 'pyrolysis' are often used interchangeably, but they do have strict definitions: pyrolysis is the thermal decomposition of matter in the absence of oxygen; devolatalisation is the thermal decomposition of matter in the presence of oxygen. Devolatalisation can lead to the combustion of the volatile matter (see homogenous combustion below), such that heat is fed back to the thermal decomposition process. This section reviews pyrolysis reactions for small and large fuel particles. Excellent reviews are given by Di Blasi (1993) and Winter (1995).

For small (isothermal) fuel particles (i.e. Bi << 0.1), thermal decomposition can be assumed to be limited by chemical kinetics. The simplest model of thermal decomposition is the single reaction pyrolysis model. It proceeds according to:

$$fuel\ (s) \rightarrow volatiles\ (g) + char\ (s)$$

The reaction rate is given by:

$$\frac{dm_f}{dt} = k_0\left(m_{f-\infty} - m_f\right)^n \tag{2.4}$$

where m_f is the mass of fuel, subscript ∞ is the final value, n is the order of reaction, and k_0 is the Arrhenius style rate constant, given by:

$$k_0 = A\exp\left(-E/RT\right) \tag{2.5}$$

A is the pre-exponential factor, E is the activation energy, and T is the fuel temperature. R is the universal gas constant. The species of gas in the volatiles are not differentiated, and the yield of volatile matter is fixed. The model cannot differentiate between the decomposition of cellulose, hemicellulose or lignin.

This last limitation can be overcome with the parallel reaction model. The fuel is split into components (e.g. cellulose, hemicellulose and lignin), and pyrolysis proceeds according to the parallel reactions:

$$fuel\text{-}cellulose\ (s) \rightarrow volatiles\text{-}cellulose\ (g) + char\ (s)$$

fuel-hemicellulose (s) → volatiles-hemicellulose (g) + char (s)

fuel-lignin (s) → volatiles-lignin (g) + char (s)

Each reaction has its own reaction rate:

$$\frac{dm_{f-cell}}{dt} = k_{f-cell}\left(m_{f-cell-\infty} - m\right)^n \quad (2.6)$$

$$\frac{dm_{f-hcell}}{dt} = k_{f-hcell}\left(m_{f-hcell-\infty} - m\right)^n \quad (2.7)$$

$$\frac{dm_{f-lig}}{dt} = k_{f-lig}\left(m_{f-lig-\infty} - m\right)^n \quad (2.8)$$

where the volatile fraction associated with component i is given by $(1\text{-}m_{f\text{-}i\text{-}\infty})$, and the reaction rate constant is given by expressions similar to (2.5).

The original reaction scheme can also be modified to give a variable volatile yield, depending on the temperature history of the particle. This is called the simultaneous competing reaction model, and it proceeds according to:

fuel (s) → (y_1) volatiles (g) + (1-y_1) char (s)

fuel (s) → (y_2) volatiles (g) + (1-y_2) char (s)

where reactions 1 and 2 have different activation energies and volatile yields. More complex schemes also exist, which include the yield of intermediary species such as tar, activated cellulose, anhydrous cellulose and others. Some kinetic data for the simpler schemes listed above is given in Table 2.1.

For large particles (described as thermally thick), the isothermal assumption

Table 2.1. Pyrolysis and evaporation parameters.

Author	Process	A *[s-1]*	E *[kJ/mol]*	h *[MJ/kg]*
Bryden et al., 2002	Wood-gas	14.4e3	88.6	-0.42
	Wood-tar	4.13e6	112.7	-0.42
	Wood-char	738e3	106.5	-0.42
	Tar-gas	4.28e6	107.5	0.04
	Tar-char	100e3	107.5	0.04
Reina et al., 1998	Furniture-gas	19.1e6	129.4	
	Forest-gas	33.8e6	136.2	
	Pallet-gas	12.3e6	127.6	
Bellais et al., 2003	Wood-char	1.03e3	74.1	
	Wood-gas	114	54.9	
Bilbao et al., 1996	Wood-gas	831e3	24.2	0.27, -0.35*
Fredlund, 1993	Wood-gas	0.55	26.3	

* cellulose and hemicellulose (initial decomposition), lignin (later decomposition)

breaks down. Temperature gradients within the particle require that the pyrolysis rate be evaluated (as above) at different points in the fuel, according to the local temperature. When the heating regime is aggressive enough, the temperature gradients become so steep that the moisture evaporation and pyrolysis regions collapse into discrete waves propagating through the particle. In such regimes, pyrolysis is no longer limited by chemical kinetics, but by the supply of heat to the pyrolysis front.

Heat transfer within the particle must be modelled with the diffusion equation:

$$\sum c\rho \frac{\partial T}{\partial t} = \frac{\partial}{\partial x}\left(k_{eff} \frac{\partial T}{\partial x} \right) \tag{2.9}$$

where the summation on the left hand side is for solid, water vapour and volatile gases, assuming that all three are in thermal equilibrium (Ohlemiller, 1985). The k_{eff} term may include conductive elements of both gaseous and solid phases and an effective radiative heat transfer term, though Panton suggests that this is only significant in larger pores and is a function of the third power of temperature (see Larfeldt et al., 2000a). Different authors suggest varying degrees of complexity concerning the conductive heat transfer coefficient, stating dependencies on parameters such as porosity (Bryden et al., 2002), density and moisture content (Ragland, see Bilbao et al., 1996; di Blassi, 1993). Similarly, specific heat varies with porosity, density and moisture content (see Table 2.2). Ragland et al. (1991; see Bilbao et al., 1996) proposed the following relationship between thermal conductivity, k, and moisture content, X_m:

$$k = \rho(194 + 406X_m) + 0.018 \tag{2.10}$$

Bryden et al. (2002) used the following relation to determine the thermal conductivity of wood:

$$k = 0.004X_m g_s + \eta(0.2X_m + 0.024) + (1-\eta)0.105 + \frac{\varepsilon}{1-\varepsilon}\sigma e d 4T^3 \tag{2.11}$$

where the first term accounts for moisture, the second for virgin wood, the third for char and the forth for radiative heat transfer. The symbols are: k, thermal conductivity; g_s, specific gravity; η, reaction progress variable (1-wood, 0-char); σ, Stefan-Boltzmann constant; e, emissivity; d, pore diameter (typically 50-100μm); and the void fraction, ε, is given by:

$$\varepsilon = 1 - \frac{\rho_w + \rho_c}{1500} - \frac{\rho_m}{1000} \tag{2.12}$$

where the subscripts w, c and m stand for wood, char and moisture respectively.

Table 2.2. Thermal parameters for wood and charcoal

Author	Material	c *[J/kg.K]*	ρ *[kg/m3]*	λ *[W/m.K]*
Fredlund, 1993	Wood (dry)	1400 – 1600	450	0.10 – 0.21
	Char	1900 – 2000	150	0.05 – 0.21
	Gas	1000 – 1100		
	Vapour	700 – 1300		
Thunman et al., 2002	Wood, solid		1480	0.73, 0.52*
	Char, solid		1950	1.47
Bruch et al., 2003	Wood, birch		750	0.53
	Char		200	0.10
Bilbao et al., 1996	Wood	1670		0.10
	Wood, wet			see below
	Char	1000		0.07
Peters & Bruch, 2003	Wood, fir	1730	330	0.2
	Char			0.1
Bellais et al., 2003	Wood	1500 + T	530	0.31, 0.2*
	Char	$420 + 2.09T + 0.000685T^2$		0.10, 0.10*
Bryden et al., 2002	Wood	$3.87(T-273)+103$		see below
	Char	$1390 + 0.36T$		0.105

* parallel and perpendicular to the grain

Convective heat transfer is associated with the movement and release of water vapour and volatile gases. As such it requires knowledge of the pressure gradient inside the fuel, which in turn requires knowledge of the void fraction or porosity of the fuel and reaction rates for both vaporisation and volatisation (discussed below). Some investigators (de Souza Costa and Sandberg, 2004) have assumed that all gases move away from the virgin fuel area, arguing that it offers a greater resistance to flow than the permeable char region. This assumption is backed up by di Blasi's very thorough simulations (1993), though it runs the risk of initially over-estimating the out-flow of gases and then under-estimating it as the last of the un-burned fuel core is consumed, since gases that do move towards the cool virgin fuel will tend to re-condense and settle. Bryden et al. (2002) and Larfeldt et al. (2000b) both assumed that the gas velocity followed Darcy's law of flow through a porous medium:

$$u = -\frac{\lambda}{\mu}\frac{dP}{dx} \tag{2.13}$$

where u is gas velocity, κ is permeability of the porous medium, μ the dynamic viscosity of the gas and P the pressure.

The fibrous nature of wood means that different values of permeability are quoted for transverse and longitudinal directions (travel along the grain being up to a thousand times more permeable, see table 2.2). Peters and Bruch (2003), Bilbao et al. (1996) and Spearpoint and Quintiere (2000) made the simplification that gases were immediately released at the surface of the fuel.

2.2.2 Heterogeneous combustion

Char combustion (heterogeneous because it takes place between materials in different phases) usually takes place after the devolatalisation process has finished, because the blowing of volatile matter through the char surface typically inhibits oxygen from reaching the char. Char is a porous medium since the devolatisation process has created a network of pores and fissures in the surface of the wood. Char combustion yields a mixture of carbon dioxide and carbon monoxide, which desorbs from the char surface and subsequently burns with secondary air in the gas phase (Arthur, 1951).

Similar to pyrolysis reactions, the char combustion reaction can be limited by one of two processes: chemical kinetics or diffusion. For particles which are either small or have a large porosity (leading to high gas diffusivity compared to the char reactivity), char combustion is limited by kinetics. In this case the concentration of oxygen throughout the particle is an approximately uniform non-zero value, and the particle burns by maintaining a constant diameter but reducing its density. For larger particles, or particles that have a lower porosity compared with the reactivity of the char, the rate of char combustion can be approximated by a surface reaction limited by the diffusion of oxygen through the species boundary layer to the char surface. In this case the bulk density of the particle remains approximately constant, and the particle changes mass by decreasing the diameter of the particle. An excellent review of char combustion models is given by Winter (1995).

Ash, the inorganic solid which remains after combustion, generally represents less than 5% of the mass of dry wood. It causes a slight hindrance to gas permeability and a more substantial hindrance to radiative heat transfer (Davies, 2005). It is common to neglect the effect of ash, assuming a small mass which is liable to be swept away by even the slightest air current (de Souza Costa and Sandberg, 2004; Thunman et al., 2002).

2.2.3 Homogenous combustion

Gas phase combustion (homogenous because reactants are in the same phase) may take place once the volatile gases have been desorbed from the fuel surface. Atreya (1998) suggests that the following criteria be met for volatiles to ignite into flaming combustion: a critical mass flux of volatile gas release must be exceeded, a critical gas temperature must be exceeded in the region of volatile and oxygen mixing, low gas velocities must be maintained and the flame must produce enough heat to overcome losses to the environment and the relatively cool fuel surface. In order to model gas phase combustion, two phenomena must be accounted for: transport of reactant, oxidant and product through the gas phase, and the mechanism that limits the rate of combustion. Two related models exist for transport:

- *Species Transport Model* requires n-1 extra continuity equations for n species, so that the distribution of each species (except the bulk carrier: nitrogen in most cases) is explicitly calculated. The behaviour of each species (i.e. diffusivity, specific heat etc.) can be controlled independently. The model is valid for both laminar and turbulent flows. Chemical reactions are affected by source terms in the continuity equations for the various species and the energy equation. The rate of chemical reaction is limited by one of the reaction schemes detailed below. The species transport model is the most general model for reacting flows and the most expensive because of the large number of extra continuity equations required.
- *Simple Chemical Reacting System (SCRS) Model* requires several assumptions to be fulfilled: the flow must be turbulent; the sources of reactants (i.e. fuel and oxygen) must be discrete; chemistry is infinitely fast; all species have identical values of diffusivity and; the Lewis number of the flow is approximately unity (i.e. thermal diffusivity is equal to species diffusivity). The chemistry of the system can then be defined by two continuity equations: one for mean mixture fraction (i.e. what fraction of the flow derived from the fuel inlet) and mixture fraction variance (i.e. how much the time averaged flow fluctuates around the mean due to turbulence). The field of individual species and temperature are all calculated from the two independent variables. The rate of chemical reaction is limited by the rate of turbulent mixing. The SCRS model is considerably cheaper than the species transport model, though there are severe limitations on the number and nature of flows entering the domain, restricting it to use with only the simplest chemical systems.

The rate of chemical reaction in homogenous combustion flows can be modelled by the following:

- *Finite-rate Chemistry Model* which assumes an Arrhenius style expression for reaction rate. This model is most applicable to systems with slow chemistry or laminar flow.
- *Eddy Dissipation Model* (a.k.a. the Eddy Break-up Model) due to Magnussen and Hjertager (1976) which assumes that reaction rate is limited by turbulent mixing of reactants (or the turbulent mixing time, k/ε). This model can only be used for turbulent flows with fast chemistry, where chemical kinetics can be ignored.
- *Eddy Dissipation Concept* due to Ertesvag and Magnussen (2000, cited by Versteeg and Malalalsekera, 2007), which is based on the Eddy Dissipation Model. In this modification, it is assumed that chemical reactions only occur in a fraction of the flow field occupied by the smallest turbulent structures, the small scales.

All the models in this section must be solved in conjunction with the Navier-Stokes equations, to resolve the velocity field and determine the mixture rate of reactants.

2.2.4 Convection Heat Transfer

Heat transfer due to non-reacting impinging jets has been investigated extensively and excellent reviews of the subject are available from Viskanta (1993) and from Jambunathan et al. (1992). Germerdonk (cited by Viskanta, 1993) showed that while a jet and a flame are aerodynamically similar, the heat transfer coefficient of a flame can be up to three times higher than for a jet. The effect of radiation varies widely, and while references cited in this section have chosen to ignore it, others have found that it is of key importance (see below).

A non-reacting jet impinging on a flat plate can be broken down into three key areas of interest: the free, stagnation and wall-jet regions (figure 2.2). In the free region, the jet leaves the nozzle, diameter d, and mixes with ambient air, and an exchange of energy and momentum takes place between the two bodies of fluid. Shear stresses cause the jet velocity profile to take on a Gaussian distribution, and may also induce turbulence. The plate is distance z from the nozzle. The stagnation region is where the plate causes the jet to change direction. The boundary layer is of approximately constant thickness, and the level of turbulence has a great influence on the heat transfer coefficient. The point of maximum radial velocity is approximately one nozzle diameter away from the stagnation point, and beyond this is the wall-jet region, where the jet air flows radially away

from the stagnation point. Heat transfer in this region is increased by turbulence, which causes good mixing of the jet air so that more of the fluid comes in to contact with the plate.

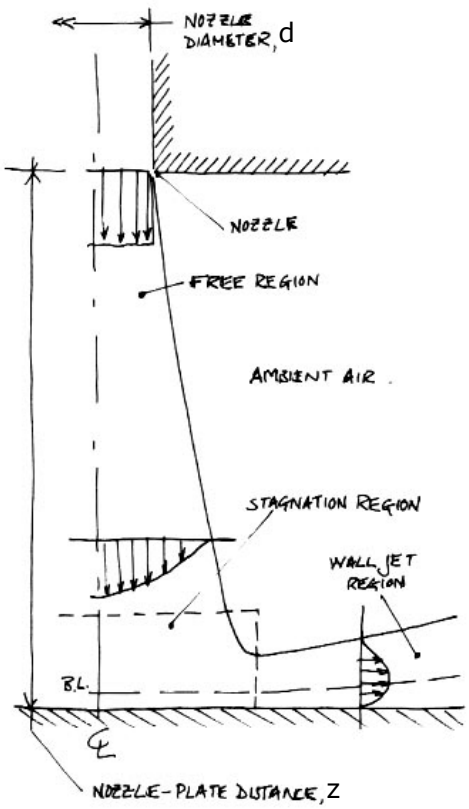

Figure 2.2. Nomenclature of a jet impinging on a flat plate (Viskanta, 1993).

Non-dimensionalised heat transfer correlations for impinging jet heat transfer usually take the form:

$$Nu_d = k\,\mathrm{Re}_d^{\alpha}\,\mathrm{Pr}^{\beta}(z/d)^{\gamma} \qquad (2.14)$$

where exponents α, β and γ are evaluated experimentally or analytically. Reynolds number, Re_d, is commonly defined in terms of the nozzle diameter, d. Saad et al. (1977) demonstrated analytically that for a laminar, flat velocity profile leaving the nozzle the Reynolds number exponent, α, should be 0.50, though values from experimental investigations have been reported in the range $0.23 < \alpha < 0.70$ (Viskanta, 1993). For turbulent flows the Reynolds number exponent generally falls in the range $0.50 < \alpha < 0.87$ (Jambunathan, 1992). Hrycak (1983) suggests $\alpha = 0.50$ for the stagnation region, and $\alpha = 0.70$ for the wall jet region, and reports an average value of $\alpha = 0.70$ for heat transfer from a plate with non-dimensional radius (R/d) = 17. Sparrow & Lovell (1980) presented data for low-Reynolds number flow, suggesting an exponent of 0.62.

Many investigators report that heat transfer maximum at the stagnation point reaches a maximum for nozzle-to-plate distances 6.0 < (z/d) < 7.0 (Jambunathan, 1992; Viskanta, 1993). For smaller nozzle-to-plate distances secondary maxima begin to appear at (R/d) = 2.0, associated with the phenomenon of hydraulic jump (Gardon & Cobonpue, 1962) or with the re-establishment of turbulent flow (Lytle & Webb, 1991). For very low nozzle-to-plate distances (typically below 0.50) a local heat transfer minimum occurs at the stagnation point, and the maximum occurs at (R/d) = 0.50, associated with the vena contracta.

Published data on low Reynolds number and low plate-to-nozzle distance jet impingement heat transfer are summarised in Table 2.3. These configurations are of particular relevance because rocket stoves are limited to velocities that can be achieved with buoyancy driven flows (typically 1 m/s), nozzle diameters comparable to the dimensions of a cooking-pot (typically 0.1 m) and very low nozzle-to-plate distances in order to maximise radiative heat transfer.

Table 2.3. Summary of low-Re, low-(z/d) impinging jet investigations.

Authors	*Re*	*(z/d)*	d *[mm]*	*(R/d)*	α	γ
Garbon & Cobonpue	3.5 – 11	0.5 – 24.0	2.3 – 9.0	0	0.50	-1
Lytle & Webb	3.6 – 27.6	0.1 – 6.0	7.8 – 10.9	1	0.57	-0.33
Hrycak	2.0 – 67.0	3.0 – 10.0	3.2 – 12.7	17	0.70	-0.17
Sparrow & Lovell	2.5 – 10.0	7.0 – 15.0	6.0	~2	0.62	---

Turning now to flames, Huo and Ko (2004) note that heat transfer of a flame impinging on a plate is affected by the type of flame, burner-plate distance, equivalence ratio and Reynolds number. Assessing the heat transfer efficiency of a natural gas flame, they concluded that the optimum flame-plate displacement is to be had when the tip of the light-blue premixed flame just kisses the plate (figure 2.3b): any higher and the core does not have space to react (figure 2.3c); any further away and the hot combustion gases begin to be diluted by excess air (figure 2.3a). Andreatta (2004) confirmed these findings when he carried out a series of experiments with non-premixed flames at low temperatures, designed to replicate the behaviour of wood flames. He noted that bringing the flame too close to the plate serves to quench the flame and cause large amounts of soot to be deposited on the plate.

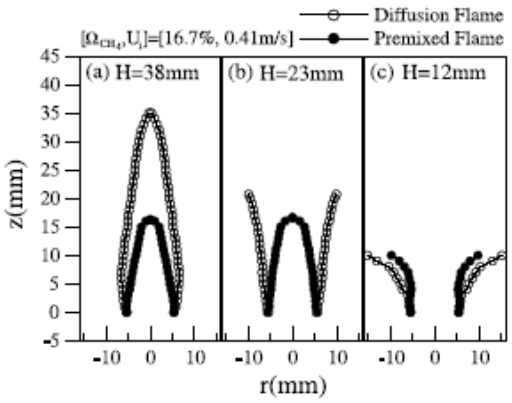

Figure 2.3. Flame types (Huo and Ko, 2004).Ω is fuel mass fraction; U is velocity; H is nozzle-to-plate clearance and; r is radial distance from stagnation point.

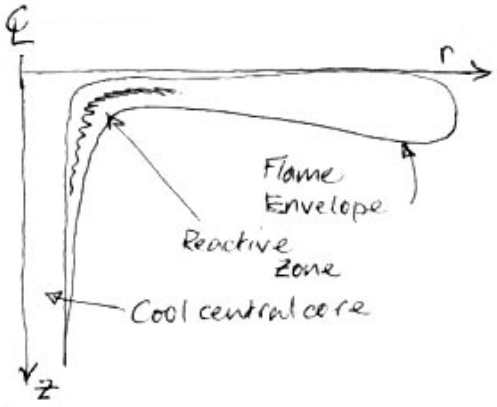

Figure 2.4. Structure of a flame impinging on a flat plate. Axial and radial distance from stagnation point defined by z and r respectively.

Meanwhile, Viskanta (1993) states that 70% of heat transfer can be attributed to convection and 30% to radiation, and that radiative heat transfer can be ignored, though his later work appears to re-evaluate this position (see below). A flame is structured around a cool central core of unreacted gas. Around this is a sleeve of fuel very well mixed with air where intense combustion takes place and adiabatic flame temperature is achievable (Figure 2.4). Viskanta also notes that there is no significant tailing off of the heat transfer coefficient with increasing radius with a flame jet: van der Meer (see Viskanta, 1993) reports local Nusselt numbers of 40-80 for jets with Reynolds numbers in the range 4000-9000.

2.2.5 Radiation Heat Transfer

Monatomic and symmetrical diatomic molecules, like O_2 and N_2, do not participate in radiative heat transfer, while asymmetric molecules, such as CO, CO_2, H_2O, NO and hydrocarbons, are classed as participative media in radiative heat transfer. Since this latter list represents the products of combustion, the phenomena can be expected to play a significant role in the overall heat transfer within the stove. For a hemispherical gas cloud interacting with an adjoining surface, Bejan (1993) gives the following relationship for heat transfer:

$$Q_{gs} = \sigma A_s (e_g T_g^4 - a_g T_s^4) \qquad (2.15)$$

where subscripts g and s refer to gas and surface respectively, and Q is heat, σ the Stefan-Boltzmann constant, A the area, e the emissivity, a the absorbtivity and T is the absolute temperature in Kelvin. The emissivity is a function of gas temperature, partial pressure of the participating media, total pressure of the gas and the radius of the hemisphere enclosing the gas. The functions are given by empirical relations collated from experiments by Hottel (see Bejan, 1993). A

factor also exists to transform hemispherical enclosures to other shapes. As a first approximation this would be a useful method, but it assumes uniform temperature and species concentrations throughout the gas, which is not generally the case for a flame.

A more thorough treatment of radiative heat transfer would require a solution to the Radiative Transfer Equation (RTE), which provides a continuity balance for radiated energy as it passes through a participating medium, undergoing absorption, emission and scattering. Denison & Webb (1993) give the following intuitive expression of the RTE:

> *(Change of energy of a pencil of radiation along a direction Ω and path length ds within a volume element dV) = - (Energy absorbed along direction Ω by dV) – (Energy scattered out of the direction Ω by dV) + (Energy emitted by dV along direction Ω) + (Energy scattered onto direction Ω by dV) + (Energy scattered/emitted into dV and onto direction Ω by all other volume and surface elements)* (2.16)

When rendered mathematically, this expression describes the variation of the independent variable, radiation intensity, I, in terms of three spatial coordinates and two angular directions. Solutions can be grouped into three broad categories: exact or analytical solutions, approximate solutions and statistical solutions. Exact solutions only exist of the most simple geometries and boundary conditions, and cannot even hope to provide an accurate account of radiation within a stove. Statistical methods, such as Monte Carlo, are accurate although they are computationally expensive and rarely compatible with solution techniques of the Navier-Stokes equation. Approximate solutions represent the only hope of modelling radiative heat transfer within a combustion chamber, and they include three broad families of techniques: zonal methods; multi-flux approximations; and spherical harmonics, moment method or P_N approximations (Viskanta, 1982).

The spherical harmonics methods simplify the RTE by turning it into a set of simultaneous partial differential equations. As the order of the approximation increases, complexity increase far more rapidly than accuracy, so many investigators have limited themselves to using only the first order, or P_1 approximation. While its simplicity is alluring, the P_1 approximation does tend to result in large errors when modelling optically thick applications. Similarly the Rosseland approximation is rather simple to implement, though is woefully inadequate in optically thin applications and near to boundaries. The discrete ordinates (or S_N) method is an attempt to simplify the RTE by discretising the

angular orientation of rays, but again, lower order approximations tend to cause substantial errors in the optically thin limit (Modest, 1993).

Finally, some hybrids exist, such as the discrete transfer radiation model, which combine elements of approximate and statistical techniques.

2.2.6 Modelling cooking stoves

The economic importance of space-heating stoves in Scandinavia and North America has meant that a good deal of effort has been invested in modelling and optimising stove performance, though the same modern engineering techniques have not been applied as widely to cooking stoves from the developing world.

Ndiema et al. (1998) used Fluent's CFD code to model the formation of gas species during the pyrolysis and combustion of wood. They burned wood chips and charcoal in a grated vented Kenyan stove. Details are scant, but their model was based upon the following assumptions: (i) the main volatile matter was methane (CH_4); (ii) the fuel bed constituted an isothermal, porous, spherical packed bed of biomass particles; (iii) the flow field was modelled as flow through a perforated plate, governed by Darcy's Law, with an assumed air velocity of $0.01\ m/s$, and (iv) methane was formed through the water-gas shift reactions. The model predicts the distribution of methane throughout the stove quite accurately, though it does not do justice to concentrations of carbon monoxide. Further details of the model are not given.

When optimising their EcoStove, Bryden et al. (2000, 2003 and 2004) made extensive use of CFD code developed by Star CD. As already noted, they aimed to optimise the temperature distribution over the heated surface of a plancha stove. They did not model the rocket type combustion chamber, instead giving a gas temperature and velocity as the inputs to the model at the entrance to the heating cavity. They were exceptionally accurate when modelling the temperature distribution and the model was later used to in conjunction with genetic algorithms to optimise the location and size of baffles inside the heating cavity. Bryden's work will be discussed further in the section on optimisation techniques.

Ravi et al. (2002) have used CFD code to model an Indian stove. The stove consists of a annular packed bed of saw-dust with a central air vent where combustion occurs. The simulation includes sub-routines which model the pyrolysis, combustion, flow field and heat transfer. The model included the following assumptions: (i) pyrolysis was a single-step first order reaction, producing CH_4 and C_2H_6, (ii) char combustion was ignored, (iii) volatile combustion was a single-step finite-rate reaction, (iv) the flow and temperature fields were given by the Navier-Stokes and energy equations, (v) heat was

transferred from gas to solid through radiation and convection and (vi) only conductive heat transfer occurred in the saw-dust bed. The results presented show a good correlation between simulation and experiment. The model was to be used to optimise the bed-to-pot spacing for heat transfer.

2.3 OPTIMISATION

2.3.1 Cooking stove optimisation programs

There exists a myriad of optimised stove designs, and the list given below is by no means exhaustive. The stoves described here demonstrate key design ideas or design methodologies of interest.

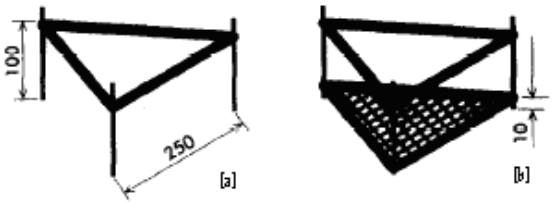

Figure 2.5. Classic (a) and improved (b) open fires (Ballard-Tremeer, 1996).

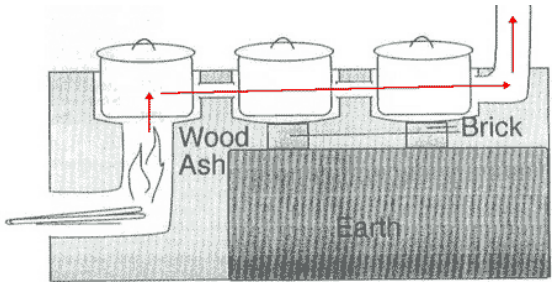

Figure 2.6. A Lorena stove (Still, 1999).

Possibly the simplest optimised stove is the improved open fire. The classic open fire is little more than a pot supported on three stones with a fire on the ground beneath it, though a tripod is sometimes used in lieu of the stones. The use of a tripod would tend to reduce the thermal mass of the stove, and also reduce restrictions to air-flow under the pot, leading to increased excess air and reduced flame temperature (figure 2.5a). The improved open fire (figure 2.5b) uses the tripod and incorporates a grate to support the burning wood. Ballard-Tremeer (1996) tested these two designs and found that the classic open fire had an efficiency in the range of 10-15%, compared to 20-25% for the improved open fire. This improvement in efficiency is coupled with a 13% reduction in CO emissions. The unchanged emission level suggests that the combustion regime has remained relatively unchanged, so that most of the efficiency gain comes from the extra insulation provided by the air between the fire and ground.

The Lorena or adobe stove was designed by the Aprovecho team (Still, 1999). A normally built fire sits under the pot, and exhaust gases are removed from the kitchen with a chimney or flue. Such 'vented' stoves have two advantages: whatever the emissions of pollutants, they practically eliminate exposure and the draught produced by the chimney aids combustion. Later generations of lorena or fogon stoves have been designed for several pots, and various geometries have

been proposed for the ducts around the second and third pots. Wood ash and brick have also been used to control heat transfer and insulation. Costs and efficiencies vary, but US$ 20 and 25% respectively appear to be typical.

Rouse (2000, 2006) reports the development of a very low cost grate in India. It consists simply of an array of fired clay bars, which are laid down over a pit to allow air to circulate. He reports that the clay bars are strong enough to resist the shocks and loads from a normal cooking routine, and cheap enough that they can be replaced occasionally. Additionally, smoke production was reduced by 50%, and efficiency was increased by 25%, though absolute values were not given. The bars cost US$ 0.10 for a set, which is approximately 20% of a comparable cast iron grate. Finally he notes that uptake in some areas was slow, and speculated that locals viewed the grates as poverty indicators, and thought it shameful to be seen to have them.

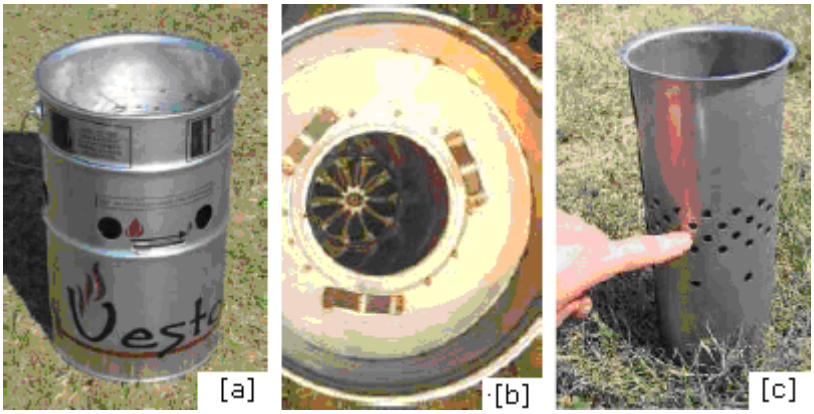

Figure 2.7. VESTO stove [a], with vortex inducing primary inlets [b] and the tapered combustion chamber with secondary air inlets [c] (Pemberton-Pigott, 2004)

Pemberton-Pigott (2004) developed the VESTO stove (Figure 2.7) used in southern Africa. It is a metal stove for cooking pots, and is made from paint tins and other reclaimed metal. It is designed to burn brush-wood, fuel-wood, agricultural residues and dung-cakes and combustion takes place in a tall tapered chamber. Primary air enters at the bottom through intakes which induce a vortex, and passes up through the bed of fuel which burns from the top down. The secondary air inlet is varied to change fire power. The whole combustion chamber is encased to insulate it, and primary air is taken from the insulation cavity, ensuring that it is preheated. The vortex flow field within the combustion chamber ensures greater mixing of secondary air and volatiles given off by the fuel, ensuring complete combustion. It also increases residence time for hot gases, thereby increasing heat transfer efficiency. Top-down burning ensures that excess volatiles are not released without being in the hottest part of the flame and

therefore stand a higher chance of being burnt. This improves combustion efficiency and reduced emissions. Efficiencies for the VESTO stove are reported to be in the range 25-35%, with excursions up to 60% when burning charcoal at very low powers, though this is not a normal operating condition, and the unit price is US$ 28 (Pemberton-Pigott, 2005).

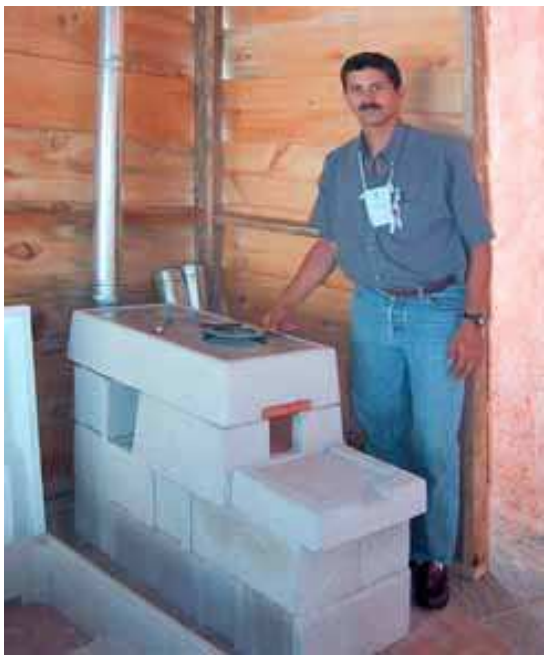

Figure 2.8. HELPS International stove (HELPS, 2005)

Figure 2.9. The jiko liner [a] and complete stove [b], showing the tongue in the foreground (GTZ, no date).

The HELPS International stove (Figure 2.8) incorporates the rocket elbow into a planca (griddle) stove for use in Guatemala (HELPS, 2005). The body of the stove is cast from concrete, and claims complete combustion, efficient heat transfer to the pot, and a 60-70% reduction in fuel consumption from classical designs, though absolute levels are not recorded.

The Maendaleo one-pot jiko (Figure 2.9) is a stove that has been developed for use in Kenya and other East African countries (GTZ, no date). It consists of a ceramic liner that is surrounded by stone and brick insulation. The liner gives optimal sizes for the floor space, combustion chamber height, door and under-pot spacing to ensure efficient combustion and heat transfer. The door restricts the amount of wood that can be burned at a time, ensuring the 'economy of smallness' (Ballard-Tremeer, 1996a). While the stove does not have a grate to raise the wood off the ground and allow air to pass underneath it, the stove promoters recommend that a 'tongue' be built in front of the stove. The tongue is a pile of stones smoothed over with clay and it raises the non-burning end of the wood off the ground, to let air circulate freely around it. The stove gives a 40%

reduction in fuel use (GTZ, no date) and costs less than a chicken. No absolute data are given.

2.3.2 Genetic Algorithms

Originally developed by Holland (1975), Genetic Algorithms (GAs) are just one of a range of computer-based search techniques and are particularly suited to examining large, highly non-linear solution spaces. They mimic Darwinian evolution, whereby only the fittest creatures are allowed to pass their genetic code to the next generation, ensuring that subsequent generations are better adapted to the problems they encounter. The GA methodology requires a problem that can be defined as an objective function to be maximised and candidate solutions (often dubbed 'creatures') to be defined by a gene or string of numbers. Each candidate solution is assessed by the objective function and assigned a fitness, and a new generation of solutions is created by recombining and mutating existing solutions. Solutions with a higher fitness have a greater chance of be selected for the mating event. Thus over successive generations weak solutions are removed, and strong solutions are adapted in the hope of finding other solutions that are stronger still. The technique has been applied to many fields, such as logistics, computer science, chemistry, engineering and product design.

Within engineering several investigators have reported success with GAs which use CFD codes to evaluate the fitness of a candidate solution. Recent applications include optimum wing design (Epstein, 2006), maximising thrust from a rocket nozzle (Cai, 2007), placement of electronic components for optimum thermal management (Dias and Milanez, 2006) and heat exchanger design (Hilbert et al., 2006).

When modelling and optimising their nozzle, Cai et al. (2006) were able to include the chemistry of combustion in their axi-symmetric CFD code. The combustion regime (for a C-H-O-N system) included 12 species and 14 competing reaction mchanisms, limited by chemical kinetics.

As already stated, Bryden et al. (2000) have used CFD to model heat transfer for their plancha stove, and they have also employed a GA to investigate the position of a baffle under the heat transfer surface in order to optimise the temperature distribution. Two aspects of their work deserve particular attention. First they used graph-based genetic algorithms (Bryden et al., 2003; Urban et al., 2002), whereby geography is imposed on the population, limiting the choice of mates for any individual. The technique is analogous to being restricted to marrying within the community, and only very occasionally is there an exchange of genetic material between communities. The result is that solutions are protected from one another and diversity is encouraged, though at a cost of slower convergence.

The second interesting aspect of their work was the use of an Artificial Neural Network (Bryden et al., 2004) which predicts the converged solution of the CFD model. In this manner the CFD need only run for several tens of iterations before the ANN has predicted the solution which would have been found after several thousands of iterations, leading to a significant time saving. The problem took a cluster of 18 CPUs, all equipped with 1 GHz processors, 24 hours to converge to a solution. This team limited themselves to modelling and optimising heat transfer in the plancha stove, arguing that wood combustion was too difficult to include.

2.4 CONCLUDING REMARKS

This chapter has reviewed experimental, numerical modelling and optimisation techniques appropriate to cooking stoves.

Many investigators have used experimental techniques (trial and error, or repeated prototype tests) to developed improved stoves. Meanwhile, many investigators in high technology branches of engineering have used genetic algorithms to optimise the design of a product. Only Bryden and co-workers have reported using genetic algorithms to develop an improved stove. Their publications demonstrated that they have had considerable success in improving the effectiveness of plancha, however they avoided modelling combustion and so did not include the combustion chamber or fuel in their search space. The work in this thesis aims to plug the gap left by Bryden and co-workers, by using a genetic algorithm (that includes the whole stove, including fuel, in its search space), to develop an improved mogogo stove for Eritrea.

In order to achieve the aim of the thesis, a model of the whole stove is required. The review of numerical modelling in this chapter has demonstrated that models exist for fuel pyrolysis, char and volatile combustion, radiation and convection heat transfer. While the models for combustion and heat transfer are sufficient for the investigation, the model of pyrolysis for thermally thick fuels requires the fuel be discretised in order to resolve the temperature field in the solid phase, and therefore determine the kinetically limited pyrolysis rate. This is computationally expensive and unnecessary. Additionally there is a great deal of data on the chemical kinetics of wood pyrolysis, but none in a format that is easily exploitable to give a global burn rate of thermally thick wood in a fixed bed and validate the cheap wood combustion model that has been proposed. The next chapter of the thesis (Chapter 3) therefore details work to develop a cheap wood combustion model and back it up with experimental data. Similarly, there is little firm data on the relative contribution of convection and radiation in cooking stoves, so the

work in Chapter 4 aims to quantify the convection heat transfer rate, and it is compared to the overall heat transfer rate in chapter 5.

The first section of the review introduced experimental techniques for assessing stove performance. While the cooking cycle test is sufficient to evaluate mogogo stove performance, it requires a large number of variables to be monitored, and is sensitive to the cooking style of the operator. As a result it is relatively cumbersome and not sufficiently accurate to collect data to develop or validate the proposed numerical model. Similarly the water boiling test has some inherent inaccuracy (the requirement to differentiate between fuel mass loss and pot mass loss), so the experimental techniques used in the remainder of this thesis are adaptations of the water boiling test that relies purely on the change of temperature of a simulated pot.

CHAPTER 3: COMBUSTION

The first step to deploying a genetic algorithm that will optimise a cooking stove is a model of wood combustion that can be used in conjunction with a CFD code. Fluent 6.2 has already been identified as a suitable candidate (Chapter 2), and it has already been demonstrated that the k-ε model is suitable for simulations of turbulent buoyant plumes above a heat source (i.e. it can resolve the velocity and temperature fields above a fuel bed; Appendix B). This chapter details a custom combustion model that was to be used as a user-defined function, tagged to the commercially available code. The requirements of the combustion model are:

- accurate prediction of wood combustion rate (to calculate the fuel consumption rate);
- accurate prediction of temperature and velocity fields above the fuel bed (to calculate heat transfer to the cooking vessel; see Appendix B);
- volume specific (so that the burn-rate of fuel is related to the volume of the fuel bed, rather than a number of fuel particles fixed in space – this requirement must be satisfied so that the genetic algorithm can easily change the output power of the fire);
- robustness (so that the genetic algorithm can operate unsupervised);
- computationally inexpensive (so that the genetic algorithm can run reasonably quickly);
- steady-state. (Though not a requirement of the model, this is a direct response to the need to be computationally inexpensive. A cook-fire is generally maintained at a constant power-rating for a prolonged period of time. Although the structure and history of the fuel bed is developing constantly, the initial assumption was that the fuel bed is fed at the same rate as it burns, giving the appearance of a quasi-steady process. The

build up of ash invalidates this assumption, but ash is generally a small fraction of wood, and was neglected for the sake of this model.)

Fluent 6.2 is packaged with a single model for solid fuel combustion, developed for modelling pulverised fuel in utility boilers. It requires a discrete phase of fuel particles, which move with the fluid flow subject to inertia, buoyancy, drag and gravity. The particles are infinitely small so that they do not displace fluid or cause a wake or turbulence. The particles develop through phases of inert heating, devolatalisation and heterogeneous char combustion. Fluent is not packaged with a model to simulate the combustion of a fixed bed, and the only option that exists is to create a cloud of reactive particles as described above and fix them in space by assigning a zero-value to the particle body forces (Lowdes, 2007). There are several problems with this approach: first the equations for motion of the discrete phase have been circumvented but not deactivated, resulting in an inefficient use of CPU resources; second the model requires a time dependant solution to allow particles to develop through the different phases of combustion; third, assumptions must be made about the special and developmental distribution of particles (i.e. how may young ones, how many old ones etc.) in addition to knowledge of the fuel parameters for devolatalisation and char combustion; fourth account still has to be made for the resistance to flow offered by the fixed bed of fuel, requiring a porous medium model to be activated. In summary, this is not a particularly graceful solution and one which was well adapted to the problem in hand. It was therefore necessary to develop a new model of wood combustion. The work presented here describes the development of such a model: it is crude, but computationally cheap and agrees with experimental data. The model was developed by conducting a series of experiments on burning wood cribs to find the burn rate and temperature field in the flame (and supplemented by further tests in Appendices C and D to give resistance to flow and other fuel bed characteristics); data from these experiments were then used to fit parameters in a numerical model. There follows a description of the experimental method used to collect data on wood combustion, a description of the numerical model, and results of both the experimental investigation and the numerical simulation.

3.1 EXPERIMENTAL STUDY OF COMBUSTION

The aim of the experimental investigation was to collect data on the burn-rate of wood and the temperature field in the flame above the wood. Cribs were built of pine blocks. All cribs were cubes, with l/h layers. Crib dimensions and properties are given in Table 3.1. To assess the impact of fuel bed structure on burn-rate

and temperature of the crib and flame, the dimensions of cribs A to I were selected as a factorial experiment in the three factors: volume (l^3), void fraction and specific area (fuel surface area per unit crib volume). The lumpiness frequency and flow resistance are discussed in section 3.2 on numerical modelling. Values of flow resistance were estimated from the Ergun equation (Ergun, 1952) and results verified with an experimental investigation (Appendix C).

Table 3.1. Crib configurations.

Crib	*Dimensions [mm]*				*Total volume*	*Void frac.*	*Sp. area*	*Mass*	*Lumpiness frequency*	*Flow resistance*
	l	z	w	n	*[m^3]*	*[-]*	*[m^{-1}]*	*[kg]*	*[m^{-1}]*	*[m^{-1}]*
A	160	20	5	13	0.004	0.6	192	0.72	500	500
B	160	20	20	3	0.004	0.6	66	0.72	200	200
C	160	20	10	13	0.004	0.2	188	1.44	~~80~~*	~~25,000~~*
D	160	20	30	4	0.004	0.3	78	1.26	150	6,000
E	140	20	12	7	0.0027	0.4	133	0.73	300	500
F	100	20	5	8	0.001	0.6	192	0.18	500	500
G	100	20	20	2	0.001	0.6	72	0.18	200	200
H	100	20	10	8	0.001	0.2	192	0.36	~~80~~*	~~20,000~~*
I	100	20	40	2	0.001	0.2	72	0.36	150	10,000
J	100	20	20	3	0.001	0.4	60	0.27	150	100

** cribs C and H not included in numerical study.*

The blocks were knot free, with the grain running the length of the block. Fuel proximate analysis was carried out according to BS1016 (except ash content, which was not analyzed), and described in Appendix D: results are summarised in Table 3.2.

Table 3.2. Fuel properties (reproduced from Appendix D).

Parameter	*Value*
Virgin fuel density	450 ± 10 kg/m^3
Moisture fraction	9.5 ± 0.6 %
Volatile fraction	74.6 ± 0.4 %
Virgin fuel gross calorific value	17.6 ± 0.2 MJ/kg
Char calorific value	29.8 ± 0.6 MJ/kg

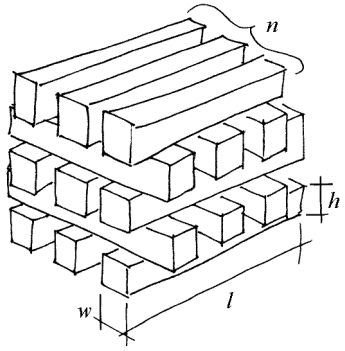

Figure 3.1. Dimensions for wood blocks for cribs: block length (l), height (h) and width (w), and the number of blocks per layer (n).

The crib was positioned on a flat plate on a balance (Mettler Toledo 32000). Four K-type thermocouples (0.75 mm bead diameter) were embedded in the crib, and a further five were suspended above the crib (Figure 3.2). An extraction hood with mean inlet velocity of 0.13 m/s was suspended 0.6m above the base of the crib. A 3-4 g charge of firelighter was inserted into the bottom centre of the crib and lit, after which mass and temperature data were logged at 0.1 Hz, until burn-out.

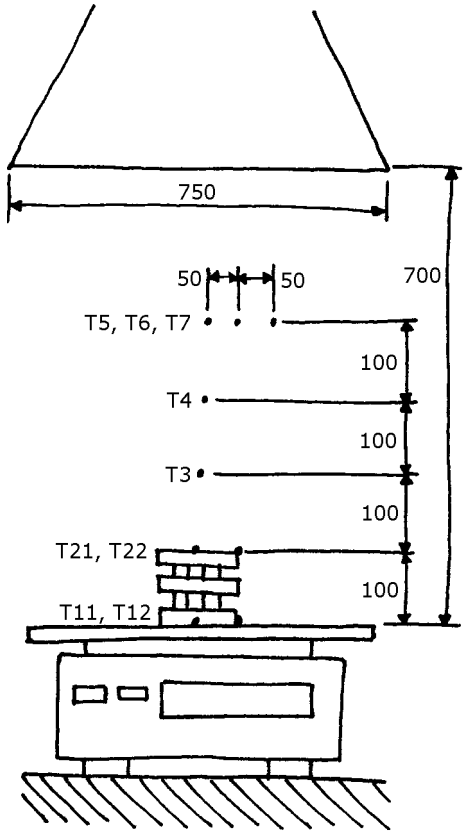

Figure 3.2. Wood-crib on the balance, with the locations of thermocouples and extraction hood. Dimensions in mm.

When processing the results, mass-rate and temperature data were taken during the period of steady flaming combustion, when non-dimensional mass (m/m_0) was in the range 0.8 to 0.2, and again in the period of steady char combustion, when non-dimensional mass (m/m_0) was in the range 0.15 to 0.05. Average burn-rate was typically calculated from 40 mass readings subject to ± 0.05 g uncertainly. Time intervals were subject to ± 0.1 s uncertainty. The act of taking a least-squares curve fit to evaluate the burn rate means the standard error is given by:

$$\hat{\sigma} = \sqrt{\frac{\sum \left(y_i - f(x_i)\right)^2}{n - p}} \tag{3.1}$$

where n is the number of readings and p is the number of parameters in the model (NIST, 2007). Equation (3.1) resulted in typical uncertainty in burn rate of ± 0.01 g/s.

Individual temperature measurements were subject to ± 10 K uncertainty. Flame temperatures were averaged over the whole flaming combustion period ($0.8 < m/m_0 < 0.2$), during which time the temperature varied by as much as 400K. Clearly the act of averaging these temperatures introduced a significant error, and the reported values are no more than approximate measures of temperatures above the crib. Results of the experimental investigation are given in section 3.3.

3.2 NUMERICAL MODEL OF COMBUSTION

The aim of the numerical model was to replicate the burn-rate of fuel in the crib, and the temperature field in the flame above the crib during the quasi-steady period of combustion. In a separate study (Appendix B), results from numerical simulations were compared with experimental data for velocity and temperature in a buoyant turbulent plume, and it was demonstrated that the k-ε turbulence model used in these simulations was able to replicate the temperature and velocity fields found above a heat source.

An initial model of fuel pyrolysis was developed with very simplified geometry and boundary conditions (Burnham-Slipper et al., 2007). In that model, the rate of char combustion was limited by diffusion of oxygen through the species boundary layer to the char surface, and the rate of pyrolysis of virgin fuel was limited by the conduction of heat through the char layer to the virgin fuel. The approach was generally successful, but the assumption of uniform velocity, temperature and oxygen concentration throughout the crib limited the accuracy of the simulations. It was concluded that a CFD model would be required to improve results. The CFD model described here attempted to address the shortcomings of the initial model. It was developed with the following assumptions:

- conditions in the crib were stable during the majority of the fuel pyrolysis period ($0.8 > m/m_0 > 0.2$), leading to a steady-state problem;
- the computational domain was axi-symmetric, and divided into a porous region representing the crib, and a non-porous region representing the surrounding air;
- flow in the crib region was laminar, while flow in the free-air region was turbulent;
- active fuel surfaces in the crib region were lumped together in a periodic fashion so that the regular lattice structure of fuel in the crib was approximated by a series of concentric tori;
- the rate of char combustion was limited by the diffusion of oxygen through the species boundary layer to the fuel surface;
- the rate of release of fuel volatiles was limited by the conduction of heat through char to the virgin fuel;
- the combustion of volatile gases in the flame was limited by turbulent mixing;
- the gases behaved as incompressible ideal gases;
- apart from density, all fluid properties were independent of temperature.

In the following sections, details are given of the governing equations, the fuel sub-model, and the computational domain, boundary conditions, and discretisation.

3.2.1 Governing equations

The Navier-Stokes Equations as described in this section were solved using Fluent 6.2. Conservation of mass, momentum and energy are given by equations (3.2), (3.3) and (3.4) respectively (Versteeg and Malalalsekera, 2007):

$$\frac{\partial}{\partial x_j}(\rho u_i) = S_m \tag{3.2}$$

$$\frac{\partial}{\partial x_i}\left(\rho u_i u_i\right) = \frac{\partial}{\partial x_j}\left[\left(\mu_m + \mu_t\right)\frac{\partial u_i}{\partial x_j}\right] + \rho g_i \tag{3.3}$$

$$\frac{\partial}{\partial x_i}\left(\rho E u_i\right) = \frac{\partial}{\partial x_j}\left[\left(k_m + k_t\right)\frac{\partial E}{\partial x_j} + \left(D_m + D_t\right)\frac{\partial \rho Y_i}{\partial x_j}\right] + S_h \tag{3.4}$$

Turbulence was modelled with the standard k-ε model (Launder & Spalding, 1974) using enhanced wall treatment (Fluent, 2007), resulting in two transport equations for turbulent kinetic energy (3.5) and its dissipation (3.6).

$$\frac{\partial}{\partial x_i}\left(\rho k u_i\right) = \frac{\partial}{\partial x_j}\left[\left(\mu_m + \frac{\mu_t}{\sigma_k}\right)\frac{\partial k}{\partial x_j}\right] + G_k + G_b - \rho\varepsilon \tag{3.5}$$

$$\frac{\partial}{\partial x_i}\left(\rho\varepsilon u_i\right)=\frac{\partial}{\partial x_j}\left[\left(\mu_m+\frac{\mu_t}{\sigma_\varepsilon}\right)\frac{\partial\varepsilon}{\partial x_j}\right]+C_{1\varepsilon}\frac{\varepsilon}{k}\left(G_k+C_{3\varepsilon}G_b\right)-C_{2\varepsilon}\rho\frac{\varepsilon^2}{k} \quad (3.6)$$

where G_k and G_b are sources of turbulence due to shear and buoyancy. Chemistry was modelled using the species-transport model (Fluent, 2007), resulting in a further four transport equations of the form (3.7) for wood volatiles, oxygen, carbon dioxide and water vapour.

$$\frac{\partial}{\partial t}\left(\rho Y_i\right)+\frac{\partial}{\partial x_i}\left(\rho Y_i u_i\right)=\frac{\partial}{\partial x_j}\left[\left(D_m+D_t\right)\frac{\partial\rho Y_i}{\partial x_j}\right]+S_i \quad (3.7)$$

where Y_i is the *i*th species and R_i is the source of the *i*th species due to homogenous reactions. The reaction between wood volatiles and oxygen took place according to:

$$CH_2O+O_2\longrightarrow CO_2+H_2O \quad (R3.1)$$

where the reaction rate was limited by turbulent mixing, according to the eddy-dissipation model (Magnussen and Hjertager, 1976). Radiation was included by using the Discrete Ordinates model (Murthy & Mathur, 1998), with the weighted-sum-of-gray-gases-model (Fluent, 2007) to calculate local absorption coefficient, giving transport equation (3.8).

$$\frac{d}{ds}I(r,s)+a_l I(r,s)=a_l {n_l}^2\frac{\sigma T^4}{\pi} \quad (3.8)$$

The effect of soot on radiation was not included in the model, despite its significance in biomass combustion. Two standard soot formation models were available in Fluent 6.2, both developed for diesel engines. Backreedy et al. (2006) have used the single-step soot model when simulating combustion of pulverised coal in a utility boiler, but no data was available to assess their suitability for wood combustion. Since it has been demonstrated that hydrocarbon soot and biomass soot behave differently from one another (Ross et al., 2005) and a soot model could not be used with confidence, it was omitted. The present model is expected to under-estimate the levels of radiative heat exchange in the flame. The effect of scattering on radiation was also ignored.

3.2.2 Fuel sub-model

An initial attempt at modelling the crib assumed that active fuel surfaces (i.e. char surfaces that combust and emit volatiles) were uniformly distributed throughout the crib region (Burnham-Slipper et al., 2007a). Total fuel surface area and mean void fraction in the crib were preserved. The approach yielded correct values of char combustion rate and devolatalisation rate, but resulted in perfect mixing of the volatiles and oxidant. Consequently the model predicted

that volatiles burned very rapidly, and gave a spurious temperature field, being too hot in the crib and too cool in the flame. A 'lumpiness function' was introduced to model discrete streams of wood volatile and oxidant, which had to mix in order to burn. The lumpiness function was given by:

$$\Psi = (1+\cos\omega z)(1+\cos\omega r) \tag{3.9}$$

where z and r are the axial and radial co-ordinates, and ω is the lumpiness frequency (Figure 3.3). Active fuel surfaces existed in computational cells where $\Psi > \Psi_L$ (dubbed 'lumps'), other cells being empty where air and combustion gases were free to flow. A fraction, ν, of the crib volume was inside the lumps. Let us first examine char combustion in these lumps, then move on to devolatalisation.

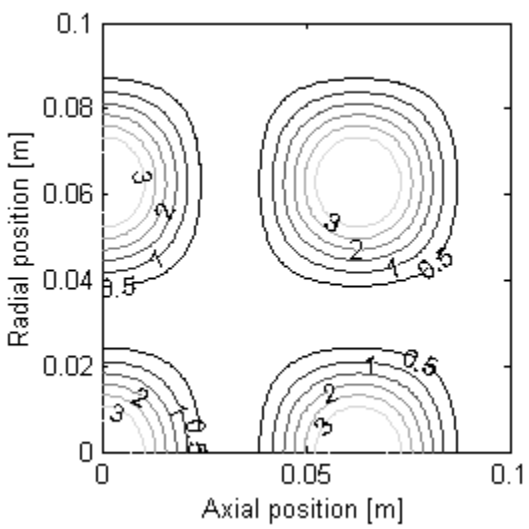

Figure 3.3. Lumpiness function, Ψ, for ω = 100 m^{-1}. Fuel is considered to exist in lumps where Ψ > 3.0.

Char was assumed to burn exothermically with oxygen to yield carbon dioxide:

$$C + O_2 \longrightarrow CO_2 \tag{R3.2}$$

Inside the lumps, oxygen diffuses through the species boundary layer to the char surface at the volume specific rate, m'_{O2} [kg/m^{3}s], according to Fick's Law:

$$m'_{O2} = \frac{a}{v} h_m \left(\rho_{O2\infty} - \rho_{O2s}\right) \tag{3.10}$$

where a is the fuel specific area [m^2/m^3], h_m is the mass transfer coefficient, ρ is density, and subscripts O2, ∞ and s refer to oxygen, free-stream and surface conditions respectively. At the char surface, oxygen is consumed at the same rate, m'_{O2}, limited by chemical kinetics:

$$m'_{O2} = k_2 \rho_{O2s} \tag{3.11}$$

Combining (3.9) and (3.10), surface oxygen density can be eliminated, leaving the oxygen consumption rate as:

$$m'_{O2} = \frac{k_2 \frac{a}{v} h_m}{k_2 + \frac{a}{v} h_m} \rho_{O2\infty} \tag{3.12}$$

The Arrhenius style kinetic rate constant for reaction (R3.2), k_2 [s^{-1}], is first order in oxygen and zeroth order in carbon since it exists in abundance:

$$k_2 = A_2 \exp(-T_2 / T) \tag{3.13}$$

where A_2 is the pre-exponential factor and T_2 is the excitation temperature. The mass transfer coefficient, h_m, for flow through an inert packed bed is given by Cussler (1997):

$$\frac{h_m}{v_0} = 1.17 \left(\frac{d v_0}{\upsilon} \right)^{-0.42} \left(\frac{D}{\upsilon} \right)^{0.66} \tag{3.14}$$

where v_0 is the superficial velocity, d the particle diameter, v the kinematic viscosity and D the binary diffusivity. Equations (3.13) and (3.14) can be evaluated using parameter values typical of experimental conditions, and it can be shown that $k_2 >> a/v\ h_m$, with the result that char combustion is limited by the diffusion of oxygen through the species boundary layer, and chemical kinetics can be neglected. Thus equation (3.12) can be simplified to:

$$m'_{O2} = -\frac{a}{v} h_m \rho_{O2\infty} \tag{3.15}$$

Additionally, from equation (3.14) the mass transfer coefficient is approximately proportional to the square root of superficial velocity, so (3.15) can be adapted to:

$$m'_{O2} = -\frac{a}{v} k_m {v_0}^{0.5} \rho_{O2\infty} \tag{3.16}$$

where k_m is a constant of proportionality. Equation (3.16) defines the rate at which oxygen diffuses through the species boundary layer, and therefore the volume specific source of oxygen in the computational domain. The negative sign indicates the oxygen was removed from the gas stream. Combining reaction (R3.2) and equation (3.16), the sources of mass, carbon dioxide and heat are given by equations (3.17), (3.18) and (3.19) respectively. Together with (3.16) these constitute the char combustion model.

$$m' = \frac{12}{32} \frac{a}{v} k_m {v_0}^{0.5} \rho_{O2\infty} \tag{3.17}$$

$$m'_{CO2} = \frac{44}{32} \frac{a}{v} k_m {v_0}^{0.5} \rho_{O2\infty} \tag{3.18}$$

$$q'_{char} = H_c \frac{12}{32} \frac{a}{v} k_m v_0^{0.5} \rho_{O2\infty} \tag{3.19}$$

Let us now turn our attention to the release of volatiles. Fuel pyrolysis was assumed to take place according to the endothermic reaction:

$$wood \longrightarrow moisture + volatiles + char \tag{R3.3}$$

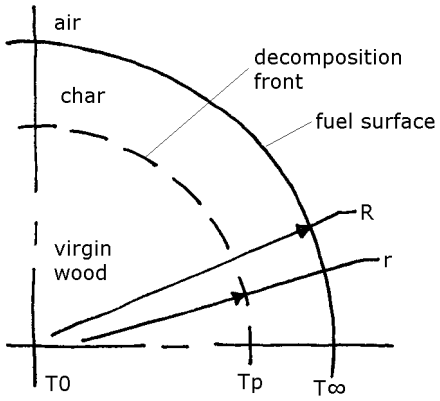

Figure 3.4. Partial section through fuel, showing decomposition front, at radius r and temperature T_p, dividing virgin fuel and char.

Although the release of moisture and volatiles occur at different temperatures (373 K and typically 550 K), it has been demonstrated that the two reactions can be superimposed on one another to produce a single thermal decomposition wave that progresses through the fuel if the heating regime is sufficiently aggressive (Bryden et al., 2002). Furthermore, Di Blasi (1993) has demonstrated that the rate of the endothermic pyrolysis reaction is limited by the supply of heat to the reaction front, rather than by chemical kinetics. For the sake of this model, it was assumed that the crib consisted of sticks with circular cross-section, and that each stick consisted of an outer layer of char, and an unreacted core of virgin fuel. The pyrolysis wave separating the virgin fuel from the char was located at a radius r and the char surface was at a radius R (Figure 3.4). Although pyrolysis takes place over a wide temperature range, it was assumed that the pyrolysis front was at a fixed temperature, T_p. The amount of heat conducted radially through the char layer (thermal conductivity, k_c) to the pyrolysis front was given by:

$$q'_{pyro} = \frac{k_c a\left(T - T_p\right)}{vR\ln\left(R/r\right)} \tag{3.20}$$

For temperatures greater than T_p, the release rate of volatile matter was therefore given by:

$$m'_{pyro} = \frac{k_c a\left(T - T_p\right)}{vR\ln\left(R/r\right)H_v} \tag{3.21}$$

where H_v is the effective enthalpy of pyrolysis, including sensible energy to raise the temperature of wood from room temperature to pyrolysis temperature, latent heat of vaporisation of moisture and latent heat of pyrolysis. H_v was estimated to be 2.5 MJ/kg of volatile matter, in agreement with experimental values (Daugaard et al., 2003). The source of mass released into the gas phase (3.20) was sub-divided into sources of moisture and wood volatiles, given by (3.22) and (3.23) respectively. The ratio of moisture to volatiles was taken from the proximate analysis. Equations (3.20) to (3.23) constitute the pyrolysis sub-model.

$$m'_{H2O} = \frac{10}{85}\frac{k_c a\left(T - T_p\right)}{vR\ln\left(R/r\right)H_v} \tag{3.22}$$

$$m'_{vol} = \frac{75}{85}\frac{k_c a\left(T - T_p\right)}{vR\ln\left(R/r\right)H_v} \tag{3.23}$$

Finally, values of inertial flow resistance coefficient for the whole crib region were calculated from the Ergun equation (Ergun, 1952) as tabulated Table 3.1. The order of magnitude of these values was verified in separate experimental studies (Appendix C and Appendix D).

3.2.3 Domain, boundary conditions & discretisation

The axi-symmetric computational domain was 700 mm high with 250 mm radius. Dimensions of the crib region were calculated to preserve crib volume and height. Two meshes were developed, with 1 mm and 2mm cell size in the crib region, growing to 20 mm at the boundary. The Richardson extrapolation (Feldman, 1999) was used to estimate the error during char burn-rate ($0.15 > m/m_0 > 0.05$) and during flaming combustion ($0.8 > m/m_0 > 0.2$) to be 4% and 7% respectively. Both values were considered acceptable, and the courser of the two meshes was used.

As shown in Figure 3.5, the domain was bounded by an adiabatic floor below and a centre-line (axis of symmetry) to the right. To the left and above was a pressure outlet, where the effect of quiescent air was achieved by allowing ambient air to enter with near-zero turbulent kinetic energy and near-zero turbulent kinetic energy dissipation. The direction vector of incoming air was parallel to the floor, though this was supplemented by a small downward component so that air could actually enter through the top of the domain, while

preserving streamlines predicted by theoretic treatment of turbulent buoyant plumes (Rouse et al., 1952).

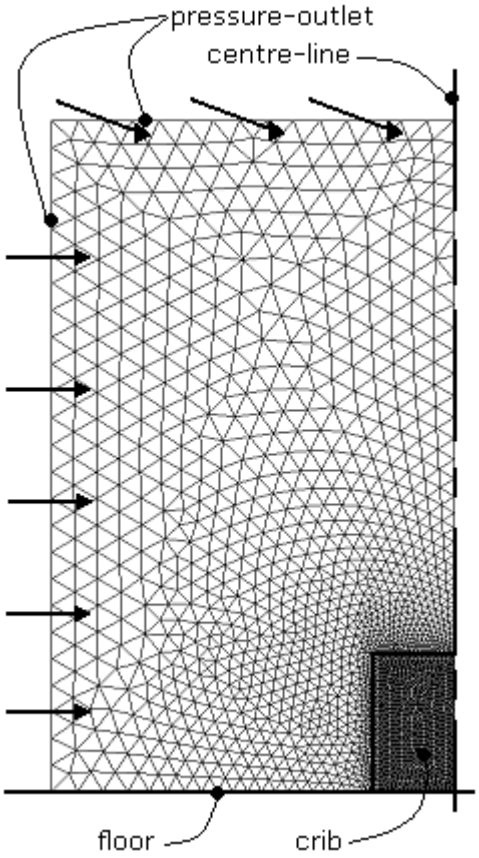

Figure 3.5. Computational domain with boundary conditions and arrows showing direction of flow entering the domain.

Partial differential equations (3.1) to (3.6) were discretised using the Second-Order-Upwind scheme. Pressure was discretised using the Body-Force-Weighted scheme. Pressure-velocity coupling used the SIMPLE scheme. The resulting equations were solved using the commercially available CFD package Fluent 6.2.

3.3 EXPERIMENTAL RESULTS & DISCUSSION

The evolution of crib mass and temperature for a typical test run is shown in Figure 3.6 and Figure 3.7. Initially, the crib burned slowly as flames spread from the fire-lighter to all the fuel surfaces. There was a period of steady mass-loss as the fuel devolatalised, until the progress variable (m/m_0) reached a value of 0.2, when all the volatiles had been driven off. Thereafter the burn-rate reduced dramatically while the char burned, until the temperature fell to a point where char combustion could not be sustained, and there remained a pile of half burned char. Meanwhile, temperature within the crib (T_{11} to T_{22}; Figure 3.6) was greatest in the char combustion period ($m/m_0 < 0.2$), and temperature above the crib (T_3

to T_7; Figure 3.7) was greatest during the devolatalisation period (0.8 > m/m_0 > 0.2), when a flame was present. It should be noted that cribs C and H did not burn with a flame, but smouldered throughout the entire test run, despite several repeats. It was concluded that the fuel was too finely cut and closely packed in these cribs to allow an adequate supply of oxygen to permeate the crib and permit flaming combustion. Since such fires are rarely used as cooking-fires, cribs C and H not included in the analysis described below.

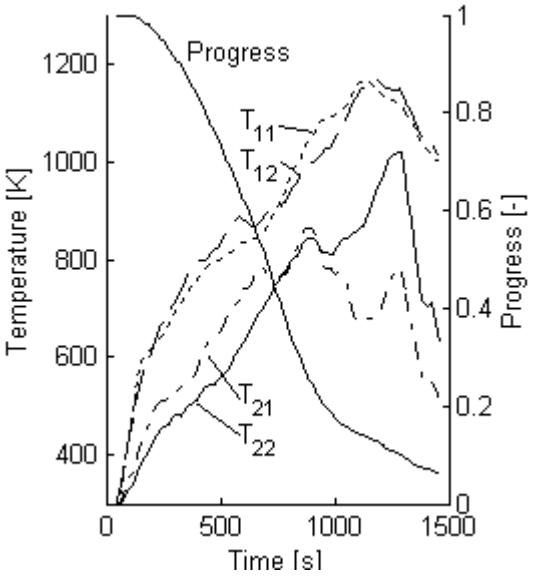

Figure 3.6. Crib J progress variable and temperatures within crib

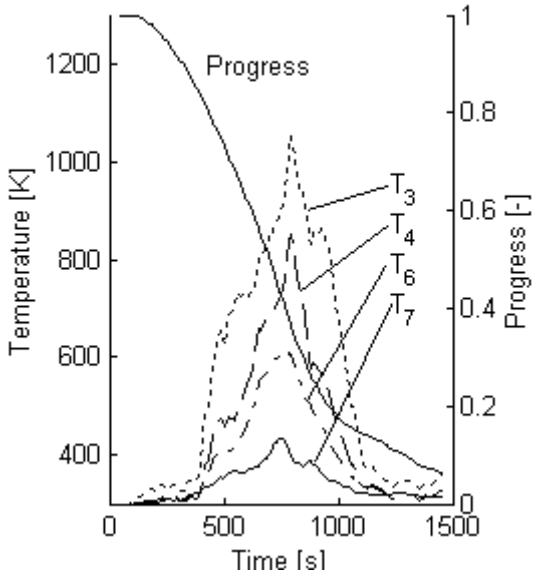

Figure 3.7. Crib J progress variable and temperatures outside crib

Burn-rate was examined in two parts: char combustion and flaming combustion. For each test run, a linear regression was used to find the mass-rate during the period 0.15 > m/m_0 > 0.05, corresponding to char combustion. The resulting char burn-rates were compiled into a single experimental correlation for char combustion, using a least-squares linear regression, in variables v, p and a, the normalised crib volume, porosity (void fraction) and specific surface area respectively (defined by equations 3.24a, b and c).

$$v_i = \frac{V_i - \overline{V}}{\sigma_V}; \quad p_i = \frac{P_i - \overline{P}}{\sigma_P}; \quad a_i = \frac{A_i - \overline{A}}{\sigma_A} \qquad (3.24a,b,c)$$

The experimental correlation for char combustion is given by (3.25) with 95% confidence.

$$m'_{char} = 0.11 + 0.05v + 0.02p + 0.02a \pm 0.03 g/s \qquad (3.25)$$

Similarly, the combined char combustion and pyrolysis rate was assessed by fitting straight line to experimental mass-loss data in the range 0.8 > m/m_0 > 0.2, using a least-squares linear regression. The burn-rates were compiled into a

single experimental correlation for wood burn-rate, using a non-linear regression. The resulting expression (3.26) gives a mean error of 10% and maximum error of 31%.

$$m'_{pyro} = 0.19\left(\frac{V}{V_{\min}}\right)^{0.95}\left(\frac{P}{P_{\min}}\right)^{0.51}\left(\frac{S}{S_{\min}}\right)^{0.56} \; g/s \qquad (3.26)$$

Table 3.3. Burn-rate during devolatalisation and char combustion for cribs A to J, with outputs for correlations 3.26 and 3.25 respectively. Note cribs C and H smouldered without a flame and were not included in the experimental correlation.

	Devolatalisation					*Char Combustion*				
Crib	*Experimental*				*Cor. 3.26*	*Experimental*				*Cor. 3.25*
A	2.29	2.20			2.38	0.063	0.068			0.085
B	1.29				1.34	0.086				0.078
C	0.22				---					---
D	0.95	0.71			0.93	0.156	0.040			0.102
E	1.21	1.13	1.01	0.93	1.08	0.107	0.097	0.085	0.076	0.075
F	0.56				0.63	0.051				0.039
G	0.31	0.30			0.36	0.022	0.032			0.037
G	0.30				0.36	0.032				0.037
H	0.24	0.24	0.20		---	0.058	0.044			---
I	0.21				0.21	0.027				0.050
J	0.33	0.37	0.37		0.38	0.026	0.057	0.043		0.042

The mean temperatures were taken for the period 0.8 > m/m_0 > 0.2. There was insufficient data to collate for T_{11}, T_{12} and T_{22}, but other temperatures were reduced using least-squares linear regression to give:

$$T_{21} = 840 + 30v + 140p - 120a \pm 110K \qquad (3.27)$$

$$T_3 = 830 - 60v + 90p - 70a \pm 110K \qquad (3.28)$$

$$T_4 = 830 + 100v + 100p - 30a \pm 180K \qquad (3.29)$$

$$T_5 = 780 + 150v + 150p + 20a \pm 170K \qquad (3.30)$$

$$T_6 = 580 + 100v + 100p + 40a \pm 120K \qquad (3.31)$$

$$T_7 = 370 + 30v + 30p + 20a \pm 30K \qquad (3.32)$$

Thermocouples T_{21}, T_3 and T_4 were permanently enshrouded in flame and received radiation from all directions. Thermocouples T_5, T_6 and T_7 were just outside the flame and they absorbed radiation from one direction only. A model of

a thermocouple in an air-stream at temperature T_a, receiving radiation from the flame at temperature T_f and emitting over the rest of its area to a background temperature T_0 was used to estimate the error between the recorded temperature of the thermocouple and the air temperature, T_a. With inputs T_f = 1000 K; T_a = 600 K; T_0 = 300 K and thermocouple bead diameter 0.75 mm, the model suggested that the thermocouple would over-estimate the temperature by as little as 5 K, an error that is well within the scatter due to averaging over time, and can be neglected.

Finally the current data can be compared to results of other investigators. Most wood cribs are investigated from the point of view of fire safety, so tend to be very large as they are expected to simulate a conflagration of a whole room. Nonetheless, Croce & Xin (2005) investigated combustion of smaller kiln-dried wood cribs in an enclosure (typical crib volume 0.005 m^3, compared to 0.003 m^3 in the current study). In Figure 3.8 Croce & Xin's data is plotted for the crib configurations A' to J' (as defined in Table 3.), along with correlation (3.25) for the current data. Croce & Xin's experimental data is on average 60% higher than correlation (3.26), though the same trends are evident in both results. Croce & Xin used kiln dried wood, rather than 10% moisture. The numerical model described above was used to predict the combustion rate for kiln dried wood, and burn-rates typically increased by 20%. While this does not completely close the gap between the current results and those of Croce and Xin, it is enough to demonstrate that the current burn-rate results are in good agreement with other published data.

Table 3.4. Crib configurations from Croce & Xin (2005).

Crib	V *[m^3]*	f_v *[-]*	S *[m^2/m^3]*
A'	0.0070	0.67	73
B'	0.0035	0.58	87
C'	0.0070	0.75	58
D'	0.0069	0.73	75
E'	0.0035	0.42	110
F'	0.0035	0.67	73
G'	0.0035	0.33	119
H'	0.0035	0.25	126
I'	0.0070	0.50	100
J'	0.0070	0.33	119

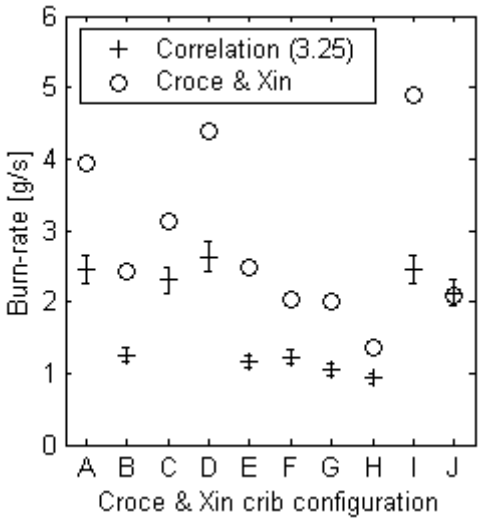

Figure 3.8. Comparison of current data and Croce & Xin (2005), for cribs A′ to J′ defined by Croce & Xin.

3.4 NUMERICAL SIMULATION RESULTS & DISCUSSION

Char combustion simulations were run for each crib configuration with the pyrolysis model disabled, using parameter values listed in Table 3.. The value of mass transfer coefficient, h_m, was initially estimated using equation (3.13), and fine-tuned to give the best match of mass-loss rate with experimental correlation (3.24). Results are shown in Figure 3.9. The sensitivity data in column 6 of Table 3. are discussed later in this section.

Table 3.5. Parameters used in numerical simulation.

Parameter		*Value*	*Units*	*Source*	*Sensitivity*
Lumpiness limit	Ψ_L	3.0	[-]		--
Pyrolysis temperature	T_p	550	K	Demirbas, 2004	-0.57
Enthalpy of char combust.	H_c	30	MJ/kg	Table 3.1	0.57
Mass transfer constant	k_m	0.2	√m/s		0.07
Char thermal conductivity	k_c	0.05	W/mK	Larfeldt et al., 2000	0.35
Char effective thickness	$R^{\sim}$	0.0005	m		-0.35
Enthalpy of pyrolysis	H_v	2.5	MJ/kg	Daugaard et al., 2003	-1.17

With the pyrolysis model enabled, simulations of all crib configurations were carried out with the parameter values listed in Table 3.5. The value of effective char thickness, $R^{\sim} = R\ln(R/r)$, was estimated for a typical configuration and fine-tuned to give the best match of mass-loss rate with experimental correlation (3.25). Results are shown in Figure 3.10, and the resulting flame temperature

distributions plotted with experimental correlations (3.26) to (3.31) in Figure 3.11. Errors in fuel burn rate have a 16% mean and 43% maximum, and are most likely to be caused by neglecting blow-off (i.e. the assumption that char combustion and devolatalisation do occur simultaneously). Errors in excess flame temperature have a 29% mean and 79% maximum and are centred on T_3 and T_4 (in the core of the flame) where there is most variability in flame temperature and most soot (generally formed in the fuel-rich region of the flame). Since soot formation and combustion was not included in this model, it should be of little surprise that the greatest errors occur here.

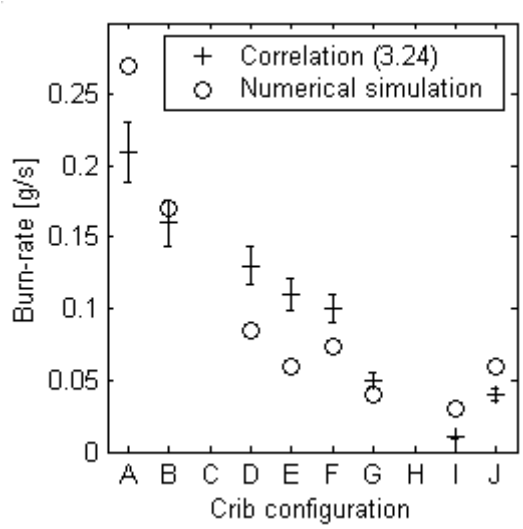

Figure 3.9. Char mass-loss data from experiment and numerical simulation.

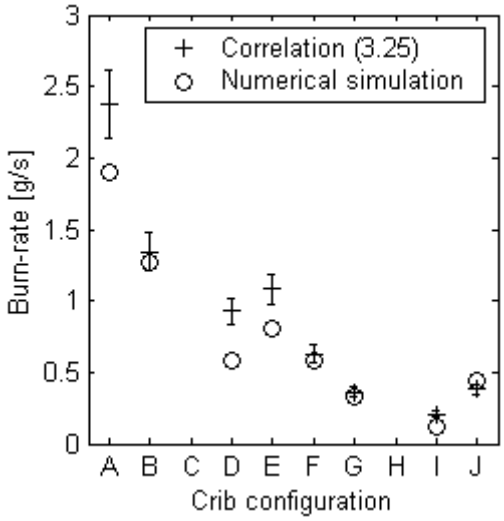

Figure 3.10. Pyrolysis mass-loss data from experiment and numerical simulation.

A sensitivity study was conducted on the model, and reported in the final column of Table 3.. The sensitivity, Σ, describes the impact a small change in the value of parameter Φ has on the rate of mass-loss, m', for small excursions from the operating point m'_0. Mathematically:

$$\Sigma = \frac{\Delta m' / m'_0}{\Delta \Phi / \Phi_0} \tag{3.33}$$

It can be seen that the model is very robust to errors in mass transfer constant, k_m, and fairly robust to errors in the effective char thickness, $R^{\sim}$. The model is very sensitive to changes in enthalpy of pyrolysis, H_v, however this does not pose a serious threat to accuracy as we are very confident of the current value.

3.5 CONLUDING REMARKS

A simplified model of wood combustion has been developed, and implemented as a user-defined function in Fluent 6.2. The model assumes that active fuel surfaces are grouped together in a regular fashion (described by a lumpiness function) in the fixed fuel bed. Fuel within the lumps behaves according to the unreacted core model, such that the pyrolysis reaction rate is limited by the supply of heat through the char layer, and the char reaction rate is limited by the supply of oxygen through the species boundary layer. The model results in 16% mean error compared to experimental results for fuel burn rate, and 29% mean error for excess temperature above the fuel bed. The source of these errors is thought to lie in the omission of blow-off and soot radiation. The model fulfils the requirements to be volume specific, robust and computationally cheap, and is accurate enough for the optimisation application in hand, especially given the highly variable nature of wood as a fuel, and the relatively large tolerances expected on stove dimensions during manufacture.

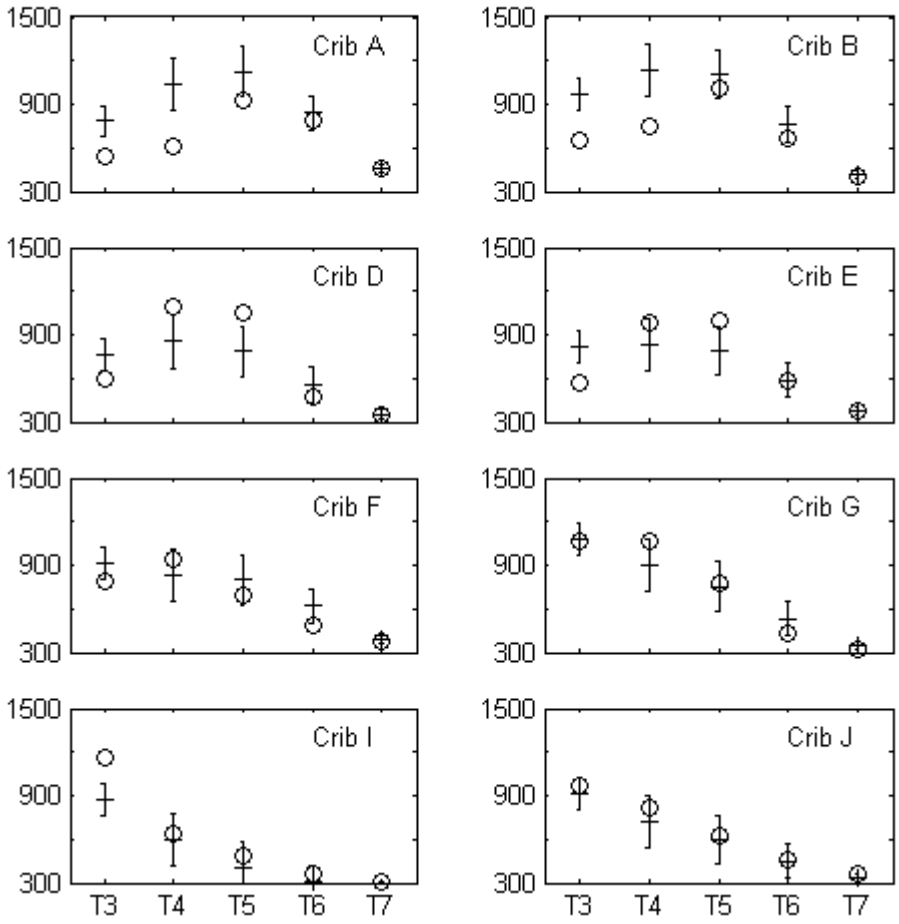

Figure 3.11. Flame temperatures from experimental correlations (22) to (26) and numerical simulation.

CHAPTER 4: CONVECTION HEAT TRANSFER

In the previous chapter a computationally inexpensive model of wood combustion was developed, and it was demonstrated that it could predict the fuel burn rate and flame temperature with 16% and 29% error respectively. In Appendix B it has been demonstrated that the k-ε turbulence model can predict the velocity profile in a turbulent buoyant plume. The aim of chapter 4 is to examine impinging jet heat transfer with the following objectives: first to experimentally evaluate the level of convection heat transfer for configurations in the rocket stove; second, to evaluate the nature and magnitude of error that the k-ε turbulence model incurs when simulating convection heat transfer. Accordingly, work in this chapter is divided into two sections. The first is an experimental investigation with a rocket stove adapted to blow cold air onto a hot plate, in order to generate a correlation for Nusselt number with stove geometry (Burnham-Slipper et al., 2007b). The second section describes a set of CFD simulations of jet impingement heat transfer. The model correctly predicts the trend of heat transfer with changing geometry and flow conditions. While significant errors are incurred under certain conditions, these conditions are unlikely to be met in rocket stoves, and the worst shortcomings of the k-ε model are avoided. Errors in the convection heat transfer model are further mitigated by the fact that they counteract errors in the radiation heat transfer model.

4.1 EXPERIMENTAL STUDY OF CONVECTION HEAT TRANSFER

The experimental investigation was carried out by blowing cold air through a nozzle onto a hot plate, and recording the temperature of the plate. The rate of heat loss due to convection was calculated from the temperature history of the plate. The nozzles were modified rocket stoves used for experiments described in Chapter 5.

The experimental apparatus consisted of two major parts: the nozzle assembly and the plate assembly (Figure 4.1). The nozzle assembly was supplied with ambient air from a compressor which fed into the bottom of the nozzle through a sudden expansion and a porous mat to diffuse the flow. Two nozzle diameters were used: 102 mm and 152 mm diameter. Both were 250 mm long and blew air directly upwards. Air velocity was monitored by a 35 mm EDRA-6 vane anemometer in the supply to the nozzle, and by another 35 mm EDRA-6 vane anemometer used to assess the uniformity of the air flow leaving the nozzle. Air velocity at the nozzle exit was varied in the range 0.5 to 1.5 m/s, with a maximum deviation from the mean velocity of 20%. The maximum uncertainty in values of Reynolds number was therefore 20%.

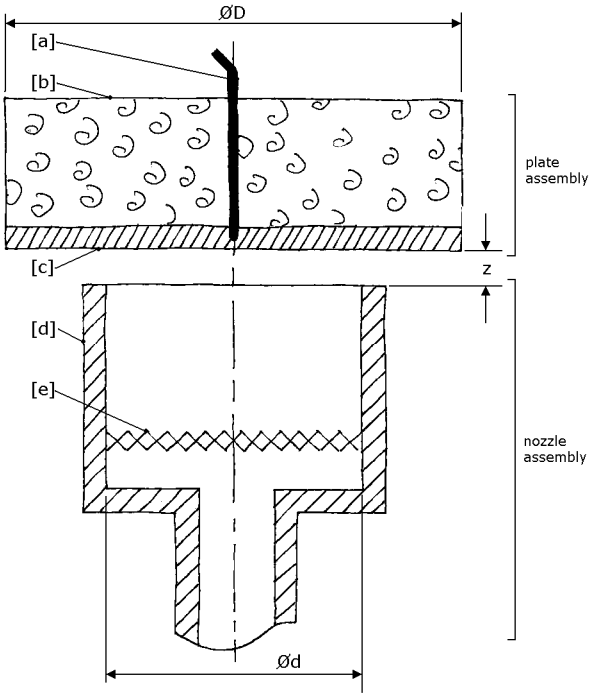

Figure 4.1. Heat transfer apparatus, showing [a] thermocouple, [b] insulation, [c] target plate, [d] nozzle and [e] porous mat.

The target plate was supported above the nozzle by an adjustable tripod. Two 16 mm aluminium plates were used, with 240 mm and 300 mm diameter. The back of the plate was insulated with 70 mm of mineral wool. The plate was initially equipped with four k-type thermocouples over the radius of the plate, but the Biot number of the plate (calculated from plate diameter, *D*) was much less than 0.1 and initial experiments demonstrated that a single thermocouple embedded 8 mm deep at the geometric centre was sufficient to monitor the temperature of the whole plate.

For each experimental configuration (Table 4.1), the plate was heated for 15 minutes in boiling water, then allowed to dry, insulated and instrumented. The

plate was then supported above the nozzle and allowed to cool under the action of ambient air impinging on its lower surface for a minimum of 420 s. Plate and ambient temperature were logged at 0.1 Hz.

Table 4.1. Experimental configurations.

Configuration	d [m]	D [m]	z [m]	v [m/s]
A	0.1	0.3	0.006	0.5
B	0.1	0.3	0.022	0.5
C	0.1	0.3	0.014	1
D	0.1	0.3	0.006	1.5
E	0.1	0.3	0.022	1.5
F	0.1	0.24	0.006	0.5
G	0.1	0.24	0.022	0.5
H	0.1	0.24	0.014	1
I	0.1	0.24	0.022	1.5
J	0.15	0.3	0.006	0.5
K	0.15	0.3	0.022	0.5
L	0.15	0.3	0.014	1
M	0.15	0.3	0.006	1.5
N	0.15	0.3	0.022	1.5
O	0.15	0.24	0.006	0.5
P	0.15	0.24	0.022	0.5
Q	0.15	0.24	0.014	1
R	0.15	0.24	0.022	1.5

4.2 NUMERICAL MODEL OF CONVECTION HEAT TRANSFER

A numerical model of the jet impinging on the plate was created using Fluent 6.2 with the following simplifying assumptions:

- the system had achieved steady-state flow conditions;
- the computational domain was axi-symmetric along the centre-line of the nozzle;
- the effects of buoyancy and radiation were neglected;
- density was that of an incompressible ideal gas;
- viscosity, specific heat and thermal conductivity were independent of temperature.

Conservation of mass, momentum and energy are given by equations 4.1, 4.2 and 4.3 respectively:

$$\frac{\partial}{\partial x_j}(\rho u_i) = 0 \tag{4.1}$$

$$\frac{\partial}{\partial x_i}(\rho u_i u_i) = \frac{\partial}{\partial x_j}\left[(\mu_m + \mu_t)\frac{\partial u_i}{\partial x_j}\right] \tag{4.2}$$

$$\frac{\partial}{\partial x_i}(\rho E u_i) = \frac{\partial}{\partial x_j}\left[(k_m + k_t)\frac{\partial E}{\partial x_j}\right] \tag{4.3}$$

Turbulence was modelled with the standard k-ε model (Launder & Spalding, 1974) using enhanced wall treatment. The transport equations for turbulent kinetic energy and its dissipation were given by:

$$\frac{\partial}{\partial x_i}(\rho k u_i) = \frac{\partial}{\partial x_j}\left[\left(\mu_m + \frac{\mu_t}{\sigma_k}\right)\frac{\partial k}{\partial x_j}\right] + G_k - \rho\varepsilon \tag{4.4}$$

$$\frac{\partial}{\partial x_i}(\rho \varepsilon u_i) = \frac{\partial}{\partial x_j}\left[\left(\mu_m + \frac{\mu_t}{\sigma_k}\right)\frac{\partial \varepsilon}{\partial x_j}\right] + C_{1\varepsilon}\frac{\varepsilon}{k}G_k - C_{2\varepsilon}\rho\frac{\varepsilon^2}{k} \tag{4.5}$$

Partial differential equations (4.1) to (4.5) were discretised using the Second-Order-Upwind scheme. Pressure was discretised according to the standard scheme. The SIMPLE scheme was used for pressure-velocity coupling. The resulting set of simultaneous ordinary differential equations was solved using Fluent 6.2.

Two sets of geometry were modelled: the first replicated the experimental set-up of Lytle & Webb (1991); the second replicated the current experimental set-up.

In the first set of simulations (replicating Lytle & Webb), the domain included a nozzle of diameter d and length $10d$, and a plate with diameter $5d$, a distance z from the nozzle (Figure 4.2). Air entered the domain through the inlet at 300 K and 10% turbulence intensity. The plate was subject to a uniform heat flux of 2500 W/m^2, resulting in a temperature difference of approximately 20 K. Cases were investigated with d = 7.8 mm and (z/d) varying in the range 0.1 to 6.0. Inlet velocity was varied to give Reynolds numbers in the range 3600 to 27600. Grid dependence was investigated by running two preliminary cases with tetrahedral meshes: the first had 0.1 mm grid spacing along the plate and end of the nozzle, coarsening to 1.0 mm elsewhere; the second had 0.05 mm grid spacing along the plate and end of the nozzle, coarsening to 0.5 mm elsewhere. The Richardson extrapolation (Feldman, 1999) was used to estimate the exact solution from these results, assuming a first-order error. The 0.1 to 1.0 mm mesh resulted in an estimated 6% error in total heat transfer. This was considered acceptable and the mesh was used for subsequent simulations. A second set of

preliminary cases demonstrated that buoyancy did not have a significant effect on heat transfer.

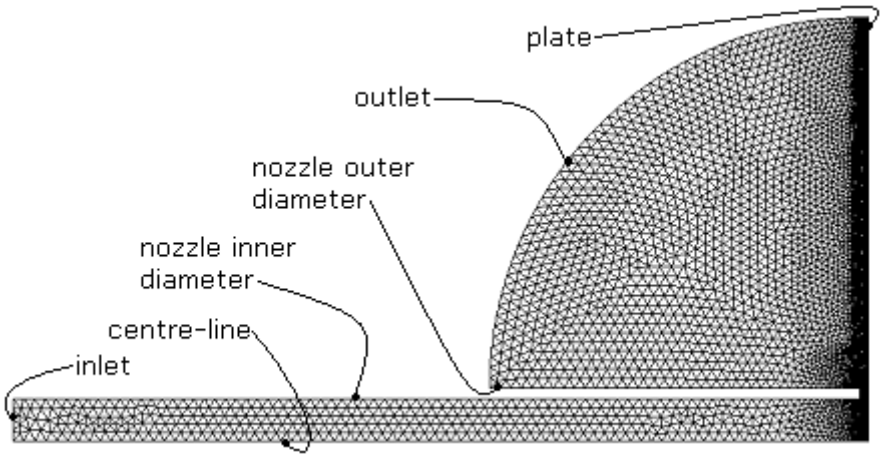

Figure 4.2. Typical computational domain to model the experiments of Lytle & Webb (1991).

In the second set of simulations (modelling the experimental set-up described in section 4.1), the nozzle was given a fixed length of 250 mm. Other dimensions were varied to reflect the experimental set-up. The domain included the edge of the plate and the first 25 mm of insulation next to the plate, though this was approximated as a smooth surface (Figure 4.3). The inlet boundary condition was developed by estimating an initial boundary condition of 10% turbulence, and recording the velocity profile just before the outlet of the nozzle. This profile was then patched onto the inlet in order to achieve a fully developed flow at the nozzle outlet. The plate was assumed to have a uniform surface temperature of 373K. Again, grid dependence was investigated using the Richardson extrapolation, and a mesh of 0.4 mm at the plate surface expanding to 4 mm elsewhere resulted in an estimated 9% error in total heat transfer: this was considered acceptable and the mesh was used for all subsequent simulations. A preliminary set of simulations were carried out with the gravity vector enabled and density calculated as for an incompressible ideal gas: the inclusion of buoyancy forces did not significantly affect heat transfer.

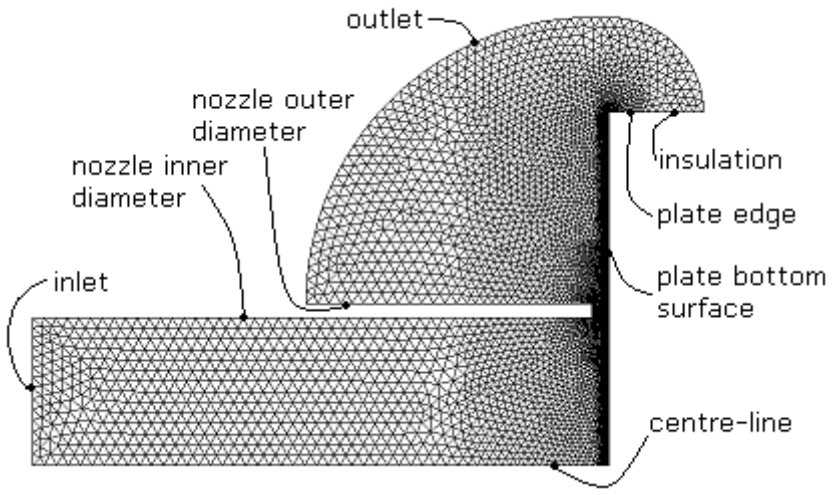

Figure 4.3. Typical computational domain to model the experimental set-up described in section 4.1.

For both sets of simulation, local Nusselt number at radius r, Nu_r, was calculated from the surface temperature and heat flux of the plate:

$$Nu_r = \frac{qd}{k(T_r - T_j)} \tag{4.6}$$

where q is the heat flux. Subscripts r and j refer to radial position and jet conditions. The Nusselt number averaged over the whole surface up to radius R was given by (Lytle & Webb, 1991):

$$Nu = \frac{1}{\pi R^2}\int_0^R 2\pi r Nu_r dr \tag{4.7}$$

4.3 EXPERIMENTAL RESULTS & DISCUSSION

Heat transfer rate was derived from the temperature history of the plate, and expressed in terms of area-averaged Nusselt number, corrected for radiation, buoyancy and edge effects as described below. The plate was modelled as a lumped-capacitance thermal inertia subject to convective heat transfer with a uniform heat transfer coefficient and radiation heat transfer with emissivity equal to 1 (since the plates were coated with a layer of wood soot):

$$\frac{dT}{dt} = \frac{1}{mc}\left[h + \sigma\varepsilon\left(T^2 + T_a{}^2\right)\left(T + T_a\right)\right]S\left(T - T_a\right) \tag{4.8}$$

where T is temperature, t is time, m is mass and c is specific heat capacity. The Stefan-Boltzmann constant is shown as σ, ε is emissivity and S is surface area. Subscript a is for ambient. Equation (4.8) was discretised using Euler's method.

The total area-average heat transfer coefficient was found by fitting the model to experimental data with a linear least-squares regression, using initial and ambient temperatures from the experimental data. It is clear from Figure 4.4 that the lumped-capacitance model is sufficiently accurate to replicate the experimental results. Although the radiation compensation was included in the model, it did not significantly change the value of heat transfer coefficient generated by the least-squares regression: toggling the value of emissivity between 0.0 and 1.0 typically changed the heat transfer coefficient by less than 1%.

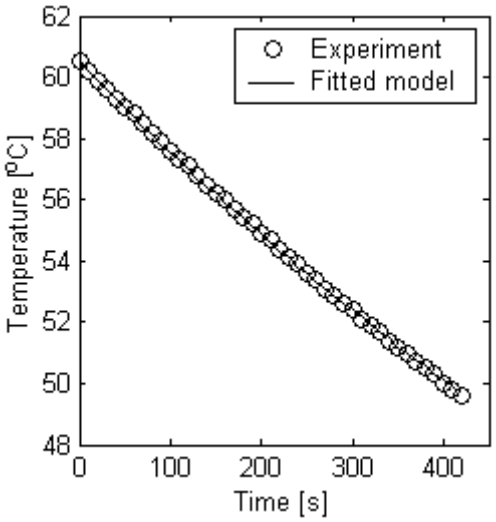

Figure 4.4. Typical experimental temperature data and fitted model to determine heat transfer coefficient (configuration: d=0.1m; z/d=0.24; D=0.3m; v=1.5m/s).

Where possible, data with the lowest temperature difference between plate and ambient air was used, to reduce the effect of buoyancy on the result. Total area-averaged Nusselt number was calculated from:

$$\overline{Nu}_{\exp} = \frac{\overline{h}d}{k} \tag{4.9}$$

where *k* is thermal conductivity of air. Uncertainty in the values of area-average Nusselt number was estimated to be 0.5%. The value of area-averaged Nusselt number as defined by (4.9) was further corrected to account for buoyancy and edge effects.

Configurations with the lowest velocity and the smallest plate diameter were close to the transition from forced to natural convection ($Gr/\mathrm{Re}^2 = O(10^{-1})$; Bejan, 2004). The Nusselt number corrected for forced convection alone was therefore calculated as:

$$\overline{Nu}_{fc} = \overline{Nu}_{\exp} - 0.27 Ra_{D/4}^{0.25} \tag{4.10}$$

where $Ra_{D/4}$ is the Rayleigh number calculated from the characteristic length $D/4$ (Bejan, 2004). To eliminate the effect of heat transfer from the edge of the plate the forced convection Nusselt number was further corrected:

$$\overline{Nu}_p = \frac{1}{A_p}\left[\overline{Nu}_{fc}\left(A_p + A_e\right) - \overline{Nu}_e A_e\right] \tag{4.11}$$

where A_p and A_e are the areas of the flat plate and edge respectively. Nusselt number for the edge of the plate was assumed to be equal to the stagnation point Nusselt number, correlated from data published by Lytle & Webb (1991):

$$Nu_0 = 0.0085\,\mathrm{Re}_d \tag{4.12}$$

This assumption was derived from the observation that buoyancy forces were relatively small for most experimental configurations, and the air generally left the bottom of the plate with a very strong radial component to its velocity. Any air that was passing over the edge of the plate was therefore part of a secondary flow that was being entrained into the primary radial flow. Velocity in this region would have been small, and heat transfer comparable with the only other low-velocity region on the plate (i.e. the stagnation point).

A non-linear least-squares regression was used to correlate plate area-average Nusselt number to Reynolds number of the nozzle flow and the non-dimensionalised nozzle-to-plate distance (z/d) and the non-dimensionalised plate radius (R/d). For Reynolds number in the range 3400 to 16000, nozzle-to-plate spacing 0.04 to 0.22 and plate radii (R/d) 0.80 to 1.50, the area-averaged Nusselt number can be correlated by:

$$Nu_d = 2.60\,\mathrm{Re}_d^{\,0.40}(z/d)^{-0.22}(R/d)^{-0.10} \tag{4.13}$$

with a mean error of 6% and maximum error or 14%. Errors in this correlation were dominated by non-uniform flow from the nozzle and uncertainty in the value of Reynolds number. The non-uniform flow would result in non-uniform cooling of the plate, but should not significantly alter the mean rate of heat transfer because of the low Biot number. The low air velocities used in these experiments mean that the air flow around the plate was susceptible to external disturbances such as air currents and drafts.

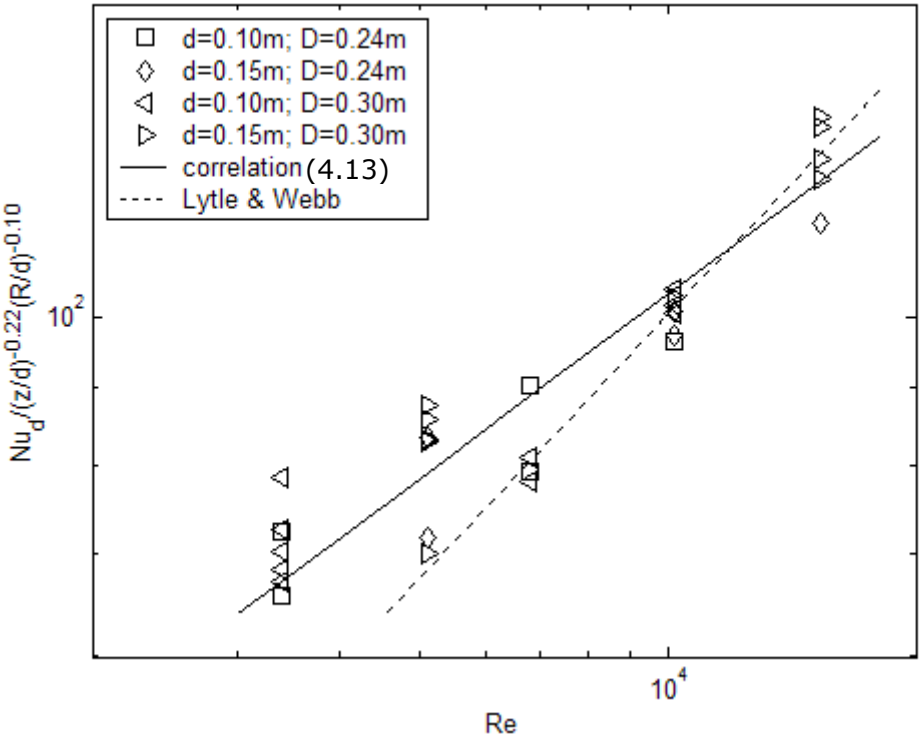

Figure 4.5. Experimental data for all configurations, with correlation and Lytle & Webb's experimental correlation.

The experimental correlation can be compared to that of Lytle and Webb (1991), who also examined heat transfer for low nozzle-to-plate distances. Though the ranges of Reynolds number and nozzle-to-plate spacing in both investigations are comparable, Lytle and Webb used much smaller diameter nozzles with higher velocities resulting in less experimental variability. They reported area-averaged Nusselt number for (R/d) < 1.0 as:

$$Nu_{Webb} = 0.424\,\mathrm{Re}^{0.57}(z/d)^{-0.33} \qquad (4.14)$$

The two correlations result in comparable values of Nusselt number (Figure 4.5), though Lytle and Webb's correlation shows a stronger dependence on both Reynolds number and nozzle-to-plate distance. The differences between the two correlations may be due to the lower range of nozzle-to-plate distances used in the current study, or to the low velocity configuration, or to another undefined short-coming in the current experimental set-up. The first hypothesis appears unlikely as the data of both Lytle & Webb and Hrycak (1983) suggest that the rate of change of Nusselt number with respect to nozzle-to-plate distance increases at lower nozzle-to-plate distances (though this is not born out by their experimental correlations). It must be concluded that the lower Reynolds exponent and nozzle-to-plate exponent in the current study are due to some

difference in experimental set-up, though further investigation is required to determine whether it is due to the low velocity configuration.

Returning to the original objective of this experimental investigation, the level of convective heat transfer from the rocket stove to a cooking pot has been investigated, and found to be in broad agreement with published data. The experimental technique used in this study has been crude by comparison to other investigators (e.g. Lytle & Webb or Hrycak), but is sufficiently accurate to give an account of convection heat transfer, given the variable nature of small wood fires and the organic and therefore changeable nature of the fuel.

4.4 NUMERICAL RESULTS & DISCUSSION

Results for the first set of simulations are presented and compared to Lytle and Webb's experimental data, to examine how the model resolved radial variations of heat transfer, then results of the second set of simulations are presented, to examine the mean heat transfer for the current experimental geometry.

Figure 4.6 shows Lytle and Webb's experimental results and data from numerical simulations for a range of nozzle-to-plate distances. For large nozzle-to-plate distances the numerical model gives a satisfactory interpretation of the experimental data, but a significant discrepancy develops as the nozzle-to-plate distance decreases. The experimental data is dominated by the heat transfer maximum in the region 1.0 < (r/d) < 2.0: a region of very high anisotropic shear suppresses turbulent oscillations as the flow passes under the nozzle. The flow is effectively re-laminarised and the heat transfer maximum at 1.0 < (r/d) < 2.0 is evidence of the subsequent re-establishment of turbulence. Meanwhile, data from the numerical simulation predicts the dominant heat transfer maximum at (r/d) = 0.50, right in the vena contraca of flow through the nozzle: the k-ε turbulence model does not account for anisotropic turbulence, nor can it account for re-laminarisation (Versteeg and Malalalsekera, 2007). According to the k-ε model, turbulence formation is directly proportional to velocity gradient or shear (Fluent, 2007):

$$G_k = \rho u'_i u'_j \frac{\partial u_j}{\partial x_i} = \mu_t S^2 \qquad (4.15)$$

where S is the modulus of the mean rate of strain tensor. As a result, the numerical simulation predicts a region of high turbulence intensity in the vena contracta (Figure 4.7), with a correspondingly high rate of heat transfer. At larger radii the model and experimental data tend to agree.

With reference to Figure 4.8, the model predicts the same trend and general level of area-averaged heat transfer as Lytle & Webb's experimental data. Taking the area-average of just the central region of the plate (r/d = 1.0), the model over-predicts heat transfer rate by an average 22%, with maximum error 42% occurring for 0.25 < (z/d) < 0.50. For the whole plate (r/d = 4.0), the average error falls to 11%, due to the better agreement away from the nozzle/relaminarisation region.

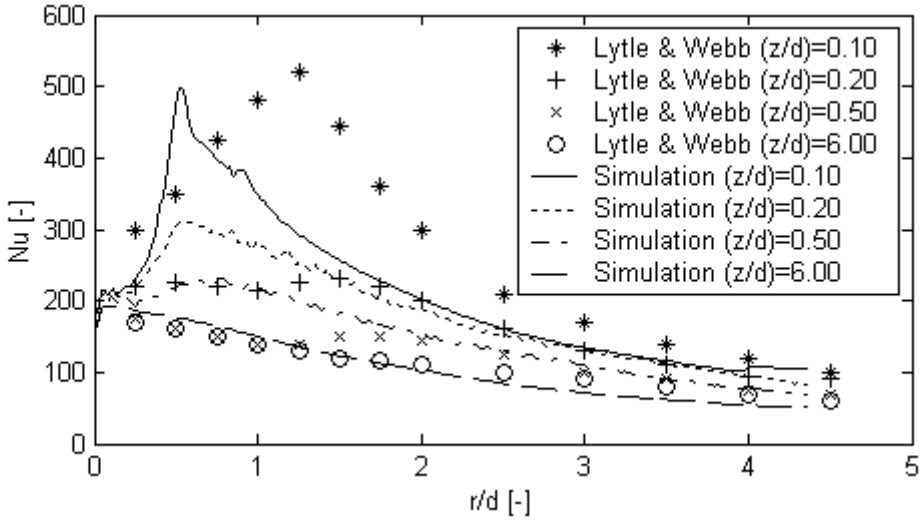

Figure 4.6. Radial variation of local Nusselt number for a range of nozzle-to-plate distances. Re=23000.

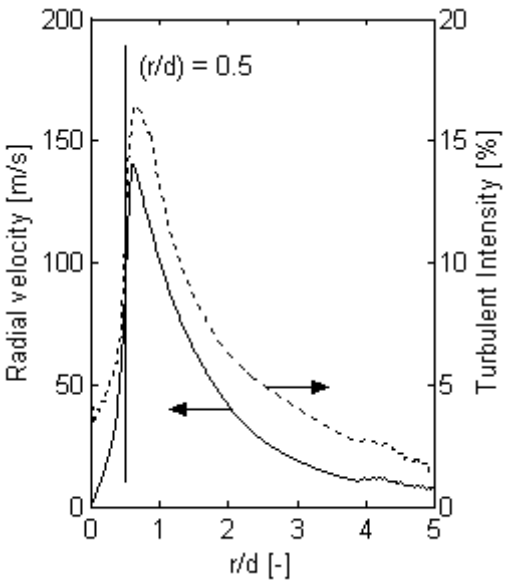

Figure 4.7. Simulated radial variation of radial velocity and turbulence intensity.

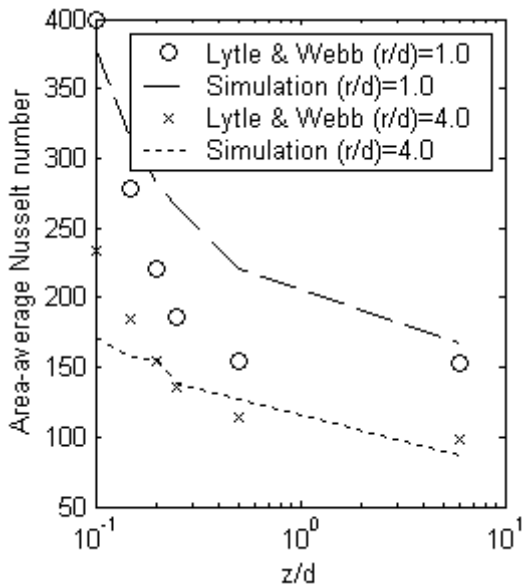

Figure 4.8. Area-averaged Nusselt number for experiment (Lytle & Webb) and numerical simulation as a function of (z/d).

Some of the cases shown in figure 4.6 were repeated with the Reynolds Stress Model (RSM) for turbulence. The RSM is a five-equation turbulence model that is able to account for anisotropic turbulence because it resolves the each element of the strain rate tensor, while the k-ε model only takes a mean value and assumes it is uniform in all directions. It was expected that the RSM would be able to model the secondary maximum of heat transfer at (r/d) = 1.25, but as Figure 4.9 shows, it has not. The heat transfer maximum remains at (r/d)=0.5, despite the clearly anisotropic turbulence field (Figure 4.10): neither turbulence model is able to model re-laminarisation, as they assume that the whole flow field in the domain is turbulent.

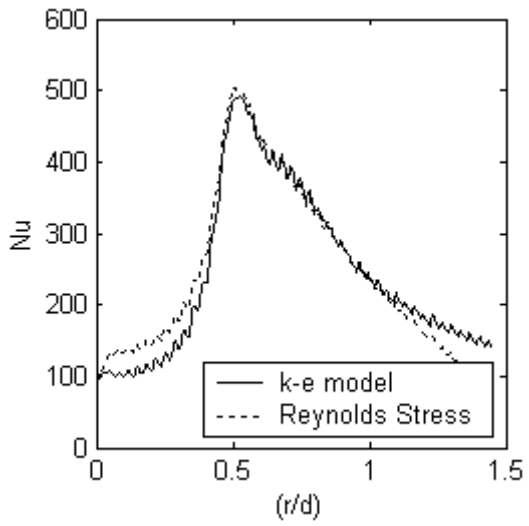

Figure 4.9. Radial variation of Nusselt number for k-ε and RSM turbulence models (Config. D).

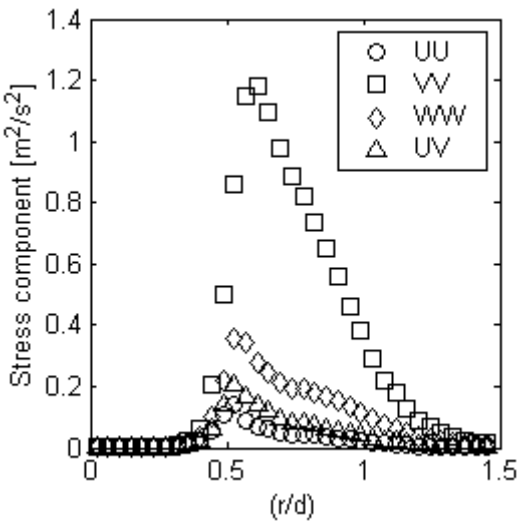

Figure 4.10. Radial variation of stress components under plate in RSM model (Config. D).

Figure 4.11 shows how heat transfer varies with Reynolds number in experiment and simulation. As the Reynolds number increases a maximum develops around (r/d) = 1.5 in the experimental data and at (r/d) = 0.5 in the simulation data. The cause is discussed above. Figure 4.12 shows that despite the different location and magnitude of the maximum, the area-averaged heat transfer is well replicated in the model (average 11% error for r/d = 4.0), though errors are more significant nearer the nozzle, posing a problem when using the model as a design tool. The numerical model correctly identifies the trends, though not the absolute value. One final point of interest: the small local maximum of heat transfer evident at (r/d) = 4.0 of the simulation data is associated with a change in grid structure at that point.

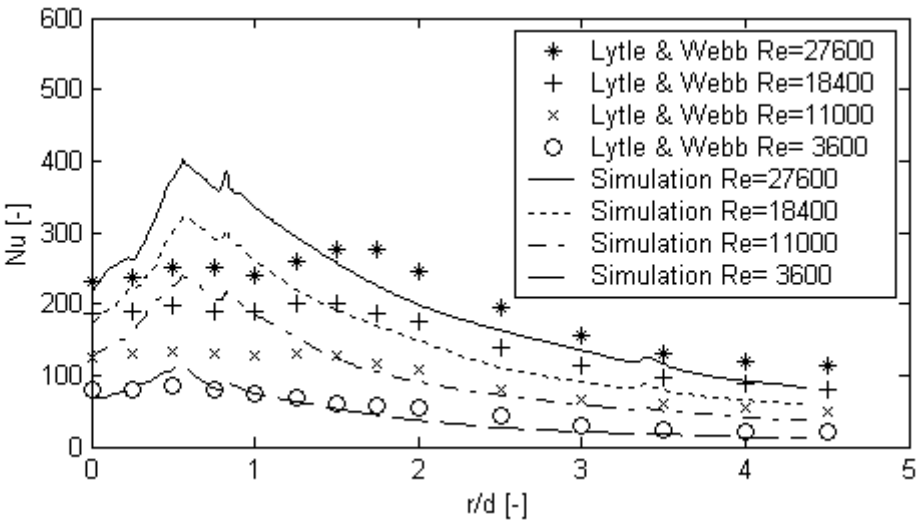

Figure 4.11. Radial variation of local Nusselt number for a range of Reynolds number. (z/d) = 0.2.

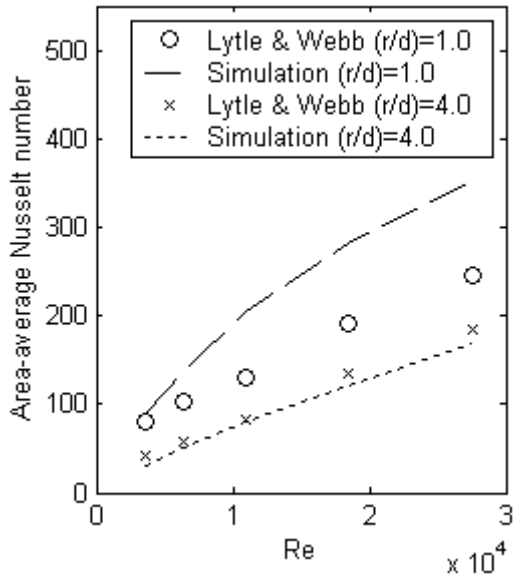

Figure 4.12. Area-averaged Nusselt number for experiment (Lytle & Webb) and numerical simulation as a function of Reynolds number (z/d = 0.2).

Let us now turn our attention to numerical simulations of the current experimental configuration. Area-averaged Nusselt number from numerical simulation results can be correlated to Reynolds number and non-dimensionalised nozzle-to-plate spacing (as for experimental data), resulting in relationship (4.16) for the whole plate including the edge, and relationship (4.17) for the bottom surface of the plate, without the edge.

$$Nu_{k-e,all} = 0.014\,\mathrm{Re}^{0.87}(z/d)^{-0.66} \tag{4.16}$$

$$Nu_{k-e,btm} = 0.021\,\mathrm{Re}^{0.84}(z/d)^{-0.66} \tag{4.17}$$

The Re-exponents of correlations (4.16) and (4.17) are approximately equal, while the quotient of (4.17) is 50% greater than (4.16). Thus it can be shown that:

$$\frac{h_s}{h_b} \approx \frac{2}{3}\left(1 - \frac{A_b}{2A_s}\right) \tag{4.18}$$

where subscripts s and b refer to the side and bottom of the plate. Evaluating (4.18) demonstrates that h_s/h_b = -0.58 for the smaller target plate (i.e. heat passes from the air to the side of the plate), which is a counter-intuitive result that requires further investigation. It is of little importance to the current investigation, since the side of a mogogo plate is embedded in the structure of the stove, so is not a heat transfer surface.

Compare (4.16) to the current experimental correlation (4.13): for (r/d) = 1.0 the simulation yields a mean error of 32% and a maximum error of 136% (Figure 4.13): for low-Re, low-(z/d) and for high-Re, high-(z/d) configurations the error is low (typically 7%), while significant errors are focussed in the high-Re, low-(z/d) configurations. It is these configurations that exhibit highest shear stresses in the fluid passing through the stove-to-plate clearance, and so are most susceptible to the previously discussed shortcomings of the k-ε model.

Compare (4.17) to similar results in literature: the Re-exponent is high, though within the reported range; the (z/d)-exponent is also high. Comparing (4.17) to the result obtained by Lytle and Webb (4.14), the k-ε model gives a mean and maximum error of 25% and 96%, with the errors focused on high-Re, low-(z/d) configurations, as above.

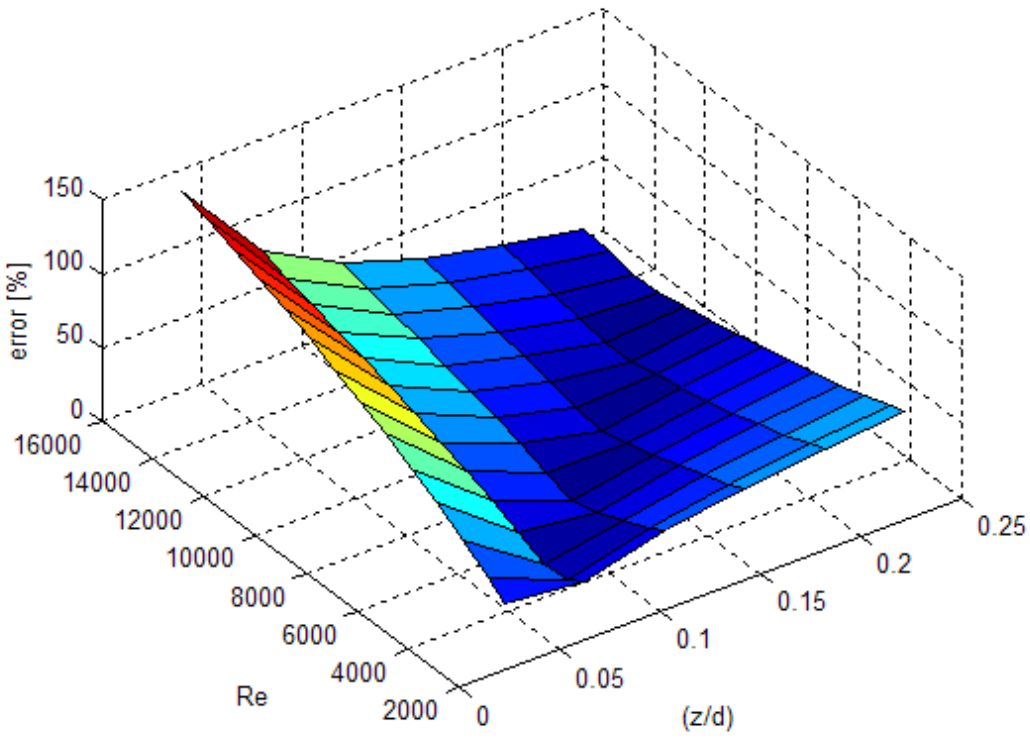

Figure 4.13. Error in area-average Nusselt number from k-ε model for the bottom of the plate, as a function of Re and (z/d).

4.5 CONCLUDING REMARKS

The aim of this chapter was to examine convection heat transfer in configurations relevant to the rocket stove, using both experimental and numerical techniques. The experimental investigation was crude, the most significant errors being in the value of Reynolds number. Nonetheless, convection heat transfer was in reasonable agreement with literature. It is unclear if the differences were due to the use of a low-velocity, large-diameter nozzle (i.e. the rocket stove configuration) or due to different measurement techniques. An initial evaluation would suggest the latter, though further work would be required to confirm this.

The k-ε model used in the numerical investigation incurred significant errors when resolving the secondary heat transfer maximum reported by Lytle and Webb at (R/d) = 1.5, and associated with the reestablishment of turbulent flow. This is most likely due to the assumption of isotropic, ubiquitous turbulence. For area-averaged heat transfer the k-ε model performed reasonably well: errors were dominated by over-predicting heat transfer in high-Re, low-(z/d) configurations.

A genetic algorithm that is set to maximise heat transfer in a stove will tend to select high-Re, low-(z/d) configurations, as they have the highest heat transfer; it

will consequently incur the highest errors if it uses the k-ε model to evaluate fitness. While this is a significant concern, a buoyancy-driven flow is unlikely to attain Reynolds number of the order 10^4, so the worst excesses are avoided. Similarly, a very low (z/d) configurations will result in a high pressure drop, reducing the fluid velocity and tending to reduce the heat transfer; consequently these will also be avoided. As a result it is expected that convection heat transfer will only ever be over-predicted by 10-20%. When taken in conjunction with the fact that there is no account for soot in the radiation model, and that radiation heat transfer will therefore be significantly under-predicted, the errors in the convection heat transfer model should cause minimal concern.

CHAPTER 5: STOVE PERFORMANCE

In previous chapters, sub-models of the stove have been presented and analysed: the combustion model in chapter 3; velocity and temperature profile in a buoyant turbulent plume in Appendix B; and convection heat transfer in chapter 4. In this chapter all the above elements are combined to give a model of a complete stove, and simulation results are compared to experimental data for a modified rocket stove. Several weaknesses in the model are identified, however it is concluded that the model is sufficiently accurate to be used to resolve the fitness function of a genetic algorithm for stove optimisation.

5.1 EXPERIMENTAL STUDY OF STOVE PERFORMANCE

The apparatus described here is similar to that used for crib combustion (see Chapter 3) and consists of five principal parts: a stove, fuel, a target plate simulating a cooking pot, an electronic balance with fuel store, and thermocouples.

The stove was based on the Rocket stove (Aprovecho, 2007). It consisted of a length of 4” or 6” steel pipe (102 or 153 mm respectively) with a window to introduce fuel, and adjustable feet and arms to change the stove-to-ground clearance and stove-to-pot clearance. Complimentary lengths of pipe were available to change the effective height of the stove. Dimensions are defined in Figure 5.1 and Table 5.1. The adjustable arms were lengths of threaded bar, ground to a point to reduce the contact area with the target plate, attached to a collar that sat atop the stove. The adjustable feet were interchangeable sets of shims, manufactured from angle-iron to maintain stability but not choke the flow of air into the stove. The complimentary lengths of pipe were equipped with a skirt that fitted tightly round the stove to inhibit the influx of fresh (secondary) air for combustion.

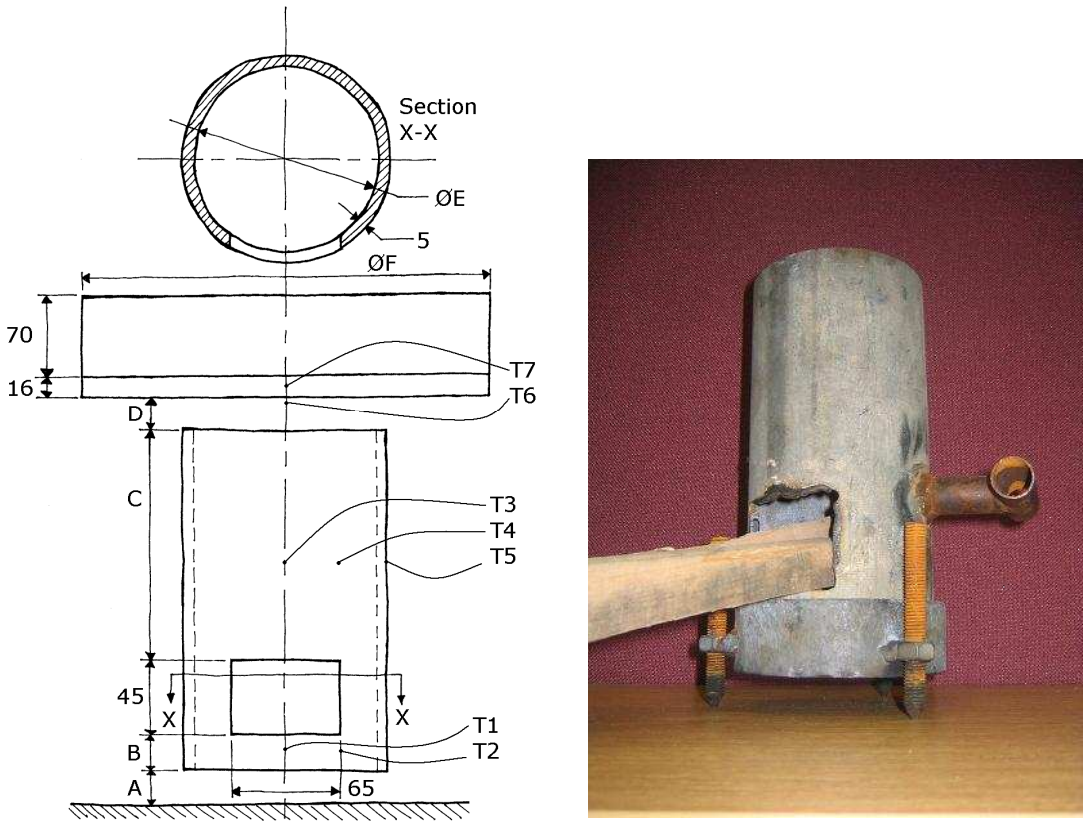

Figure 5.1. (a) Principal rocket stove dimensions. Variable dimensions A to F defined in Table 5.1. (b) Rocket stove with adjustable feet and fuel in window.

Table 5.1. Variable stove dimensions.

Dimension	Value [mm]
A	6 or 24
B	40 or 72
C	150 or 250
D	6 or 24
E	100 or 150
F	240 or 300

The fuel was sticks of knot-free, air-dried pine. All sticks had square 20 x 20 mm section, and 300–400 mm in length. Proximate analysis (except ash content) was executed to BS 1016 as reported in Table 3.2. The fuel window was just large enough to admit two layers of fuel sticks, each containing three pieces. The two layers were skewed in opposite directions to (a) block the window as much as possible and (b) present as large a surface area to the air flow as possible.

The targets were 16 mm thick aluminium plates, diameter 240 mm or 300 mm, insulated with 70 mm of rock wool on the back, and equipped with a single

thermocouple embedded 8 mm into the centre of the plate. It has already been demonstrated (section 4.1) that the plate's Biot number was sufficiently low to assume isothermal conditions.

The stove and target plate assembly was positioned on an insulated platform on a Mettler-Toledo 32000 electronic balance. Extra fuel was stored in a magazine in the platform, so that the balance registered the mass of the whole stove, target plate and all the unburned fuel. The balance was accurate to ± 0.1 g, and logged at 0.1 Hz. Typically six data points were used to calculate the burn rate of fuel, and the standard error (calculated from equation 3.1) was ± 0.02 g/s.

K-type thermocouples were used to log temperature at locations indicated in Figure 5.1: inlet region between the char and wood (T1 and T2); flame (T3 and T4); the stove wall (T5), the stagnation point (1mm below the centre of the plate, T6) and; the plate (T7). Temperatures were logged at 0.1 Hz with accuracy ±10K. Thermocouples were either entirely immersed in flame or completely shrouded from it, so there were no errors associated with uncorrected radiation.

For each experimental configuration (listed in Table 5.2) the stove was fired up with a 3-4 g charge of fire lighter. Fuel was fed into the stove through the fuel window, so that it touched the far wall. Excess char was knocked off approximately every 5 minutes. Char was allowed to collect at the bottom of the stove, where it preheated the primary air and radiated heat onto the fuel above it, aiding pyrolysis. Once the stove wall temperature achieved a steady state (typically 20–30 minutes), the target was placed on the support and allowed to heat up to 120^{o}C. Only data in the range 100^{o}C to 120^{o}C was used to calculate the heating-rate of the target plate, as this is the approximate temperature range of a cooking pot containing water-based food. Replica test runs were carried out after quenching the target plate in cold water for 60 seconds, then drying it and re-applying the insulation and thermocouple. The fire was not extinguished between tests with different configurations, but a ten minute pause was taken, to allow conditions to restabilise. Test Batch 1 contained all permutations of dimensions A, C and D; Batch 2 contains all permutations of dimensions D, E and F. The results of each batch were used as a 2^3 factorial experiment during analysis.

Table 5.2. Experimental configurations. A letter in the table indicates the dimension took the larger value Table 5.1, otherwise the smaller value was used.

Batch	Experimental configurations							
1	---	A--	-C-	AC-	--D	A-D	-CD	ACD
2	---	D--	-E-	DE-	--F	D-F	-EF	DEF

5.2 ANALYTICAL MODEL OF STOVE PERFORMANCE

An analytical model of the rocket stove was made under the following simplifying assumptions:

- the combustion chamber of the stove was a well mixed reactor with one uniform temperature;
- the combustion of char lying on the floor was neglected;
- the mixture of gases maintained the properties of air, and behaved as an ideal gas;
- air entered the stove through the ground-to-stove clearance (dimension A) and left through the stove-to-plate clearance (dimension D), with no secondary air entering through the fuel window;
- air flow through the stove was driven by buoyancy induced pressure difference, and resisted by pressure drops across the inlet and outlet orifices and inertial resistance of the fuel;
- resistance to flow due to combustion (i.e. hot loss) was neglected;
- viscous resistance to flow was neglected.

The continuity equation relates the superficial velocity through the fuel and stove to velocities in orifices A and D:

$$\rho A_c u_c = \rho_0 A_a C_{da} \sqrt{\frac{2\Delta p_a}{\rho_0}} = \rho A_d C_{dd} \sqrt{\frac{2\Delta p_d}{\rho}} \tag{5.1}$$

were ρ, A, u, p and C_d are density, cross-sectional area, velocity, pressure and discharge coefficient respectively. Subscripts a, c and d refer to inlet, combustion chamber and outlet conditions respectively (defined by dimensions in Figure 5.1). The pressure drop associated with flow through the porous fuel bed is given by the Ergun equation (Ergun, 1952), without the viscous term:

$$\Delta p_c = \frac{1.75\rho L}{D_p} \frac{(1-\varepsilon)}{\varepsilon^3} u_c{}^2 \tag{5.2}$$

Summing pressure losses through the stove:

$$(\rho_0 - \rho) g h = \Delta p_a + \Delta p_c + \Delta p_d \tag{5.3}$$

Combining (5.1) to (5.3) and re-arranging yields:

$$u_c = \sqrt{\frac{2(\rho_0 - \rho) g h}{\rho (k_a + k_c + k_d)}} \tag{5.4}$$

where:

$$k_a = \frac{\rho}{\rho_0} \left(\frac{A_c}{A_a C_{da}} \right)^2 ; \quad k_c = \frac{3.5\rho L}{D_p} \frac{(1-\varepsilon)}{\varepsilon^3} ; \quad k_d = \left(\frac{A_d}{A_a C_{dd}} \right)^2$$

There are five principal heat fluxes in the stove: convection from the flame to the plate, Q_{cp}; radiation from the flame to the plate, Q_{rp}; radiation from the flame to the stove wall, Q_{rw}; radiation from the flame to the floor and, Q_{rf}; radiation from the plate to ambient, Q_{ra}. These five fluxes are given by (5.5) to (5.8). Convection to the stove wall was negligible.

$$Q_{cp} = h_p A_p (T - T_p) \tag{5.5}$$

$$Q_{rp} = Q_{rf} = \sigma \varepsilon_f A_c (T^4 - T_p{}^4) \tag{5.6}$$

$$Q_{rw} = \sigma \varepsilon_f A_w (T^4 - T_w{}^4) \tag{5.7}$$

$$Q_{ra} = \sigma \varepsilon \left(A_f - A_c\right)(T_p{}^4 - T_a{}^4) \tag{5.8}$$

The only unknown that remains is the temperature of the flame, T_f. This can be found in one of two ways: either (a) taken from experimental data or (b) found through an energy balance on the stove:

$$mc_p \frac{dT}{dt} = Q_{char} + Q_{vols} - \left(Q_{adv} + Q_{cp} + Q_{rp} + Q_{rf} + Q_{rw}\right) \tag{5.9}$$

where energy released due to char combustion, Q_{char} is given by:

$$Q_{char} = H_{char} k_{mtc} \sqrt{u_c} A_{fuel} 0.23\rho \tag{5.10}$$

and energy released due to flaming combustion is given by:

$$Q_{vols} = \frac{H_{vols}}{H_{pyro}} \frac{k_{char} A_{fuel}}{x} \left(T - T_{pyro}\right) \tag{5.11}$$

Heat lost from the stove due to advection (i.e. the current of cold air entering the bottom of the stove, replacing hot air from the top of the stove) is given by:

$$Q_{adv} = \rho A_c u_c c_p \left(T - T_0\right) \tag{5.12}$$

The partial model (i.e. with temperature taken from experimental data) does not require an iterative solution, while the full model (including combustion and advection) required the energy equation (5.9) be integrated using Euler's method with time steps of 0.1s, until there was no further change in temperature.

5.3 NUMERICAL MODEL OF STOVE PERFORMANCE

A numerical model of the test apparatus was made in Fluent 6.2 with the following simplifying assumptions:

- steady state conditions applied;
- the computational domain was axi-symmetric.

The model consisted of the continuity equation and transport equations for axial and radial momentum, energy, turbulent kinetic energy, turbulent kinetic energy

dissipation, gas species (wood volatiles, O_2, CO_2 and water vapour) and radiation intensity as defined in equations 3.2 to 3.8. In addition the custom solid fuel combustion model detailed in section 3.2.2 was used to describe volatile release and char combustion.

The computational domain (Figure 5.2) was bounded by an axis of symmetry on the right, an adiabatic floor at the bottom, a pressure inlet-outlet on the left and top-left, and walls at 373 K (100^{o}C) representing the target plate bottom and edge at the top. The interior of the domain was divided into five regions: (1) free air which had no special modelling requirements; (2) wood which devolatalised to leave volatiles and burning char according to section 3.2.2; (3) char, which burned according to section 3.2.2 (parameters commensurate with 20 mm diameter spheres, packed orthogonally); (4) fuel window which approximated the air gaps between the stove and fuel as an axi-symmetric porous region allowing secondary air to enter the stove; and (5) stove walls with thermal properties of mild steel. Properties of the five regions are summarised in Table 5.3.

The domain was meshed with tetrahedral cells, side 2 mm in regions (2), (3), (4) and (5). The free air (region 1) was meshed with tetrahedral cells of 2 mm side at solid surfaces, increasing to 50 mm at the boundary. Error in fuel burn-rate and target heating rate were estimated to be 3% and 11% respectively, using the Richardson extrapolation (Feldman, 1999).

Table 5.3. Special modelling requirements for regions in stove model.

Region	*Properties*
(1) Free-air	no special modelling requirements
(2) Wood	Wood pyrolised according to equations 3.20 to 3.23. Char burned according to equations 3.16 to 3.19. Porous characteristics: lumpiness frequency, 200 m^{-1}; specific area, 72 m^{-1}; inertial flow resistance coefficient, 200 m^{-1}. Other fuel characteristics per Table 3..
(3) Char	Char burned according to 3.16 to 3.19. Porous characteristics: void fraction, 0.5; lumpiness frequency, 314 m^{-1}; specific area, 156 m^{-1}; inertial flow resistance coefficient, 800 m^{-1}. Other fuel characteristics per Table 3..
(4) Fuel window	Void fraction, 0.05; inertial flow resistance coefficient, 10 000 m^{-1}.
(5) Stove walls	Mild steel: density, 8000 kg/m^3; specific heat capacity, 500 J/kg-K; thermal conductivity, 16.3 W/m-K.

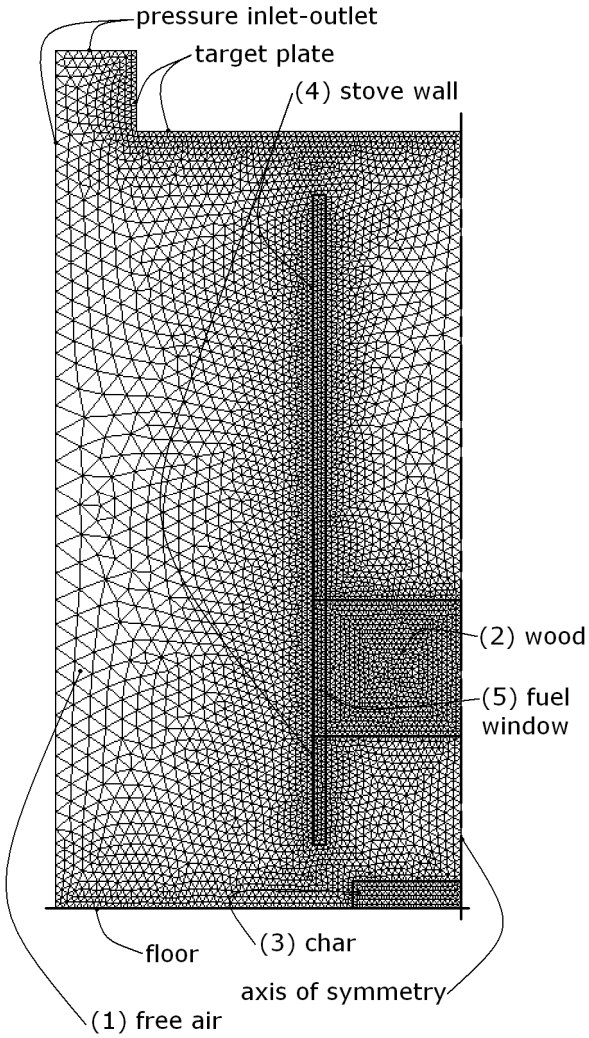

Figure 5.2. Computaional domain for rocket stove modelling, showing boundary conditions and interior regions. Configuration: A-D.

5.4 EXPERIMENTAL RESULTS & DISCUSSION

Typical temperature data for a stove during warm-up are shown in Figure 5.3. After ignition, the inlet temperature increased quickly because of the fire-lighter. The stove wall achieved a quasi-steady temperature after 1500 s. Stove inlet and wall temperatures fell steadily from 1700 s to 2300 s, when the fire was not tended. At 2300 s the char was crushed off the wood (according to the experimental procedure), falling to the stove inlet and allowing fresh fuel to be added to the stove: thereafter the inlet temperature increased suddenly and the stove wall temperature started to increase, though flame temperatures were unaffected until fire had spread to the new fuel surfaces at 2600 s. The target plate temperature, T_7, was in the range 100°C to 120°C during the time period

2380 < t < 2470 s. Note that the inlet temperature suddenly rose to a level that was higher that the flame temperature after t=2300s: it appears that the char built up around the thermocouple, completely enveloping it, and causing it to record the temperature inside that char bed, not the temperature between the char bed and the virgin fuel.

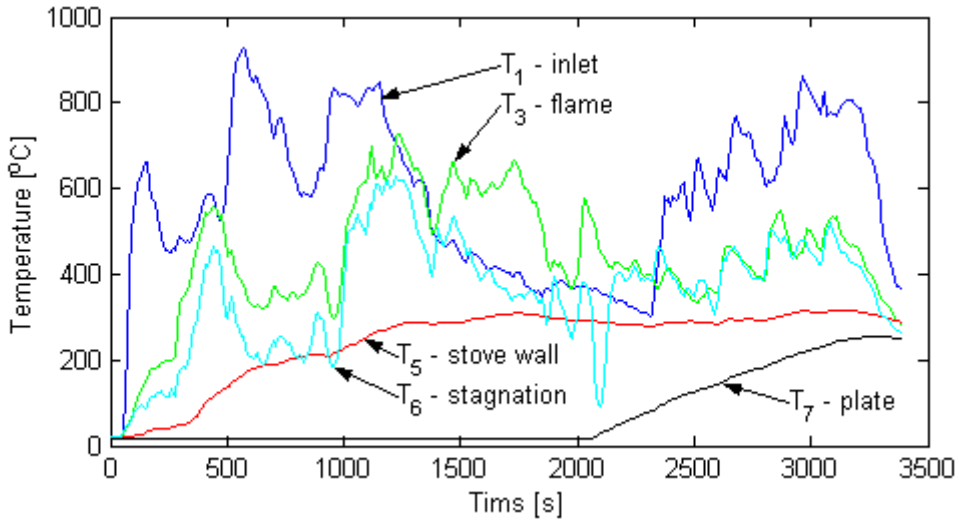

Figure 5.3. Experimental temperature traces.
Configuration: d=0.15m; v=0.5-1.0m/s; z=0.024m; D=0.3m.

5.4.1 Preliminary Experimental Results

A preliminary set of experiments were carried out during the development of the stove and test procedure. Dimensions A, B, C and D were varied as in Table 5.1, and for each permutation the fuel burn rate was recoded over a period of approximately 300 s. During that time, the target plate was heated three times to estimate the heat transfer. Results are given in Table 5.4, and ANOVA was used to give the statistical correlations 5.13a&b for fire power, P, and efficiency, η, with 95% confidence.

Table 5.4. Raw data for preliminary test on rocket stove, varying A, B, C and D.

Permutation	*Burnrate [g/s]*	*Heat to target plate [W]*		
----	0.21	603	669	572
A---	0.20	498	885	800
-B--	0.12	314	361	499
AB--	0.09	261	280	404
--C-	0.20	715	719	598
A-C-	0.15	259	308	662
-BC-	0.17	427	432	499
ABC-	0.11	283	368	327
---D	0.24	740	482	829
A--D	0.18	795	530	380
-B-D	0.17	439	444	465
AB-D	0.15	358	363	411
--CD	0.28	218	769	757
A-CD	0.17	251	299	693
-BCD	0.09	143	107	211
ABCD	0.21	354	563	487

$$P = 4.2 - 0.1a - 0.6b + 0.3c + 0.2d + 1.1e \pm 0.9kW$$
$$\eta = 14.4 + 1.3a - 1.0b - 0.1c - 1.8d - 2.4e \pm 1.9\% \qquad (5.13a\&b)$$

Many of the features of these results are discussed below with further data, but one single point should be highlighted: the fire power of the stove is very strongly influenced by the height B, between the char bed and the virgin fuel. Increasing the height significantly reduces the fuel burn rate (hence power) of the stove. Two opposing mechanisms appear to be at work: a higher stove would tend to induce a greater draft, therefore improve combustion efficiency (as per the positive c-coefficient in correlation 5.13a). This is expected to be a linear relation with height. Conversely a greater distance between char and virgin fuel would tend to reduce the radiative and convective heat transfer from the char to the virgin fuel, and reduce the rate of devolatalisation. The effect of convective heat transfer is expected to be approximately linear with height, however the more dominant effect of radiative heat transfer is expected to be the square of height (inverse square law, backed up by radiation shape factors for parallel concentric disks; e.g. Holman, 1992). The result is that for subsequent tests, dimension B was not varied, but kept at a minimum while respecting the material integrity of the stove.

5.4.2 Radiation and convection heat transfer

Heating for the target plate in Figure 5.3 can be modelled with the energy equation:

$$m_p c \frac{dT_p}{dt} = Q_{cp} + Q_{rp} - Q_{ra} \tag{5.13}$$

where convection and radiation heat fluxes are given by equations (5.5) to (5.7). Taking the experimental temperature traces for the stagnation point and the flame, the results can be plotted with the experimental plate temperature, T7 (see Figure 5.4). The difference between the pure convection line (where emissivity of the plate was set to zero) and the combined convection and radiation line demonstrates that radiation plays a significant role in heat transfer to the plate, accounting for approximately 20% of the heat entering the plate. This figure appears low, but it should be noted that the current calculation includes heat loss through radiation. Had the whole lower surface of the plate be subject to both convection and radiation (and other boundary conditions remain unchanged), then radiation would have accounted for 60 to 70% of heat transfer.

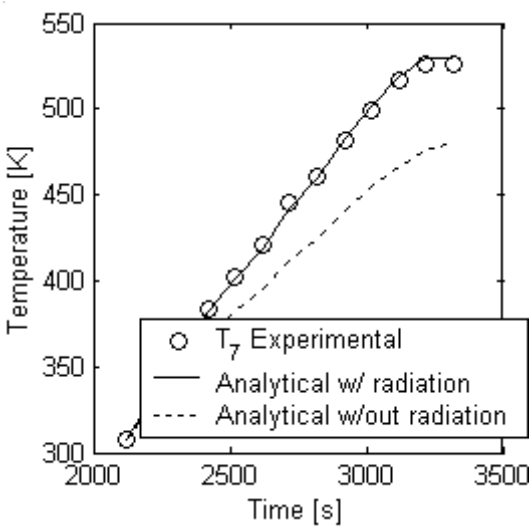

Figure 5.4. Numerical model of heat transfer to the target plate due to convection and radiation, per equation 5.13.

Let us now examine how stove performance varies with geometry, first by examining fuel burn rate and heat transfer to the plate for configurations in Batch A and comparing them to the analytical model, then doing the same for configurations in Batch B.

5.4.3 Batch 1 (ACD) experimental correlations

For stove configurations in Batch 1 (where dimensions A, C and D were varied; see Table 5.2), linear statistical correlations were calculated by least-squares

regression for fuel burn-rate (5.14) and target plate heating rate (5.15) with 95% confidence.

$$m'_{ACD} = 0.33 + 0.01a + 0.04c + 0.01d \pm 0.03g/s \quad (5.14)$$

$$q'_{ACD} = 750 + 70a + 10c - 50d \pm 110W \quad (5.15)$$

where a, c and d are the normalised values of dimensions A, C and D, following the format given in equation (3.24). Correlations 5.14 and 5.15 are plotted along with raw experimental data in Figure 5.5.

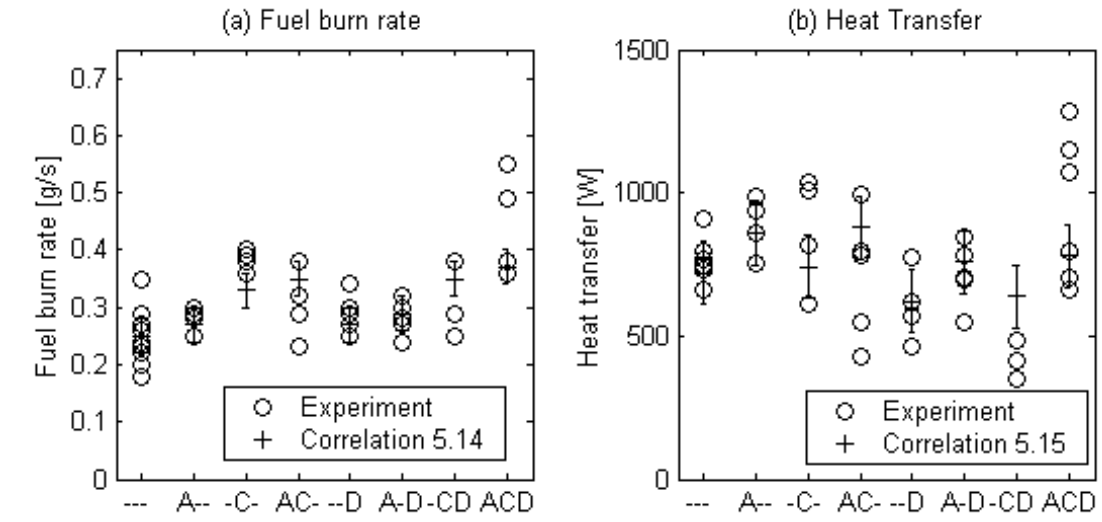

Figure 5.5. Experimental stove behaviour for Batch A (ACD).

Experimental data suggest that increasing dimension A (ground-to-plate clearance) increases fuel burn rate and heat transfer. The mechanism suggested by the analytical model is that A reduces the resistance to flow, allowing more oxygen into the stove, allowing more fuel to burn, and increasing the velocity of air over the plate, therefore improving convection heat transfer. Similarly D (stove-to-plate clearance) reduces flow resistance, therefore increasing velocity, burn rate and heat transfer, though it simultaneously increases the quantity (z/d) which Chapter 4 demonstrated reduces convection heat transfer. Increasing dimension C (stove height) also has the effect of increasing fuel burn rate and heat transfer, and the mechanism is a taller chimney leading to a bigger draft (as in equation 5.4). While the increase in velocity is clearly demonstrated in the partial analytical model (see Figure 5.6), the full analytical model predicts a decrease of burn rate when increasing stove height, C. The mechanism appears to be increased stove height initially leads to a greater draft (as already discussed) which causes a greater heat loss from the stove due to advection (as in equation 5.12), leading to a lower temperature, and finally a lower burn rate

and lower heat transfer. This clearly contradicts the experimental data, and demonstrates the shortcomings of a well-mixed reactor model: a single control volume is not sufficient to describe a through–flow process. More appropriate would be several control volumes in series, connected by a transport delay or better still the advection-diffusion equation, leading seamlessly to the need for a CFD model.

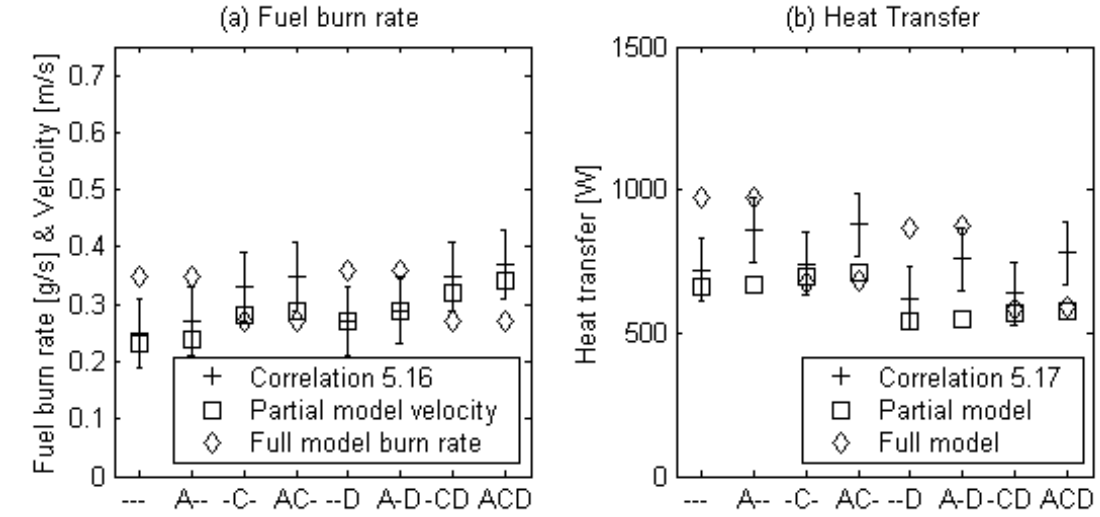

Figure 5.6. Stove behaviour predicted by analytical model.

5.4.4 Batch 2 (DEF) experimental correlations

For Batch 2 of the experimental investigation, where dimensions D, E and F (stove-to-plate clearance, stove diameter and target plate diameter; see Table 5.2) were varied, the fuel burn-rate and target plate heating rate are given by experimental correlations 5.16 and 5.17, and plotted in Figure 5.7.

$$m'_{DEF} = 0.28 + 0.03d + 0.10e + 0.01f \pm 0.02g \,/\, s \qquad (5.16)$$

$$q'_{DEF} = 840 + 90d + 250e + 70f \pm 70W \qquad (5.17)$$

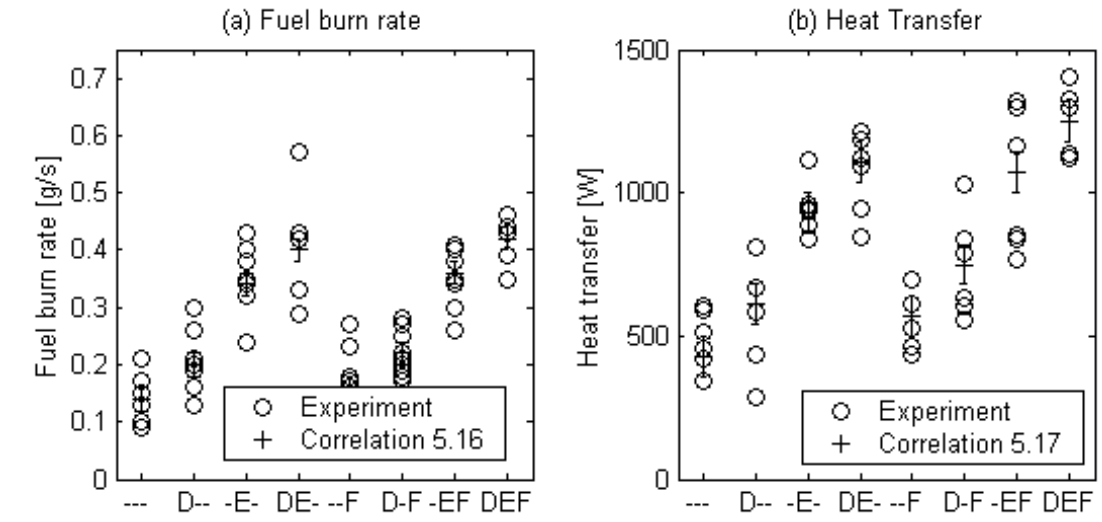

Figure 5.7. Experimental stove behaviour for Batch B (DEF).

First, compare the nominal values and D quotient for these correlations and those for Batch 1 (equations 5.3 and 5.4). For fuel burn rate, the nominal value for Batch A (0.33±0.03 g/s) and Batch B (0.28±0.02 g/s) agree, and the D-quotients (0.01 and 0.03 for Batch A and B respectively) are comparable. For heat transfer, the nominal value for Batch A (750±110 W) and Batch B (840±70 W) also agree, however the D-quotients are very different (-50 and +90 for Batch A and B respectively). The D-quotient for Batch B contradicts the findings of Chapter 4, where a greater stove-to-plate clearance led to less heat transfer. As already discussed, a greater stove-to-plate clearance also reduces the resistance to flow, leading to higher velocity, therefore better combustion and heat transfer. It may be that one effect dominated in one batch and the other in the second batch, due to uncontrolled variations in experimental technique, fuel, atmospheric conditions etc.

Reviewing the impact of the other dimensions, E (stove diameter) allows a larger surface area of fuel to be admitted to the stove, leading to a greater fuel burn rate, and to better convection and radiation heat transfer. Note however that fuel surface area increases linearly with stove diameter, while the volume of the combustion chamber increases as the square of stove diameter. Dimension F (plate diameter) has no impact on fuel burn rate but increases surface area available for heat transfer.

In this section experimental results have been presented for stove behaviour, measured by fuel burn rate and heat transfer to the plate. The experimental results have been reduced to statistical correlations, and have been discussed in terms of an analytical model of the stove. The assumption of a well-stirred reactor in the analytical model lead to errors when changing the stove height, and

has highlighted the need to model the stove with more subtle techniques (CFD). In the following section results will be presented for such a model (the numerical model described in section 5.3), and compared to experimental results.

5.5 NUMERICAL RESULTS & DISCUSSION

5.5.1 Numerical Prediction of Temperature Field

For configuration DEF, the temperature field is plotted in Figure 5.8 from results of the CFD model. The layer of burning char is visible on the floor, as are the hot 'lumps' of fuel inside the stove near the fuel window. The hot combustion gases form a plume above the fuel, impinge on the target plate, and leave the stove. Comparing these simulated temperatures with mean temperatures in experiment (Figure 5.9) it is clear that there are two problems: first the numerical model under-estimates temperatures T1 and T2 (between the char and virgin fuel) and over-estimates T3 and T4 (above the virgin fuel). It has already been suggested that thermocouples T2 and T2 were embedded in the char bed, rather than being suspended above it, and that experimental values of T1 and T2 are artificially high. With respect to T3 and T4, it appears that insufficient air being drawn in, resulting in high flame temperatures (since there is no excess air). Unburned volatiles are then burning as they leave the stove, resulting in the hot region stretching from the lip of the stove, where oxygen and turbulence exist in abundance.

5.5.2 Numerical Prediction Stove Behaviour with Changing Geometry

Experimental correlations 5.14, 5.15, 5.16 and 5.17 for fuel burn-rate and plate heat transfer in experimental Batches 1 and 2 are compared with the predictions of the same data from the numerical simulation in Figure 5.10 and Figure 5.11. Mean and maximum errors for fuel burn rate for both batches are 30% and 63% respectively. Mean and maximum errors for heat transfer for both batches are 22% and 80% respectively. Several problems with the model are immediately apparent:

- Fuel burn rate does not respond to changes in stove height (C).
- Fuel burn rate responds excessively to changes in stove diameter (E).
- Heat transfer behaves erratically with changes in stove diameter (E) and plate diameter (F).

In all other aspects, the CFD model of stove performance gives an adequate description of the stove.

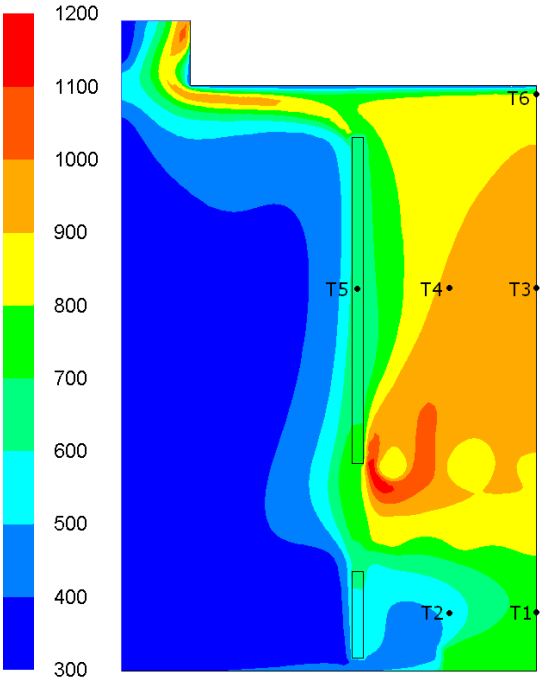

Figure 5.8. Temperature field [K] from numerical simulation of stove configuration DEF.

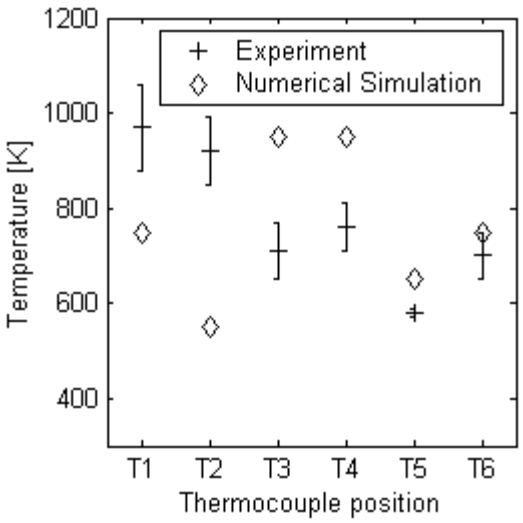

Figure 5.9. Comparison of temperature field [K] from numerical simulation and experiment. Configuration DEF.

The first of these issues (fuel burn rate does not respond to changes in stove height, C) is difficult. Table 5.5 shows that configuration –C- has resulted in a larger flow of primary air, as would be expected. The temperature of the virgin fuel bed remains relatively unchanged (782 K and 793 K for configurations --- and –C- respectively), with the result that fuel burn rate (which is driven by the temperature difference across the layer of char around the fuel) also remains little affected. This is clearly a significant drawback of the model, as stove height is an obvious design parameter and clearly has a significant effect on stove performance.

Concerning the second of these problems (fuel burn rate responds excessively to changes in stove diameter, E) it has already been stated that in the experimental set-up the surface area of fuel increased linearly with stove diameter, while the stove volume increases as the square of stove diameter. The lumpiness model assumes that the amount of fuel is proportional to the volume of the fuel bed. Consequently, changing from configuration --- to –E- increased the experimental fuel surface by a factor of 1.5 but increased the simulated fuel surface by a factor of 2.25. This discrepancy is reflected in the artificially high burn rate of –E-, DE-, -EF and DEF in simulation.

Finally, the erratic heat transfer with changes of E and F can be explained by the behaviour of the jet as it leaves the stove and comes to the edge of the plate. In

configuration –E- the flow leaves plate and continues to expand radially, entraining ambient air which cools the side of the plate. In configurations DE-, -EF and DEF the buoyancy forces acting on the jet are strong enough to curl the hot gases round the edge of the plate so that they also transfer heat to the side of the plate, resulting in the significantly higher heat transfer rate. Note that while this has caused a significant error in these results, a mogogo plate would be embedded in a clay and stone structure so that the edge of the plate (such that it is) would not be in contact with hot combustion gases, and this failure mode does not apply.

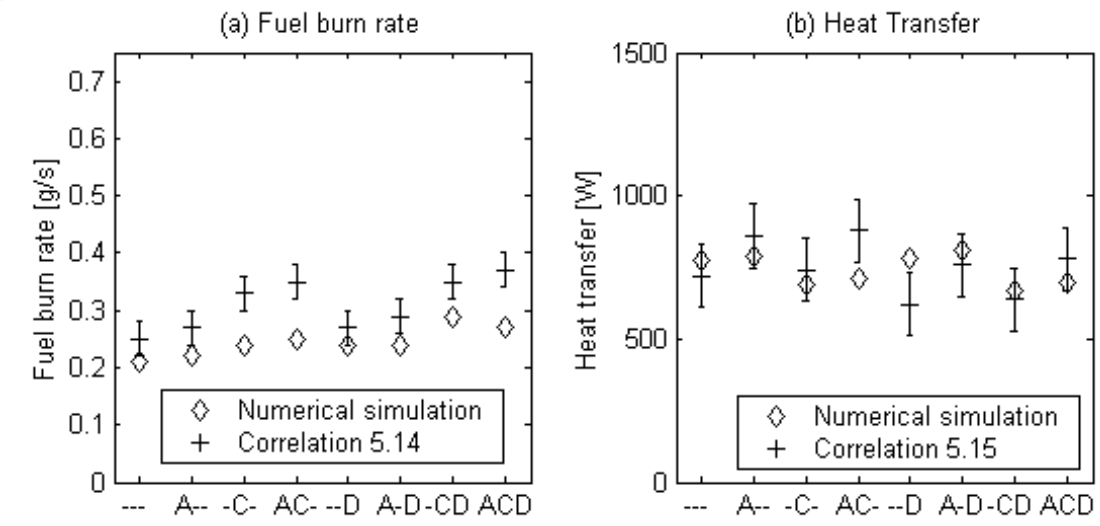

Figure 5.10. Batch 1 (ACD) prediction of stove behaviour from simulation.

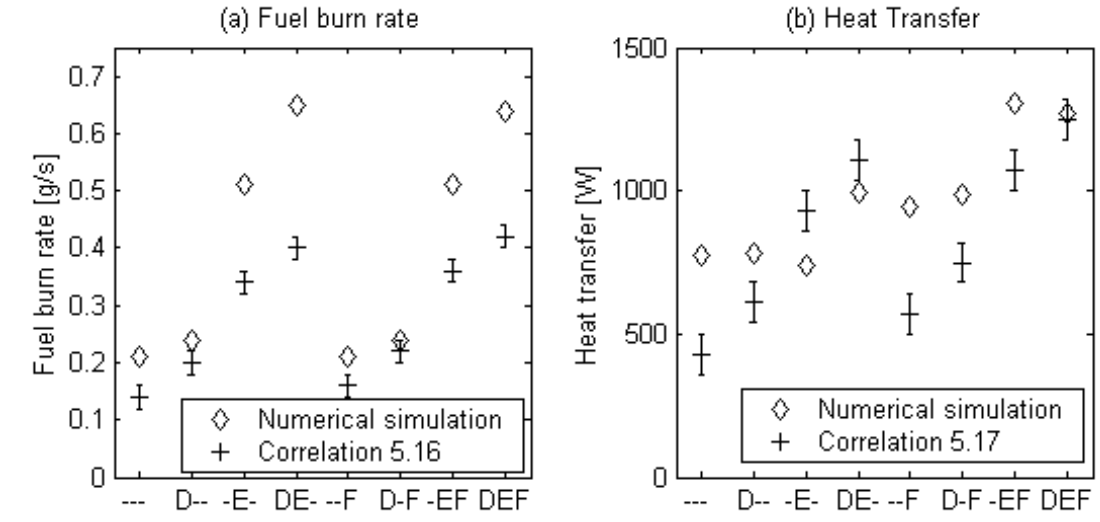

Figure 5.11. Batch 2 (DEF) prediction of stove behaviour from simulation.

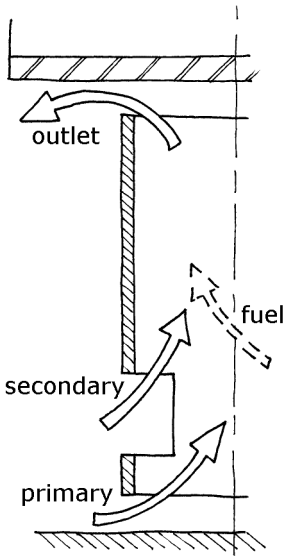

Figure 5.12. Schematic for mass flows in the rocket stove.

Table 5.5. Mass flows in g/s for stove configurations [---] and [-C-]. Flows defined in Figure 5.12.Configurations defined in Table 5.2.

	[---]	[-C-]
primary	0.61	0.76
secondary	0.01	0.02
fuel	0.21	0.25
outlet	0.83	1.03

5.6 CONCLUDING REMARKS

Experimental results for a rocket stove have been presented, along with two models: an analytical model and a numerical model. Results from the experimental investigation were used to demonstrate that radiation does play a significant part in heat transfer to the target plate, accounting for 20% of total heat transfer for a target surface with edges, and accounting for an estimated 60% of heat transfer for a target surface without edges. An accurate radiation model is therefore imperative, and the lack of an adequate soot model in CFD simulations to date is expected to play a significant part in the weakness of any predictions.

Results of CFD simulations of the rocket stove have also highlighted two other shortcomings. First, the model is fairly insensitive to changes in stove height. This is a serious flaw, and no explanation was forthcoming. Second, the model was over-sensitised to changes in stove diameter. The mechanism for this is understood. Despite these shortcomings, the model shows reasonable agreement with experimental data. While the results of simulations may fall short of the expectations of research focussed purely on combustion science, the model is sufficiently mature to be used as a design tool for the optimisation of a wood-fired cooking-stove, where fuel is not accurately metered into the combustion chamber, and combustion chamber dimensions are not tightly controlled during manufacture.

CHAPTER 6: STOVE OPTIMISATION

In Chapter 3 a model was developed of fuel in a fixed bed, and in Chapter 4 CFD simulations were carried out on impinging jet heat transfer. In Chapter 5 these models were brought together to simulate a whole stove, and to investigate the effect of changing key stove dimensions. In this chapter the model is used to assess the objective function of a genetic algorithm (GA) with the aim of optimising the stove for heat transfer and fuel burn rate. The GA uses one of two methods to convert the gene to a CFD mesh: these methods are compared and discussed. Other aspects of the GA are standard procedures, such as roulette-wheel selection, single point cross-over and mutation. The GA was for eight heats, and the winners of the eight heats were put together in three run-offs. The resulting stove displays evolved many features that are recognised as beneficial to combustion and effective heat transfer. The stove was subjected to a sensitivity analysis and attempts were made to redesign some aspects of the stove to achieve a reasonable compromise between performance and manufacture.

6.1 OPTIMISATION METHOD

The genetic algorithm presented in this chapter was similar in many regards to algorithms cited in the literature review (Chapter 2), using standard techniques such as roulette-wheel selection, single point crossover and random mutation. It was a bespoke code written as a Matlab m-file, essentially consisting of a pair of nested for-loops to visit each creature in each generation (see the pseudo-code in Figure 6.1). For each creature (candidate stove), it was necessary to convert the genetic code in to a mesh which could be read by the CFD code. Two such gene-to-mesh methods were investigated: the vector-geometry method (VGM; see Hilbert et al., 2006) and the apparently novel mesh-deformation method (MDM),

which are described in detail in sections 6.1.1 and 6.1.2. Once a mesh had been created, it was imported into Fluent 6.2, and solved using the model described in Chapter 5 and the fuel sub-model described by the user-defined function (UDF) in Chapter 3. The UDF exported data on fuel burn rate, and Fluent 6.2 exported data on heat flux across the top of the mogogo plate. One of two objective functions (presented and discussed in section 6.1.3) was used to calculate the fitness of the candidate stove.

Once the fitness of all stoves in one generation had been found, the GA progressed to the mating phase. Initially the roulette-wheel method was used to select mates (though this was later modified; see section 6.2.1). In the roulette-wheel method, a virtual roulette-wheel is formed each generation, with N_c bins for the N_c creatures. The sizes of the bins are in proportion with the fitness of each creature. The roulette-wheel is spun with two balls to randomly select two parents (though creatures with a higher fitness are more liable to be selected). The two parents mate: the child takes genes from the first parent up to a randomly selected cross-over point; thereafter the child takes genes from the second parent. Each of the N_b bases in the child's gene is then subject to a $1/N_b$ chance of a random mutation. This mating process is repeated N_c times to give N_c new creatures, and the cycle repeats for N_g generations.

```
initialise random genome of creatures
FOR each generation
      FOR each creature
            transform gene into mesh
            call CFD to calculate fluid flow
            calculate fitness from CFD results
      ENDFOR creature
      select mates
      cross-over to create new generation
      mutation on new generation
      new generation usurps old generation
ENDFOR generation
```

Figure 6.1. Pseudo-code of Genetic Algorithm.

6.1.1 Mesh Deformation Method

In the mesh-deformation method a coarse generic mesh was deformed according to data in the gene, then exported to Fluent 6.2 where it was refined for use as a CFD domain (Figure 6.2).

To execute mesh deformation, it was assumed that the mesh represented a network of N_b springs, connected at N_n nodes. The N_b bases of the gene represented scaling factors to be applied to the initial lengths of the springs, giving their natural lengths: when the mesh was allowed to relax so that the N_b springs tend to their natural lengths, the boundaries deformed and changed the shape of the stove (Figure 6.2). Some nodes (on the centre-line and mogogo plate) had their positions fixed by assigning them an infinite mass. The other nodes (on the deformable part of the stove, the outlet and the interior of the domain) were assigned an arbitrary mass, m, and viscous friction coefficient, c. The springs were assigned an arbitrary stiffness, k, and natural length, l_0. Each base, b, of a creature's genome was an integer in the range 1 to 9. The natural length of the ith spring was given by:

$$l_{i,n} = l_{i,0} \frac{2g_i}{g_{\max}} \tag{6.1}$$

During mesh deformation, Newton's second law was applied to each node in the x and y directions:

$$\begin{aligned} m_{i,x} \frac{dx_i}{dt} &= k\left(\left|R_{ij}\right| - l_{ij,n}\right) - c\frac{dx}{dt} \\ m_{i,y} \frac{dy_i}{dt} &= k\left(\left|R_{ij}\right| - l_{ij,n}\right) - c\frac{dy}{dt} \end{aligned} \tag{6.2a,b}$$

where the first and second terms on the right hand side of equations 6.12 are the sum of spring forces applied by neighbouring nodes on the ith node, and the force due to viscous friction. R_{ij} is the relative position of node j with respect to node i, and $l_{o,ij}$ is the natural length of the spring connecting nodes i and j. Equations 6.2 were discretised using Euler's method and solved for a fixed number of time-steps, $N_{\Delta t}$. The solution was artificially damped according to a dynamic relaxation scheme: the total kinetic energy of the system was monitored at every time-step, and if a maximum was detected, the velocity of every node was returned to zero. By this method it was expected that the mesh motion was frozen near its equilibrium position, and a minimum number of time-steps would be required to achieve its relaxed deformed state (Adrianssens, 2001). The resulting mesh was written to file and exported to Fluent 6.2, where it was refined for use as a CFD domain.

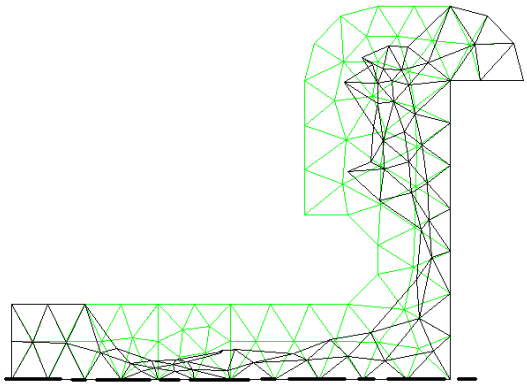

Figure 6.2. Generic mesh (green) and deformed mesh (black) for a detail of a stove nozzle. The view is axi-symmetric, with the centre-line on the x-axis, the nozzle inlet is on the left, and the section on the right is the bottom of the mogogo plate.

6.1.2 Vector Geometry Method

In the vector geometry method (VGM) the mesh was rebuilt completely for each creature. Bases of the gene were used as scaling factors for vectors describing the positions of nodes on the surface of the stove. Positions of the nodes were imported to the mesh-generation software, Gambit 2.16, then joined by edges to make faces, which were meshed. The mesh was then exported to Fluent 6.2, where boundary conditions were applied, and the heat and fluid flows calculated. The coordinates of some nodes was absolute, while others were positioned with respect to other pre-defined nodes. For example in Figure 6.3, the y-coordinate of node 2 is defined as the y-coordinate of node 1, plus a length calculated from a pre-defined maximum and a scale derived from the gene; the x-coordinate of node 2 and the x- and y-coordinates of node 1 are defined by a scalable length from the origin. Stated mathematically:

$$x_n = x_{precedent,n} + \left[\frac{g_{x,n}}{g_{\max}} \left(x_{\max,n} - x_{\min,n} \right) + x_{\min,n} \right]$$

$$y_n = y_{precedent,n} + \left[\frac{g_{y,n}}{g_{\max}} \left(y_{\max,n} - y_{\min,n} \right) + y_{\min,n} \right] \qquad (6.3a,b)$$

where x, y and g are the x-coordinate, y-coordinate and base of the gene for node n. Subscripts min and max refer to the minimum and maximum values of the vector, and precedent refers to the node from which the current node position is calculated. Values for the minima, maxima and precedents are given in Table 6.1. The gene was constructed as a list of integers in the range 1 to 9, hence g_{max} = 9. The system of precedents and special rules (Tables 6.1 and 6.2) was

formulated to give a high probability of a coherent stove shape (i.e. the boundary of the stove does not cross itself).

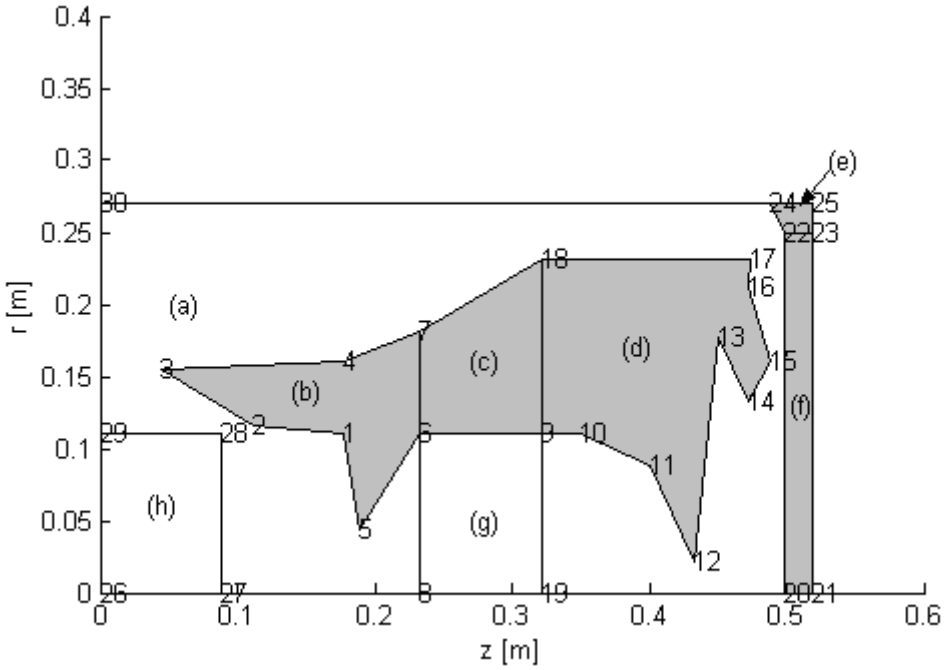

Figure 6.3. Schematic of node numbers and their connectivity for the vector-geometry method of mesh formation. Regions of the domain are (a) free air; (b) stove bottom; (c) fuel window; (d) stove top; (e) stove lip; (f) mogogo plate; (g) fuel; and (h) char. The x-axis is the rotation of symmetry, the y-axis is the ground and solid material is shown shaded.

6.1.3 Objective Functions

Two objective functions were used to assess the fitness of candidates (equations 6.4 and 6.5). Both aimed to reward three aspects of a stove's performance: (a) achieving a target heat flux through the mogogo cooking surface; (b) achieving a uniform heat flux across the mogogo cooking surface and; (c) minimising fuel consumption.

$$f_1 = \frac{1}{m'_f} \frac{1}{\sum \left(q''_i - q''_t\right)^2} \tag{6.4}$$

$$f_2 = g(q'') + \frac{h(q'')}{m_f{}'} \tag{6.5}$$

Table 6.1. Data for vector-geometry method.

Node	x-precedent	x-minimum	x-maximum	y-precedent	y-minimum	y-maximum
1	0	0	0.2	0	0	0.2
2	0	0	0.2	1	0	0.05
3	0	0	0.2	2	0	0.05
4	0	0	0.2	3	0	0.05
5	1	0	0.05	0	0	0.2
6	5	0	0.05	0	0	0.2
7	6	0	0	0	0	0
8	6	0	0	0	0	0
9	6	0	0.2	0	0	0.2
10	9	0	0.05	0	0	0.2
11	10	0	0.05	0	0	0.2
12	11	0	0.05	0	0	0.2
13	12	0	0.05	0	0	0.2
14	13	0	0.05	0	0	0.2
15	14	-0.02	0.02	14	0	0.05
16	15	-0.02	0.02	15	0	0.05
17	16	-0.02	0.02	16	0	0.05
18	9	0	0	0	0	0
19	9	0	0	0	0	0
20	0	0	0.1	0	0	0
21	20	0.02	0.02	0	0	0
22	20	0	0	0	0.25	0.25
23	21	0	0	0	0.25	0.25
24	22	-0.02	0.02	0	0.02	0.02
25	21	0	0	24	0	0
26	0	0	0	0	0	0
27	0	0	0	0	0	0
28	27	0	0	0	0	0
29	0	0	0	28	0	0
30	0	0	0	24	0	0

Table 6.2. Special requirements for vector-geometry method.

Vector	Special requirement
x5	precedent is maximum of nodes 1 to 4
y5	normal, except must be less than y2
y17	precedent is greatest of nodes 9 to 17
y18	precedent is greatest of nodes 9 to 17
x20	precedent is greatest of nodes 14 to 17
y24	precedent is greatest of nodes 1 to 23
x27	0.5 * x1
x28	0.5 * x1

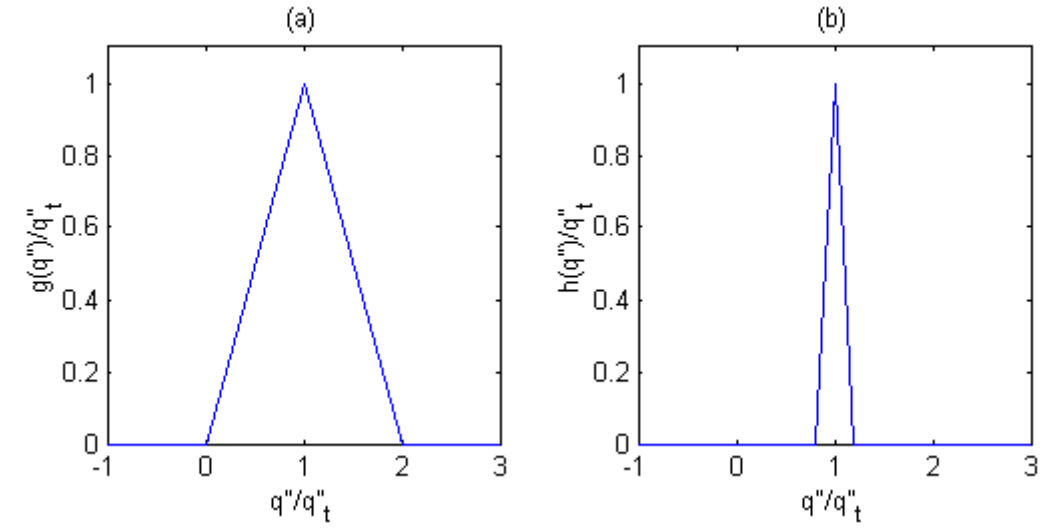

Figure 6.4. Functions g(q") and h(q"), which contribute to the overall objective function.

where m'_f is the fuel burn rate, q_i" is the heat flux through cell i on the mogogo cooking surface, and $q"_t$ is the target mogogo heat flux. Functions g(q") and h(q") are described in Figure 6.4 and discussed below.

Objective function f_1 (6.4) was used while developing the algorithm (see results in section 6.2.1), however a candidate stove was able to achieve a fitness either through achieving a uniform heat flux near the target flux (via the sum of squares of residuals in the denominator) or though minimising the fuel burn rate, or through both methods simultaneously. Many of the candidate stoves achieved high fitness solely by minimising fuel consumption, resulting in stoves that did not burn fuel: while it was a fitness function suitable for development of the GA, it was not suitable for optimising a working stove, hence the need for the second objective function.

Objective function f_2 (6.5) used two Δ-functions centred on the target heat flux, g(q") and h(q") in Figure 6.4 (a) and (b) respectively. The second Δ-function, h(q") has a far tighter range ($0.8 < q/q_t < 1.2$) than the first ($0.0 < q/q_t < 2.0$), with the result that a candidate stove must be very close to achieving the target heat flux before it can be rewarded for low fuel consumption. This might be described as a sequential multi-objective genetic algorithm (SMOGA).

The target heat flux was found through a series of experiments using a mogogo constructed at the University of Nottingham, operated by members of the Eritrean Diaspora to produce passable ingera. Target heat flux was estimated as $q_t" = 5090$ W/m^2, first by Fourier's law of one-dimensional heat conduction given the temperature gradient across the plate, the thickness and thermal conductivity (Appendix E), and second by estimating the sensible heat required to raise the temperature of the batter, and the latent heat required to drive off moisture and gelatinise the flour. Full details of the mogogo, test procedure and analysis are given in Appendix F.

6.1.4 Analysis Procedure and Algorithm Parameters

The optimisation process was carried out in three stages. The aim of the first stage of analysis was to determine which of the two gene-to-stove methods was more efficient (i.e. reviewed a greater range of stoves designs and converged on a solution more rapidly). The GA was executed with objective function f_1 (equation 6.4), first for two runs with the MDM, then with the VGM. Using the most efficient mesh-to-stove method and objective function f_2 (equation 6.5), the second stage was a series of eight heats to identify preliminary candidate stoves. The third and final stage was a series of three run-offs between these eight candidates and a further two randomly generated genes to identify an optimum stove design. This optimum stove was then subjected to a sensitivity analysis to ensure the design was robust.

Throughout the process, the GA was run with N_c =10 creatures in the gene pool for a maximum of N_g = 50 generations. The MDM required N_b = 300 bases in the gene and the VGM required N_b = 60 bases in the gene. These values and the number of runs were considered to be a reasonable compromise between conducting an exhaustive search of the solution space and the limited resources available. The full code of the GA, Gambit and Fluent journal files and the Fluent UDF are given in Appendix G.

6.2 RESULTS AND DISCUSSION

6.2.1 Gene-to-Stove Methods

Two runs each of the vector-geometry method (VGM) and the mesh-deformation method (MDM) were carried out to identify which was the most efficient (Figure 6.5). Mean fitness of the MDM started at approximately 0.0001 and rose to approximately 0.0005. Mean fitness for the VGM started from a similar level (as it should for randomly generated genomes), however it rapidly rose to relatively high values of the objective function (almost an order of magnitude higher than the MDM) and exhibited large fluctuations (e.g. from geration 20 to generation 30 of run 1, the mean fitness ranged from 0.001 to 0.007). In run 1 of the VGM, mean fitness slumped just after generation 40, from values of about 0.007 down to 0.004.

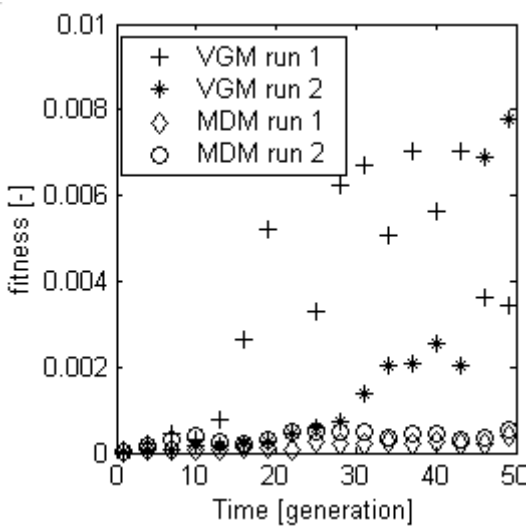

Figure 6.5. Generation average fitness for GA runs with the vector-geometry method (VGM) and the mesh deformation method (MDM), using objective function 6.4. The VGM evolves high-fitness creatures far more rapidly than the MDM.

Several conclusions can be drawn from this: first, that the VGM has been able to examine a wider range of stove configurations; second that within that range some very successful configurations have been identified; and thirdly, that despite finding these successful configurations, the pure roulette-wheel selection method was not able to retain them.

Reasons for the relative inefficacy of the MDM are twofold. In the first instance, a single mesh had to fulfil two purposes: it was to be a deformable structure for the mesh-deformation method itself, and also a computational domain for the CFD calculations. CFD typically requires a fine mesh with non-skewed elements, else the solution will not converge. These conditions are diametrically opposed to

mesh-deformation where a sparse mesh would be more easily deformed, resulting in highly-skewed elements: a compromise mesh must be used for the method to meet with any success. This leads to the second shortfall: any compromise mesh has a degree of redundancy, such that a radical change in the length of a single edge can easily be absorbed by the flexibility of its neighbours. This results in a very stable geometry where several edges need to be adjusted in consort before a single node on the boundary of the stove geometry can significantly change position. The genes affecting these changes might be located on non-consecutive bases within the gene, and a system of cross-over and random mutation is unlikely to achieve the required combination by chance. The efficiency of the method might be improved by reducing the number of edges, however this returns to the problem of poor mesh quality for CFD calculations. In the final analysis, the VGM was far more efficient at rapidly moving through the solution space, and was selected for use in the initial heats and the final run-offs for stove optimisation.

It was also noted that the pure roulette-wheel selection method was unable to retain all the fittest stoves. While this is not necessarily a problem (the GA searches the solution space, and it is relatively easy to keep track of past solutions, successful or otherwise) optimum solutions are expected to be bunched around a local maximum even in a non-linear solution space. As a result, the pure roulette-wheel was modified such that the first creature in the new generation was the fittest to date, and the other positions were filled using the standard roulette wheel. This encouraged the GA to continue exploring the highest maximum that it has discovered, but did allow it to move from one maximum to another if it was found to be higher.

6.2.2 Champions from Initial Heats

The GA was run eight times (labelled a to h) using the vector-geometry method, the modified roulette wheel and the objective function f_2. Using a 3.2 GHz processor and 1 GB of RAM, the CFD code took 1000-1500 cpu seconds for every creature in every generation to converge. Consequently a generation of 10 creatures was assessed in 4-5 hours, and a simulation of 50 generations (the default value) took approximately 1 week. Mean and maximum fitness are plotted for a typical run in Figure 6.6. Fitness of the best stoves are given in Table 6.3, and the best stoves are plotted schematically in Figure 6.7 (see Figure 6.3 for description of the regions in Figure 6.7).

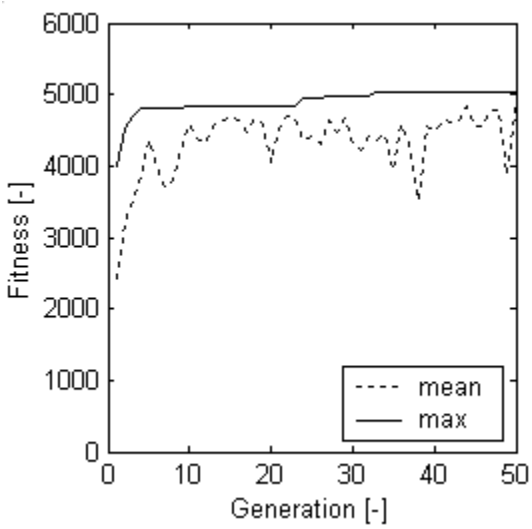

Figure 6.6. Fitness for creatures in run (c), using objective function 6.6.

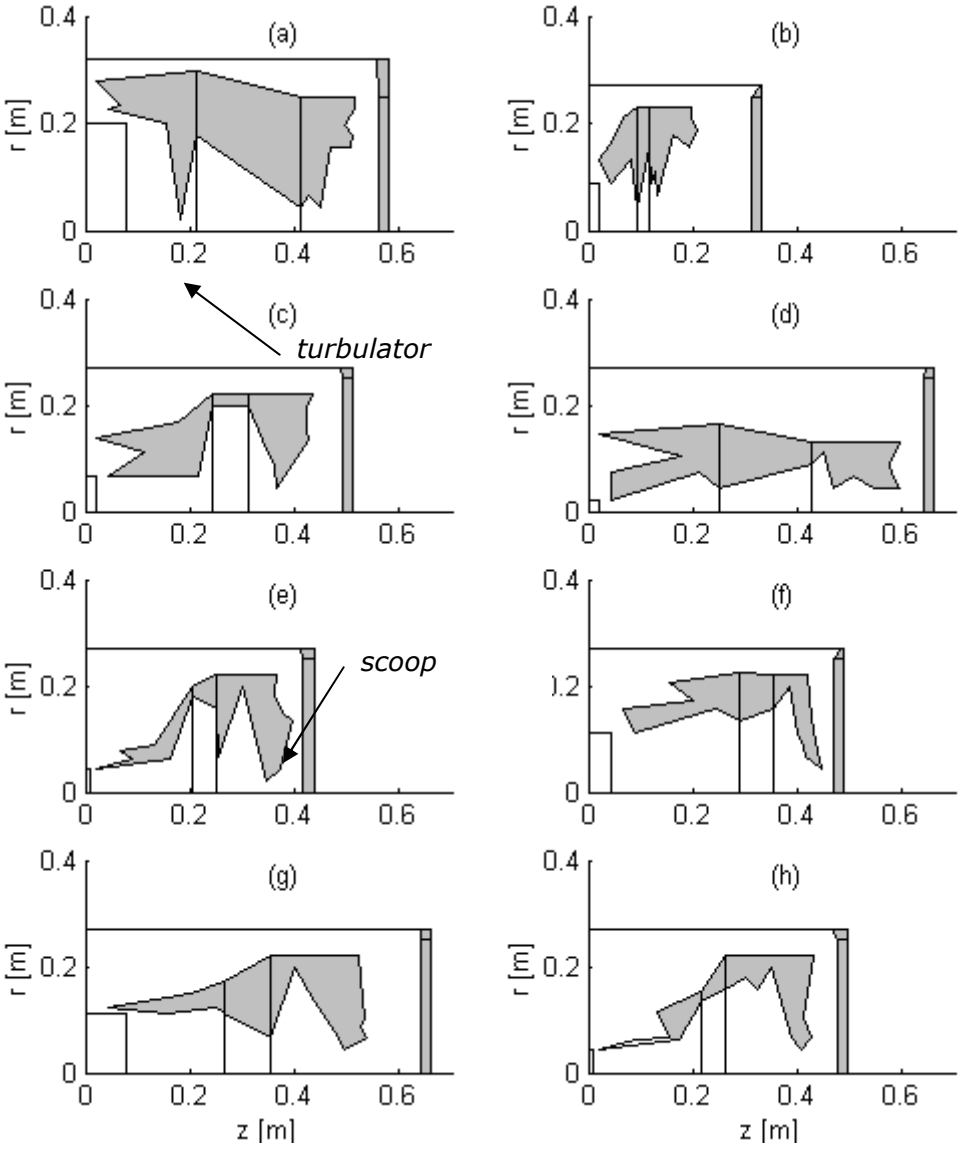

Figure 6.7. Stoves with highest fitness after a single 50 generation run.

Table 6.3. Results for heats a to h.

Run	Mean heat flux [W/m2]	Fuel burn rate [g/s]	Fitness, f_2 [-]
a	4668	2.85	4873
b	0	0	0
c	4713	1.88	5047
d	4782	0.86	5590
e	4625	0.46	5789
f	3858	0.90	3858
g	3014	1.65	3014
h	4678	1.62	5038

Of all the stoves in Figure 6.7, stove (b) sticks out as a runt. The combustion reaction was sustained in none of the candidate stoves of run (b), they all achieved a fitness of zero, and the stove in Figure 6.7b is creature 1 of generation 1. Reviewing the other seven stoves, several features quickly become apparent:

- There are many sharp edges (such as in stove (a), at (z,r) coordinates (0.18, 0.02)) which induce turbulence thereby improving mixing, with benefits for both combustion and heat transfer.
- These 'turbulators' tend to come in pairs at the inlet and outlet of the stove (see stoves a, c, d, e and h), creating a region of recirculation. While this is of clear benefit at the outlet, where hot flue gases are in contact with the mogogo plate, the advantage is not so clear at the inlet. Nonetheless, four of the seven stoves have evolved this feature, indicating that it is unlikely to have been selected by chance. One possible explanation is that it further increases turbulence, and this is an effective method of increasing the supply of oxygen into the char bed on the stove floor (Figure 6.8).
- The virgin fuel (region (g) in Figure 6.3, adjoining the centre-line) is a wide flat region, as in stoves c, e, f and h. This configuration will tend to minimise resistance to flow, and result in a relatively small fuel window. This will encourage use of more finely prepared fuel, which is encourages good combustion, but is difficult to prepare (and liable to have an impact on the marketability and saleability of the stove).
- The combustion chamber above the bed of virgin fuel is bracketed by two turbulators to create a region of recirculation, thereby increasing the residence time of flue gases and encouraging complete combustion.

Examples in stoves (e) and (g). Note that the leeward side of a bluff body will generally support a region of recirculation, which is liable to induce regions of shear and turbulence. Thus a bed of fuel is likely to create its own turbulence to help combustion. However the model of the fuel bed is a laminar region, with no source of turbulence. The GA has therefore promoted turbulent mixing in the combustion chamber by including turbulators directly down stream of the virgin fuel region.

- In almost all stoves, the height of the stove (especially the lower region) has been maximised to induce a greater air flow. This overturns concerns raised in Chapter 5 for the sensitivity of the CFD model to changes in height of the stove (Figure 5.10): clearly the model is sensitive to stove height. However it overlooks an aspect that was only briefly touched upon in the preliminary results in Chapter 5. Heat transfer from char to virgin fuel is expected to be dominated by radiation (that char glows is evidence), subject to an inverse square law. Hitherto the quality of the radiation model has not been discussed in great detail, but it appears that this effect has not been accurately captured: practical experience would suggest that few of the stoves in Figure 6.7 would sustain vigorous combustion because the char is too far from the virgin fuel. This highlights serious flaws in the radiation model and preparation of the GA.

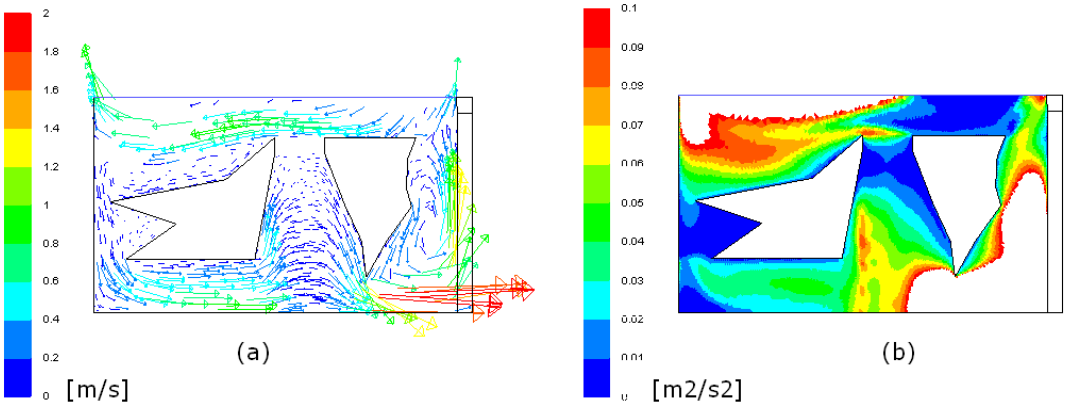

Figure 6.8. Velocity vectors (a) and turbulent kinetic energy (b) for stove (c). The turbulator protruding into the combustion chamber augments buoyancy driven turbulence and the double turbulator at the inlet appears to induce turbulence, with the possible result of improving aeration for the char bed.

The outlet of stove (e) deserves some further attention. A restriction at z = 0.32m creates a high speed jet, improving the impingement heat transfer to the mogogo plate around the stagnation point. At approximately z/d = 1.0, this configuration should have its heat transfer maximum at the stagnation point

(from the predictions of Lytle & Webb, 1991), followed by a reasonably flat characteristic as the jet passes through the stagnation region (r/d < 1.0). There follows a region of recirculation, which should press the jet into firmer contact with the wall, and promote mixing the the flue gases, to maximise heat transfer (though it will also introduce a pressure drop, reducing flow).

The is a second restriction at r = 0.12m followed by a scoop in the region 0.12 < r < 0.20. These two features have the effect of forcing the hot flue gases onto the mogogo plate, introducing tertiary air (Figure 6.9a) and inducing turbulence (not shown). From the plot of volatile mass fraction (Figure 6.9b) it is clear that insufficient air has been drawn in to the stove to allow for complete combustion of the volatile gases within the combustion chamber, and the scoop for tertiary air permits a region of secondary combustion towards the perimeter of the mogogo plate. Both Viskanta (1993) and Chander & Ray (2005) discuss the considerable increase in Nusselt number due to flaming impinging heat transfer (as opposed to inert impinging heat transfer), Viskanta citing radiation as the principal mechanism.

The GA has blindly exploited some useful heat transfer mechanisms to maximise Nusselt number for stove (e), following the predictions of the CFD model. However, returning to the discussions of chapters 4 and 5, there are considerable concerns about the accuracy of the CFD model, notably the prediction of insufficient primary and secondary air and the consequent incomplete combustion of volatile gases within the stove (Figures 5.8 and 5.9 and associated discussion). This would negate the principal advantage of the scoop in stove (e), however it would continue to force the jet onto the bottom of the mogogo plate.

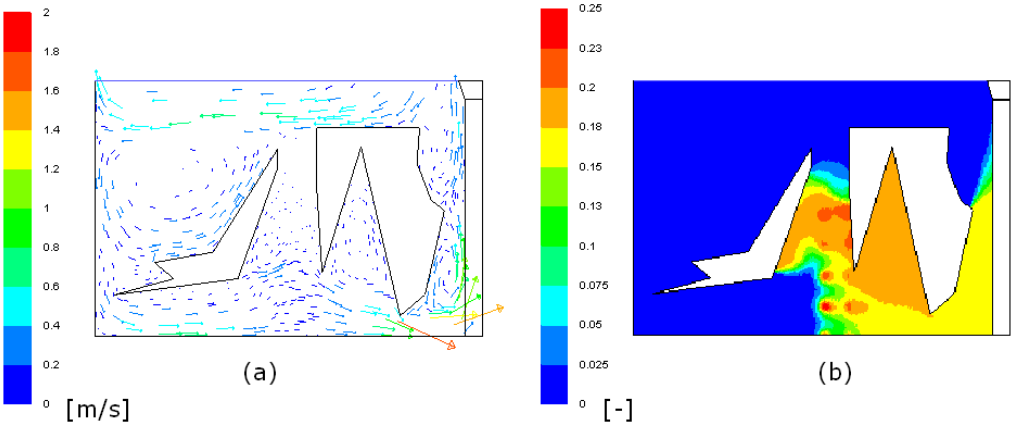

Figure 6.9. Velocity vectors (a) and volatile mass fraction (b) for stove (e).

6.2.3 Champion of Champions & Sensitivity Analysis

Stoves (a) to (h) from Figure 6.7 and two other randomly generated stoves were put head-to-head in three run-offs to produce an optimised stove. One run-off produced a new creature with no features carried over from the initial input stoves (fitness, f_2 = 5850). The other two run-offs yielded slight variations on stove (e), with fitness 6034 and 6090. The highest scoring stove (fitness 6090) is illustrated in Figure 6.10. It features the outlet from stove (e), one turbulator and a recirculation region in the combustion chamber, a wide thin virgin fuel region, a tall lower section, and no turbulators on the inlet, all of which have been discussed above. Errors in heat flux and fuel burn rate for the optimum stove were estimated to be 2% and 40% respectively using the Richardson extrapolation: results concerning the fuel burn rate should be treated with circumspection.

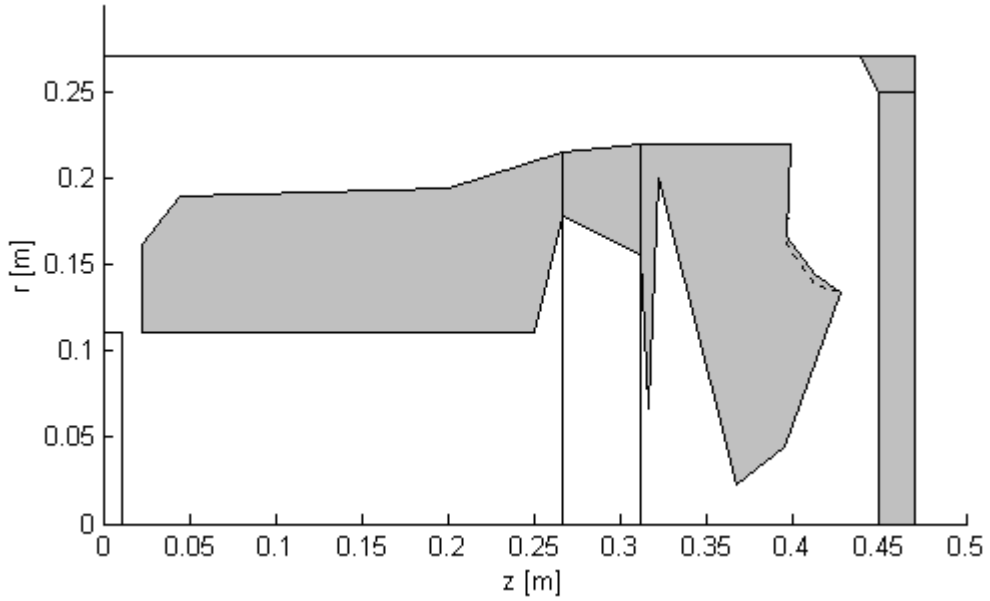

Figure 6.10. Schematic of the best stove proposed by the GA. The dashed line shows an improvement identified by the sensitivity analysis (ref. AA). The x-axis is the rotation of symmetry, the y-axis is the ground and solid material is shown shaded.

The stove was subject to a sensitivity analysis to examine the robustness of the design. Each base of the gene was altered by values of +1 and -1, subject to the range $1 < b < 9$, and the effect on fuel burn rate and heat transfer observed. The nine results of interest are given in Table 6.4 and plotted in Figure 6.11.

Table 6.4. Sensitivity analysis on optimised stove design. The columns b0, b-1 and b+1 represent data at the base value identified by the GA, and bracketed by minus and plus one. Ref. AA improves the fitness of the stove; all others cause a significant reduction.

	Heat Flux [W/m2]			Burn Rate [g/s]			Fitness, f2 [-]			
base	b-1	b0	b+1	b-1	b0	b+1	b-1	b0	b+1	ref.
1	4670	4670	3173	0.41	0.41	1.34	6090	6090	3173	a
2	3528	4670	4504	1.29	0.41	0.37	3528	6090	5663	b
7	3818	4670	4670	0.49	0.41	0.41	3818	6090	6090	c
17	4056	4670	3461	0.33	0.41	0.56	4056	6090	3461	d
24	4670	4670	617	0.41	0.41	1.13	6090	6090	617	e
30	4726	4670	4606	0.37	0.41	0.41	6470	6090	5892	AA
31	4670	4670	1915	0.41	0.41	2.89	6090	6090	1915	f
39	3836	4670	3001	0.40	0.41	0.61	3836	6090	3001	g,h

The modification to base 30 (ref. AA) was the only modification with the effect of increasing fitness. It modified the stove outlet, making the scoop more pronounced (see the dashed line in Figure 6.10). Other modifications caused a deterioration in performance, either through altering the resistance to air flow (modifications a, b and c), by altering the amount of fuel in the stove (modification d), or by altering the convective heat transfer performance (modifications e, f, g and h). It is interesting to note that modifications (g) and (h) both adjust the stove-to-plate clearance, with a dramatic deterioration in performance: clearly this is a very well tuned parameter which would require a very tight tolerance in manufacture. A finer investigation of $1.0 < b_{39} < 2.0$ in 0.25 intervals demonstrated that the maximum heat flux was indeed to be found at $b_{39} = 2.0$, rather than a non-integer value of the base. Other dimensions are relatively insensitive to change in one direction, but very sensitive to change in the other: for robust manufacture of such a stove in it would be prudent to detune most of these parameters slightly (with a small drop in performance) in order to move away from a highly sensitive (but optimum) design condition, thereby making a more robust design.

The stove features a turbulator with a very thin section (z = 0.33 m) and a very thin neck (z = 0.34 m) which supports a massive block of material. It is anticipated that these two features could easily break and render the stove useless, so a further sensitivity analysis was conducted on this region of the stove. Reducing the turbulator size reduces fitness from 6470 to 4220. Removing the turbulator completely results in a further decease to 3980. Clearly the large turbulator is important for mixing and heat transfer: a smaller version is almost

as useless as no turbulator at all, and a final design would have to include some sort of insert in this region to (a) act as the turbulator and (b) strengthen the neck. This is unfortunate as it would significantly alter the price of the resulting stove, and move away from the initial design philosophy that the optimised stove could be manufactured on an ad hoc basis by rural women without specialist training nor recourse to purchasing components. Rouse (2000) has demonstrated that even a relatively cheap component can act as a poverty indicator and is liable to reduce the uptake of any stove. Further work is required to identify a stove design that does not require any additional components.

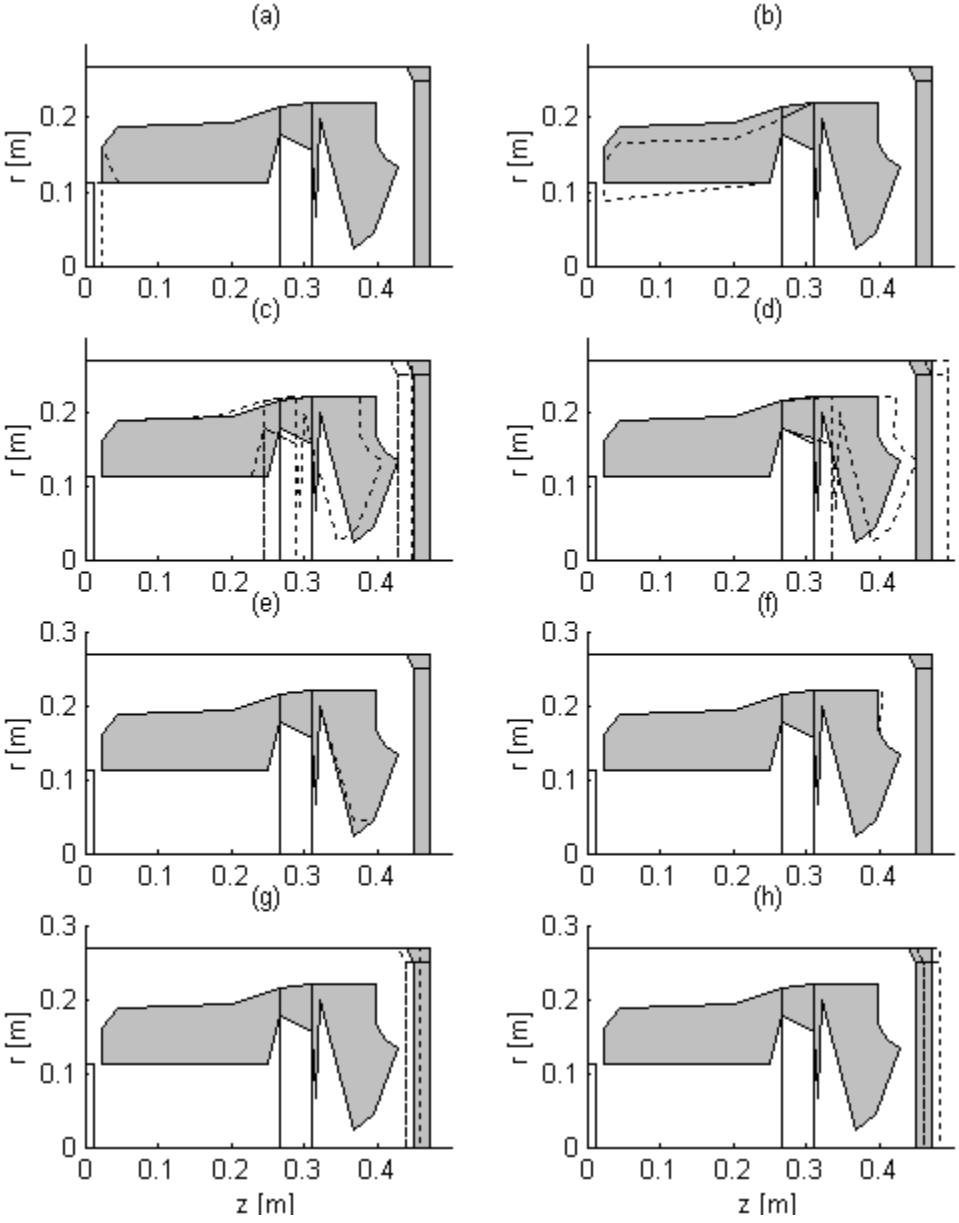

Figure 6.11. Schematic of modifications (a) to (h) identified by the sensitivity analysis as most detrimental to heat transfer rate. The optimum stove is shown in solid line, and the modification is shown in dashed.

6.3 SUMMARY AND CONCLUSION

A genetic algorithm has been used to optimise a mogogo stove in terms of heat flux and fuel burn rate. An initial investigation has demonstrated that although novel, the mesh-deformation method for converting the GA gene to a CFD mesh is inappropriate because it results in a very stable mesh that is insensitive to changes in the gene: the vector-geometry method (Hilbert et al., 2006) is more robust and moves through the solution space far more rapidly. The choice of objective function is critical to attaining the desired output from the GA. The use of a single processor to run the GA (and specifically to run CFD cases to evaluate the objective function) has resulted in glacial progress. It would have been of considerable interest to investigate variations on the current GA, such as modifying the structure of the VGM, use of a larger population, use of multiple cross-over points in the mating algorithm etc., however resources did not allow it. Turning now to the solution itself, the GA has proposed an optimised stove which uses commonly understood features: maximising time, temperature and turbulence (Bryden et al., 2005) and use of impinging and wall jet heat transfer (Viskanta, 1993). The proposed stove achieves the target cooking heat rate (997W, while the target was 1000W), using fuel at a rate of 0.6 g/s. This performance is equivalent to 12% efficiency or specific fuel consumption 0.4 kg fuel per kg food, compared to 0.5 for the classic mogogo or 0.27 for the ERTC mogogo. This result has not been experimentally verified, and should be viewed with circumspection given the shortcomings of the CFD model. Nonetheless, the proposed stove requires only one bought component, with an estimated cost US$ 1, which compares favourably to the cost of the optimised ERTC mogogo (US$ 40), and in that respect it has realised the requirements of the project. Considerable further work is required to adapt the design to manufacturing requirements and to successfully bring it to market in Eritrea.

CHAPTER 7: CONCLUSIONS & RECOMMENDATIONS

A mogogo stove for Eritrea has been optimised using computational fluid dynamics and genetic algorithms. Several secondary objectives have been realised in the course of the work:

- A review has been conducted of literature concerning experimental and numerical techniques relevant to stove optimisation (Chapter 2). The review found that models are in place for combustion (e.g. devolatalisation, homogenous and heterogeneous combustion, radiation and convection heat transfer), but not in a format that can be easily and cheaply exploited in conjunction with a genetic algorithm. It was therefore necessary to develop a new fuel devolatalisation model. Similarly, experimental techniques are in place to assess the efficiency of cooking stoves (e.g. water boiling test), but none that could simultaneously quantify fuel burn rate and heat transfer to the cooking vessel (since both currently rely on weight loss). It was therefore necessary to modify an existing technique: fuel burn rate was measured though mass loss of the whole stove assembly, and heat gain to the pot was assessed by monitoring rate of change of temperature.
- A model of wood combustion was developed (Chapter 3). The model assumed that fuel devolatalisation was limited by the transfer of heat though the fuel char layer, and that char combustion was limited by the supply of oxygen through the species boundary layer. A structured experiment was used to provide data on fuel burn rate and temperature profile in the flame above the fixed bed of fuel. The model gave mean error of 16% and 30% in fuel burn rate and excess temperature in the flame respectively, and is good agreement with burn rates from literature (Croce & Xin, 2005).

- A CFD model was developed of an inert turbulent buoyant plume above a heat source (Appendix B). The model predicted the axial and radial rates of decay of temperature and velocity above the heat source, in agreement with an analytical solution (Rouse et al., 1952).
- A secondary investigation was carried out to quantify the resistance to flow presented by a structured bed of wood (Appendix C). The results demonstrated that flow resistance was anisotropic, but in broad agreement with a prediction from literature (Ergun, 1952).
- A structured experiment was carried out to quantify convective heat transfer due to an impinging jet at low jet-to-plate clearances (Chapter 4). The results are in agreement with literature (Lytle & Webb, 1991), despite crude apparatus. A CFD model using the k-ε model correctly simulated the average heat transfer to the plate, though the position of the secondary maximum was not correctly modelled due to the assumption of anisotropic turbulence under the nozzle.
- A series of secondary experiments were conducted to estimate fuel proximate analysis (Appendix D: moisture, 10%; volatile content, 75%; char and ash, 15%; wood calorific value, 19 MJ/kg; char calorific value, 30 MJ/kg; char inertial flow resistance, 815 m^{-1}) and thermal properties of the mogogo plate (Appendix E: thermal conductivity, 0.41 W/m.K; specific heat capacity, 900 J/kg.K).
- A structured experiment was carried to evaluate the effect of changing the geometry of a rocket-type stove (Chapter 5). A simplified analytical model of the stove was shown to be inadequate, principally due to the assumption that the stove behaved as a well-stirred reactor. A CFD model was developed, incorporating the fuel sub-model discussed above. The model predicted the trends found in experimental results, with some notable exceptions: the model was found to be relatively insensitive to changes in stove height; the model was found to be over-sensitive to changes in stove diameter; the model did not include a soot-formation sub-model, leading it to under-predict radiation heat transfer between fuel, flame and walls.
- A mogogo stove was constructed and used to estimate the fuel consumption and efficiency of a base-line stove (Appendix F). The stove was operated by members of the Eritrean community in Nottingham, and results showed it to be less efficient that tests on other mogogo stoves in Eritrea (4-7%, compared to 10% for the traditional mogogo; van Buskirk, 2004), but comparable to other open fires (Ballard-Tremeer, 1996).

- A genetic algorithm was developed to optimise the internal structure of a mogogo stove (Chapter 6, Appendix G). The GA used the CFD model developed in Chapters 3, 4 and 5 to evaluate the objective function. The resultant stove evolved many features known to improve combustion and heat transfer, such as increased residence time for flu gases, increased turbulence and recirculation zones. (Bryden et al., 2005; Viskanta, 1993), and is estimated to double efficiency over the base-line stove, while only incurring a small cost penalty (estimated to be 1 US$).

7.1 LIMITATIONS AND RECOMMENDATIONS FOR FURTHER WORK

The finite extent of this project has required that some aspects of work be overlooked. Future work on stove optimisation should examine some or all of the following, starting with aspects of numerical modeling:

- The CFD work in this thesis has ignored the swirl component of flow in the stove. Swirl has been demonstrated to improve combustion at all scales from the Vesto stove (Pemberton-Piggot, 2005) to tangentially-fired utility boilers, by increasing residence time of flu gases in the combustion chamber and below the heat transfer surface and by reducing the risk of flame attachment to walls.
- CFD work has also ignored soot formation and combustion in the flame. Soot adds significantly to the radiation load, and would have helped predict the correct heat transfer from char to virgin fuel and from flame to mogogo surface. A simple but robust soot model for biomass combustion would add significantly to this and other work as biomass enjoys a revival in the UK fuel mix.
- The simplified chemistry of wood combustion employed in this thesis has been adequate, but further increases in accuracy could be made by using two- or three-step devolatalisation mechanisms available in the literature, and by employing more subtle models of flaming combustion. Indeed, the latter is likely to be a prerequisite for the soot formation model discussed above.

Looking further afield, the following recommendations are made for stove programs:

- The wood used as fuel in this research was sourced from European softwood. While most woody biomass is comparable in its ultimate and proximate analysis, the reactivity of different wood species is known to differ widely and be catalyzed by trace elements (Jones et al., 2007). It would therefore have been appropriate to source samples of typical

Eritrean wood species to conduct the wood combustion experiments in Chapter 3 and the stove geometry experiments in Chapter 5.

- The objective function for the genetic algorithm in Chapter 6 should be extended to include the total life-cycle cost of the stove. This should include the cost measured in days for: sourcing found materials, working to earn money for bought materials; training and construction; collecting fuel (based on a duty cycle of cooking events per month and expected life of the stove); ill-health in the household due to exposure to pollutants (requiring the more detailed chemistry and soot models discussed above).
- The stove proposed in Chapter 6 of this thesis should be evaluated in the laboratory, and taken to Eritrea for dissemination. The current political climate in Eritrea is not conducive to international non-governmental organizations, however the National Union of Eritrean Women (NUEW) is a quasi-autonomous non-governmental organization (QUANGO) that enjoys some security and authority, and is in an ideal position to roll out a stove program 'by women for women'. This is the most likely route to a successful low-cost stove program in Eritrea.
- While this PhD program has gone some way to achieving its aim of producing an optimized mogogo stove, an experimentally based program based in Eritrea is likely to have made significantly more progress. Numerical modeling of combustion is an extremely complex process (Torero, 2007), and future stove optimisation programs should be based in the country of interest and only involve numerical modeling as a last resort or to resolve very precisely defined aspects of the optimisation process.

7.2 ORIGINAL CONTRIBUTION OF THE THESIS

Aspects of the work that have demonstrated 'the creation and interpretation of new knowledge… at the forefront of an academic discipline' (University of Nottingham, 2008) are:

- the numerical model of wood combustion, which predicts the devolatalisation rate in terms of bed temperature and the char combustion rate in terms of the free-stream oxygen concentration;
- the lumpiness function to group fuel surfaces into a regular heterogeneous matrix in the fuel bed, thereby allowing diffusion limited volatile combustion;
- the use of a metal disc in lieu of a cooking pot to assess heat transfer in a stove optimisation project;

- the application of a genetic algorithm to optimize not only heat transfer, but also combustion conditions within a stove for the developing world;
- the application of dynamic relaxation during mesh deformation to convert a GA gene into a CFD mesh.

Work in this thesis has also yielded two conference papers (Burnham-Slipper et al., 2007a, 2007b).

APPENDIX A: REFERENCES

AHUJA DR et al., 1987. Thermal performance and emission characteristics of unvented biomass-burning cookstoves: a proposed standard method for evaluation. Biomass 12(4):247-270.

ANDREATTA D, 2004. A report on some heat transfer experiments [on-line]. Eugene, OR: BioEnergy Lists. Available at: <info.bioenergylists.org> [accessed 26th April 2008].

APROVECHO, 2007. Design principles for wood burning cook stoves [online]. Eugene, OR: Aprovecho. Available at: <www.aprovecho.org> [accessed 3rd August 2007].

APROVECHO, no date. Aprovecho's stove research page [on line]. Eugene, OR: Aprovecho. Available at: <www.efn.org/~apro/AT/attitlepage.html> [accessed 9th February 2005].

ARTHUR, 1951. Modelling reactions between carbon and oxygen. Trans. Faraday Society 47:164-178.

ATREYA A, 1998. Ignition of fires. Philosophical Transactions of the Royal Society, 356:2787-2813.

BACKREEDY RI et al., 2006. Modelling pulverised coal combustion using a detailed coal combustion model. Combustion Science and Technology 178: 763-787.

BAILIS R et al., 2004. The Water Boiling Test. Household Energy and Health Programme, Shell Foundation. Available at: <ehs.sph.berkeley.edu> [accessed 27th January 2005]

BALLARD-TREMEER G & JAWUREK HH, 1996. Comparison of five rural, wood-burning cooking devices: Efficiencies and emissions. Biomass and Bioenergy, 11(5):419-430.

BALLARD-TREMEER G & JAWUREK HH, 1999a. The "hood method" of measuring emissions of rural cooking devices. Biomass and Bioenergy 16(5):341-345.

BALLARD-TREMEER G & JAWUREK HH, 1999b. Evaluation of the dilution chamber method for measuring emissions of cooking devices. Biomass and Bioenergy, 17(6):481-494.

BEJAN A, 1993. Heat transfer. New York: Wiley & Sons.

BEJAN A, 2004. Convection Heat Transfer (3rd edition). John Wiley & Sons, Hoboken, NJ, USA.

BELLAISA M et al., 2003. Pyrolysis of large wood particles: a study of shrinkage importance in simulations. Fuel 82:1541–1548.

BHATTACHARYA SC, ALBINA DO & KHAING AM, 2002. Effects of selected parameters on performance and emission of biomass-fired cookstoves. Biomass and Bioenergy 23(5):387-395.

BHATTACHARYA SC, ALBINA DO & SALAM PA, 2002. Emission factors of wood and charcoal-fired cookstoves. Biomass and Bioenergy 23(6):453-469.

BRUCH C, PETERS B & NUSSBAUMER T, 2003. Modelling wood combustion under fixed bed conditions. Fuel 82:729–738.

BRYDEN KM & MCCORKLE DS, 2004. Evolutionary optimization of energy systems using population graphing and neural networks. Advances in Engineering Software 35:289–299.

BRYDEN KM et al., 2000. A study of the effectiveness of a plancha stove: preliminary results. In: International Conference on Biomass-based fuels and cooking systems.

BRYDEN KM et al., 2002. Modelling thermally thick pyrolysis of wood. Biomass and Bioenergy 22:41-53.

BRYDEN KM et al., 2003. Optimization of heat transfer utilizing graph based evolutionary algorithms. International Journal of Heat and Fluid Flow 24:267–277.

BRYDEN KM et al., 2005. Design Principals for wood burning cook stoves [online]. Eugene, Oregon: Aprovecho Research Centre. Available at <www.aprovecho.net> [accessed 25th April 2008].

BRYDEN KM, RAGLAND KW & RUTLAND CJ, 2000. Modelling thermally thick pyrolysis of wood. Biomass and Bioenergy, 22, 41–53.

BURNHAM-SLIPPER H et al., 2007a. A simplified wood combustion model for use in the simulation of cooking fires. In: 5th Int. Conf. Heat Transfer, Fluid Mechanics and Thermodynamics, Sun City, South Africa.

BURNHAM-SLIPPER H et al., 2007b. Jet impingement heat transfer for low nozzle-to-plate clearances. In: Proceedings of 10th UK National Heat Transfer Conference. Edinburgh, 10-11 September 2007.

BUTCHER SS et al., 1984. Emission factors and efficiencies for small-scale open biomass combustion: towards standard measurement techniques. In: Annual Meeting of the American Chemical Society.

CAI G et al., 2007. Performance prediction and optimisation for liquid rocket engine nozzle. Aerospace Science and Technology 11:155-162

CENTRAL INTELLIGENCE AGENCY (CIA), 2005. The World Factbook [online]. Washington: CIA. Available at: <www.cia.gov> [accessed 26th April 2008].

CROCE & XIN, 2005. Scale modelling of quasi-steady wood crib fires in enclosures. Fire Safety Journal 40:245-266.

CUSSLER EL, 1997. Diffusion: mass transfer in fluid systems (2nd edition). Cambridge: Cambridge University Press.

DAUGAARD DE & BROWN RD, 2003. Enthalpy for pyrolysis of several types of biomass. Energy & Fuels 17:934-939.

DAVIES J, 2005. Radiative heat transfer. Stove Digest [on line], 7(16), 4 (18 Feb). Available at: stoves@listserv.repp.org.

DE SOUZA COSTA F & SANDBERG D, 2004. Mathematical model of a smoldering log. Combustion and Flame 139:227–238.

DEMIRBAS, 2004. Combustion characteristics of different biomass fuels. Prog. Energy Comb. Sci. 30:219-230.

DENISON MK & WEBB BW, 1993. A Spectral Line-Based Weighted-Sum-of-Gray-Gases Model for Arbitrary RTE Solvers. J. Heat Transfer, 115:1002-1012.

DI BLASI C, 1993. Modelling and simulation of combustion processes of charring and non-charring solid fuels. Progress in Energy and Combustion Science 19(1):71-104.

DI BLASI C, 1993. Modelling and simulation of combustion processes of charring and non-charring solid fuels. Prog. Energy Combust. Sci. 19:71-104.

DIAS T AND MILANEZ LF, 2006. Optimal location of heat sources on a vertical wall with natural convection through genetic algorithms. International Journal Heat Mass Transfer 49:2090-2096

DRYSDALE D, 2004. An introduction to fire dynamics. Chichester: John Wiley & Sons.

EPSTEIN B, PEIGIN S AND TSACH S, 2006. A new efficient technology of aerodynamic design based on CFD driven optimisation. Aerospace Science and Technology 10:100-110.

ERGUN S, 1952. Fluid Flow through Packed Columns. *Chem. Eng. Prog.*, 48(2):89-94.

FELDMAN J, 1999. The Richardson Extrapolation [online]. Vancouver: The University of British Columbia. Available at: <www.math.ubc.ca/~feldman> [accessed 3.5.7].

FLUENT, 2007. Fluent 6.2 Documentation. Lebanon, NH: Fluent Inc.

FREDLAND B, 1993. Modelling of heat and mass transfer in wood structures during fire. Fire Safety Journal 20:39-69.

FRIEDL et al., 2005. Prediction of heating values of biomass fuel from elemental composition. Analytica Chimica Acta 544:191-198.

GARDON R AND COBONPUE J, 1962. Heat transfer between a flat plate and jets impinging on it. International Developments in Heat Transfer, Second Int. Heat Trans. Conf., pp. 454-460, ASME, New York.

GELLER HS, 1982. Cooking in the Ungra area: Fuel efficiency, energy losses, and opportunities for reducing firewood consumption. Biomass 2(2):83-101.

GEORGE WK, ALPERT RL & TAMANINI F, 1977. Turbulence measurements in an axisymmetric buoyant plume. Int. J. Heat Mass Transfer 20:1145-1154.

GESELLSCHAFT FUR TECHNISCHE ZUSAMMENARBEIT (GTZ), 2008. GTZ in Ethiopia [online]. Escborn, Germany: GTZ. Available at: <www.gtz.de> [accessed 26th April 2008].

GHEBREHEWIT D, 2002. Very high efficiency wood and dung mogogo in Eritrea. Physica Scripta, 97:110-112.

GTZ, no date. A guide to make your own Maendeleo one-pot jiko [on line]. Available at: <www.gaia-movement.org> [accessed 15th February 2005].

GUPTA S et al., 1998. Emission factors and thermal efficiencies of cooking biofuels from five countries. Biomass and Bioenergy, 14(5-6):547-559.

HEALTH CANADA, 1995. Exposure guidelines for residential indoor air quality [on-line]. Ottawa: Health Canada. Available at: <www.hc-sc.gc.ca> [8.4.5].

HEDON, 2008. Sustainable scaling up of the dissemination of the Mirt stove in Ethiopia [online]. London: HEDON. Available at: <www.hedon.info> [accessed 26th April 2008].

HELPS INTERNATIONAL, 2005. Stove site [on line]. Guatemala: HELPS International. Available at: <www.fni.com/~dononeal> [9.2.5].

HILBERT R et al., 2006. Multi-objective shape optimisation of a heat exchanger using parallel genetic algorithms. Int. J. Heat Mass Transfer 49:2567-2577.

HOLLAND JH, 1975. Adaptation in Natural and Artificial Systems. Ann Arbour: University of Michigan Press.

HOLMAN JP, 1992. Heat Transfer (7th edition). London: McGraw-Hill.

HOU SS & KO YC, 2004. Effects of heating height on flame appearance, temperature field and efficiency of an impinging laminar jet flame used in domestic gas stoves. Energy Conversion and Management 45:1583–1595.

HRYCAK P, 1983. Heat transfer from round impinging jets to a flat plate. Int. J. Heat Mass Transfer 26(12):1857-1865.

JAMBUNATHAN K et al., 1992. A review of heat transfer data for single circular jet impingement. International Journal of Heat and Fluid Flow 13(2):106-115.

JONES JM et al., 2007. An investigation of the thermal and catalytic behavior of potassium in biomass combustion. In: Proceedings of the Combustion Institute 31:1955-1963.

JOSHI V, VENKATAMARAN C & AHUJA DR, 1989. Emissions from burning biofuels in metal cookstoves. Environmental Management 13(6):763-772.

JOSHI V, VENKATAMARAN C & AHUJA DR, 1991. Thermal performance and emissions characteristics of biomass-burning heavy stoves with flues. Pacific & Asian Journal of Energy 1:1-19.

LARFELDT J, LECKNERA B & MELAAEN MC, 2000a. Modelling and measurements of heat transfer in charcoal from pyrolysis of large wood particles. Biomass and Bioenergy 18:507-514.

LARFELDT J, LECKNERA B & MELAAEN MC, 2000b. Modelling and measurements of the pyrolysis of large wood particles. Fuel 79:1637-1643.

LAUNDER BE AND SPALDING DB, 1974. The Numerical Computation of Turbulent Flows. *Computer Methods in Applied Mechanics and Engineering*, 3:269-289.

LOWDES IS, 2007. The computational modelling of flame spread along a conveyor belt. Fire Safety Journal 42: 51-67.

LYTLE D & WEBB B W, 1991. Secondary heat transfer maxima for air jet impingement at low nozzle-to-plate spacing, in Experimental heat transfer, Fluid Mechanics and Thermodynamics, 1991, Keffer JF, Shah RK and Ganic EN (eds), pp 776-783, Elsevier, New York.

MAGNUSSEN BF & HJERTAGER BH, 1976. On mathematical models of turbulent combustion with special emphasis on soot formation and combustion. In: 16th Symp. (Int'l.) on Combustion. The Combustion Institute, 1976.

MCCRACKEN J & CHARRON D, 2003. Evaluation of the Efficacy and Effectiveness of the EcoStove [online]. Available at: <ceihd.berkeley.edu> [accessed 25th January 2005].

MODEST MF, 1993. Radiative heat transfer. New York: McGraw Hill.

MURTHY JY AND MATHUR SR, 1998. A Finite Volume Method For Radiative Heat Transfer Using Unstructured Meshes. AIAA-98-0860.

NAEHER LP, 2001. Carbon monoxide as a tracer for assessing exposure to particulate matter in wood and gas stoves in highland Guatemala. Environmental Science & Technology 35:575-581.

NDIEMA CKW, MPENDAZOE FM & WILLIAMS A, 1998. Emissions of pollutants from a biomass stove. Energy conservation Management 39(13):1357-1367.

NIST, 2007. NIST/SEMATECH e-handbook of statistical methods [online]. <www.itl.nist.gov/div898/handbook> [accessed 30th May 2007].

OHLEMILLER TJ, 1985. Modelling of smouldering combustion propagation. Prog. Energy Combust. Sci. 11:277-310.

PEMBERTON-PIGOTT C (crispin@newdawn.sz), 2005. RE: Ethiopian & Eritrean stoves (14.2.5). Email to: Burnham-Slipper H (eaxhb@nottingham.ac.uk).

PEMBERTON-PIGOTT C, 2004. VESTO: the variable energy stove [on-line]. Swaziland: New Dawn Engineering. Available at: <www.newdawnengineering.com> [accessed 14.2.5].

PETERS B & BRUCH C, 2003. Drying and pyrolysis of wood particles: experiments and simulation. J. Anal. Appl. Pyrolysis 70:233-250.

RAVI MR, KOHLI S & RAY A, 2002. Use of CFD simulation as a design tool for biomass stoves. Energy for Sustainable Development 6(2):20-27.

REINA et al., 1998. Thermogravimetric study of the pyrolysis of waste wood. Thermochimica Acta 320:161-167.

ROSS AB et al., 2005. A study of different soots using pyrolysis-GC-MS and comparison with solvent extractable material. Journal of Analytical and Applied Pyrolysis 74:494-501.

ROUSE H, YIH CS & HUMPHREYS HW, 1952. Gravitational convection from a boundary source. Tellus 4:201-210.

ROUSE J, 2000. Clay grate development in Chibau Khera, India. Boiling Point 20:35-37.

SAAD et al., 1977. Prediction of heat transfer under axisymmetric laminar impinging jet. Ind. Eng. Chem. Fundam. 16:148-154.

SCHUMAKER, 1973. Small is Beautiful. London: Pergamon.

SCOTT P, 2006. Rocket stoves for sub-Saharan Africa. Boiling Point 50:7-8.

SHABBIR A & GEORGE WK, 1994. Experiments on a round turbulent buoyant plume. J. Fluid Mechanics 275:1-32.

SPARROW E M AND LOVELL B J, 1980. Heat transfer characteristics of an obliquely impinging circular jet. J. Heat Transfer 102:202-209.

SPEARPOINT MJ & QUINTIERE JG, 2000. Predicting the Burning of Wood Using an Integral Model. Combustion and Flame 123:308–324.

STILL D, 1999. From lorenta to estufa: rethinking the Latin American stove [on-line]. Eugene, OR: Aprovecho. Available at: <www.aprovecho.net> [14.2.5].

THUNMAN H & LECKER B, 2002a. Thermal conductivity of wood: models for different stages of combustion. Biomass and Bioenergy 23:47-54.

TORERO JL, 2007. Heat and mass transfer in fires: scaling laws and their applications. In: Proceedings of 10th UK National Heat Transfer Conference. Edinburgh, 10-11 September 2007.

UNITED NATIONS DEVELOPMENT PROGRAMME (UNDP), 2004. Human Development Report 2004: Cultural Liberty in Today's Diverse World [on-line]. New York: UNDP. Available at: <hdr.undp.org> [accessed 30th April 2005].

UNIVERSITY OF NOTTINGHAM, 2008. University of Nottingham Qualifications Framework: Appendix A [online]. Nottingham: University of Nottingham. Available at: <www.nottingham.ac.uk> [accessed 26th April 2008].

URBAN GL, BRYDEN KM & ASHLOCK DA, 2002. Engineering optimization of an improved plancha stove. Energy for Sustainable Development 6(2):9-19.

VAN BUSKIRK, 2004. Private communication.

VAN BUSKIRK, nd. Eritrean stove efficiency [on line]. Berkley, USA: Punchdown. Available at: <www.punchdown.org> [accessed 9 February 2005].

VAN MAELE K & MERCI B, 2006. Application of two buoyancy-modified k-ε turbulence models to different types of buoyant plumes. Fire Safety Journal 41:122-138.

VERSTEEG HK & MALALALSEKERA W, 2007. An introduction to computational fluid dynamics: the finite volume method. London: Longman.

VISKANTA R, 1982. Radiation heat transfer: interaction with conduction and convection and approximate methods in radiation. In: Grigull et al., ed. Heat Transfer. Washington DC: Hemisphere, pp. 103-120.

VISKANTA R, 1993. Heat transfer to impinging isothermal gas and flame jets. Experimental Thermal and Fluid Science, 6(2):111-134.

WINTER F, 1995. Single fuel particle and NOx/N2O emission characteristics under circulating fluidised bed combustor conditions. PhD thesis, University of Technology, Vienna.

ZHANG et al., 1999a. Carbon monoxide from cookstoves in developing countries: 1. emission factors. Chemosphere, 1(1):353-366.

ZHANG et al., 1999b. Carbon monoxide from cookstoves in developing countries 2: exposure potential. Chemoshere, 1(1):367-375.

ZHANG et al., 2000. Greenhouse gases and other airborne pollutants from household stoves in China: a database for emission factors. Atmospheric Environment, 34(26):4537-4549.

APPENDIX B: TURBULENT BUOYANT PLUMES

In chapter 3 a model is developed of flaming combustion above a fixed bed of fuel. While the thrust of the chapter is directed towards the behaviour of the solid fuel in the fixed bed, it is also necessary to correctly predict the velocity and temperature profile in the buoyant plume above the fuel, so that (a) the rate that oxygen is drawn into the fixed bed is correctly predicted and (b) the rate of heat transfer to a surface above the fixed bed is also correctly predicted. This appendix presents work to demonstrate that the k-ε model of Fluent 6.2 can correctly resolve the temperature and velocity fields. Data from CFD simulations is compared to experimental data from literature, and it is concluded that the standard k-ε model is adequate.

B.1 INTRODUCTION

Buoyancy driven flow is caused by temperature differences (and therefore density differences) within the fluid. This may be exemplified by the plume of smoke rising from a burning cigarette in quiescent air: heat supplied to the fluid directly surrounding the hot tip causes it to expand and applies a buoyancy force which drives the air up. The initial motion is laminar, as demonstrated by the clearly uninterrupted filaments of smoke, but as the height increases, the laminar regime breaks down and is replaced by a divergent turbulent plume of eddies. It is the fields of temperature and velocity within this type of plume that is of interest in this investigation.

Rouse et al. (1952) used a hot air gun embedded in the floor to create a plume, and surrounded it with a mesh to reduce external disturbances. They took measurements of the temperature and velocity fields using thermocouples and specially constructed vane anemometers. Defining the buoyancy produced per unit time at the source,

$$F_0 = 2\pi \int_0^\infty \overline{wg} r dr \tag{B.1}$$

and local buoyancy,

$$\overline{g} = g\left(1 - \frac{T_0}{T}\right) \tag{B.2}$$

the distributions of vertical velocity, $\overline{w}$, and local buoyancy, $\overline{g}$ (analogous to temperature), were given by:

$$\overline{w} = 4.7\left(F_0 / z\right)^{1/3} \exp\left(-96r^2 / z^2\right) \tag{B.3}$$

$$\overline{g} = 11.0\left(F_0^{\,2} / z^5\right)^{1/3} \exp\left(-71r^2 / z^2\right) \tag{B.4}$$

where z is the axial height above the heat source and r is the radial distance from the centre-line. It is clear that both excess temperature and velocity decay as power law functions as height along the centre-line increase, and that both decay as a Gaussian distribution as the radial distance increases.

George et al. (1977) made a very similar investigation, using hot wires for both temperature and velocity readings. They reported the following correlations for velocity and buoyancy:

$$\overline{w} = 3.4\left(F_0 / z\right)^{1/3} \exp\left(-55r^2 / z^2\right) \tag{B.5}$$

$$\overline{g} = 9.1\left(F_0^{\,2} / z^5\right)^{1/3} \exp\left(-65r^2 / z^2\right) \tag{B.6}$$

giving slightly lower values for temperature and velocity on the centre line, but a broader plume. Other investigators (Nakagome & Hirata, Papanicolaou & List, Chen & Rodi; see Shabbir & George, 1994) report very similar results.

Van Maele & Merci (2006) used these experimental results (as well as other canonical flows) to investigate the accuracy of various turbulence models, concluding that the realizable k-ε model performed best (not surprising, given that this model was built to overcome the inadequacies of the standard k-ε model concerning circular jets).

Moving away from the axisymmetric case of a heat source on a boundary, several authors have investigated turbulent plumes above a line heat source, including Frostrum & Sparrow (1967) and Gebhart et al. (1970).

The current investigation aims to replicate some of Van Maele & Merci's work in order to evaluate which flavour of the k-ε model is most accurate, and evaluate the error incurred by the model. Note that the results of the model are not valid near small values of z (i.e. directly above a bed of fuel), due to the disturbance of individual structures within the source, but far from the heat source results are expected to be valid.

B.2 MODEL FORMULATION

Equations for the continuity of mass, momentum, enthalpy, turbulent kinetic energy and dissipation of turbulent kinetic energy (equations 3.1 to 3.5) were solved using Fluent 6.2. Two formulations of the turbulence model were used: the standard and realisable k-ε models. The realisable k-ε model differs from the standard version in two respects: firstly the model constant C_μ is sensitised to turbulence and deformation of the flow; secondly the continuity equation for dissipation of turbulent kinetic energy (c.f. 3.5) is modified to:

$$\frac{\partial}{\partial x_i}(\rho\varepsilon u_i) = \frac{\partial}{\partial x_j}\left[\left(\mu_m + \frac{\mu_t}{\sigma_\varepsilon}\right)\frac{\partial \varepsilon}{\partial x_j}\right] + \rho C_1 S_\varepsilon - \rho C_2 \frac{\varepsilon^2}{k+\sqrt{\nu\varepsilon}} + C_{1\varepsilon}\frac{\varepsilon}{k}C_{3\varepsilon}G_b + S_\varepsilon \tag{B.7}$$

Density was modelled as an incompressible ideal gas; pressure discretization used the body-force-weighted scheme; all other variables were discretized with first order upwind; pressure-velocity coupling used the SIMPLE scheme.

The experimental apparatus of Rouse et al. (1952) was modelled using an axisymmetric domain of 4870 triangular cells (Figure B.1). The domain was 1 m radius, 3 m high, with a pressure inlet to model the ingress and egress of fluid to atmosphere, and a wall with a 64 mm nozzle embedded in it to model the floor. Air that entered the domain from atmosphere was assumed to have turbulent kinetic energy of 1e-6 m2/s2 and a turbulent energy dissipation rate of 1e-9 m2/s3 and temperature of 300 K. Air from the hot air gun in the floor was released at 573 K and 0.67 m/s with a turbulent intensity of approximately 0.5%.

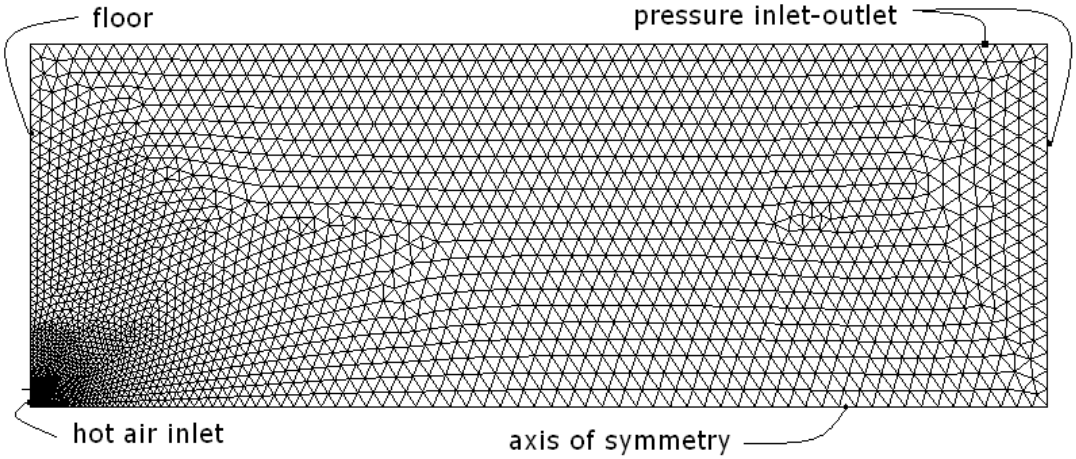

Figure B.1. Axi-symmetric computational domain.

B.3 RESULTS & DISCUSSION

Figure B.2 and Figure B.3 show flow conditions on the centre-line of the plume. It is clear that both k-ε models correctly predict the rate of decay of both velocity and temperature as height above the source increases. Figure B.4 shows three profiles of normalised velocity (define as $\overline{w}\left(z / F_0\right)^{1/3}$) at three heights above the source. It is clear that both models show scaleable results, with the standard k-ε model most closely aligned to the data of George et al, while the realisable k-ε model is most closely aligned with Rouse et al. Meanwhile, normalised temperatures (defined as $g\beta\Delta T\left(z^5 / F_0{}^2\right)^{1/3}$) at the same three heights are shown in Figure B.5: again the results show that the temperature profile is scalable, though there is a large spread of results near the centre of the plume (η<0.1), especially for the realisable k-ε model, resulting in an over-prediction of temperatures near the centre-line.

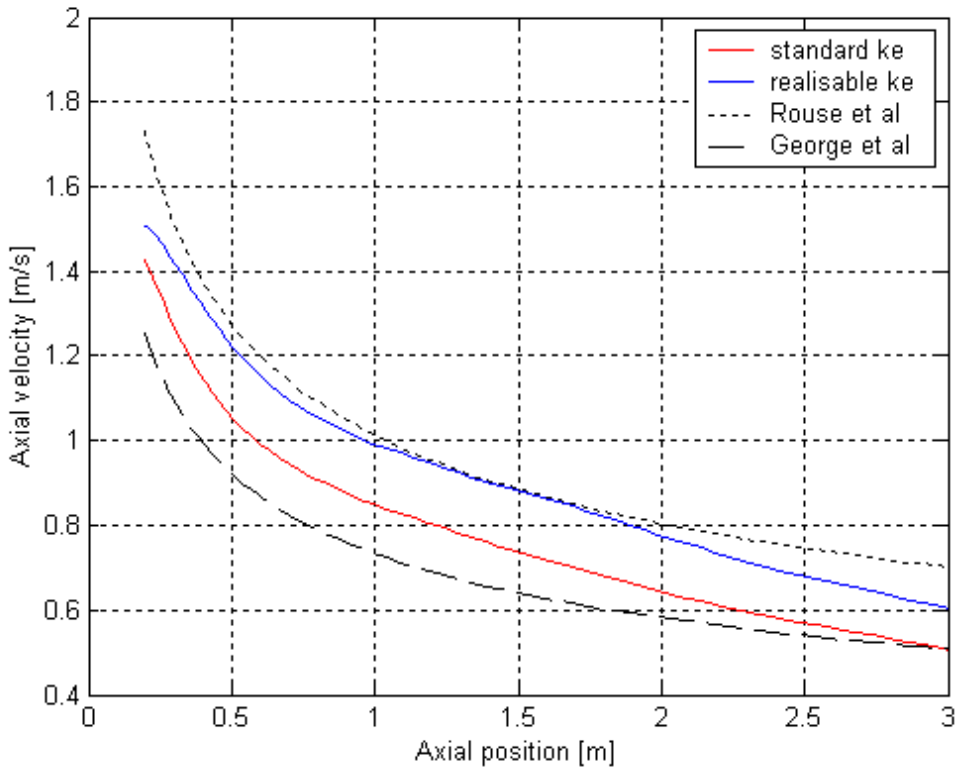

Figure B.2. Axial velocity as a function of height above the source.

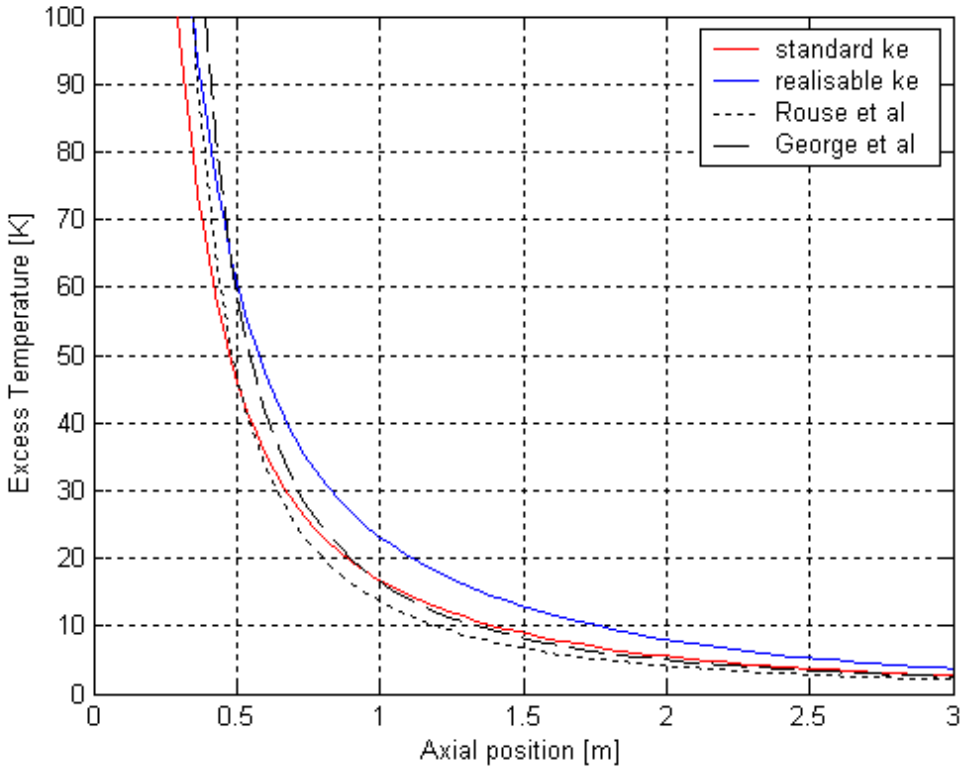

Figure B.3. Excess temperature as a function of height above the source.

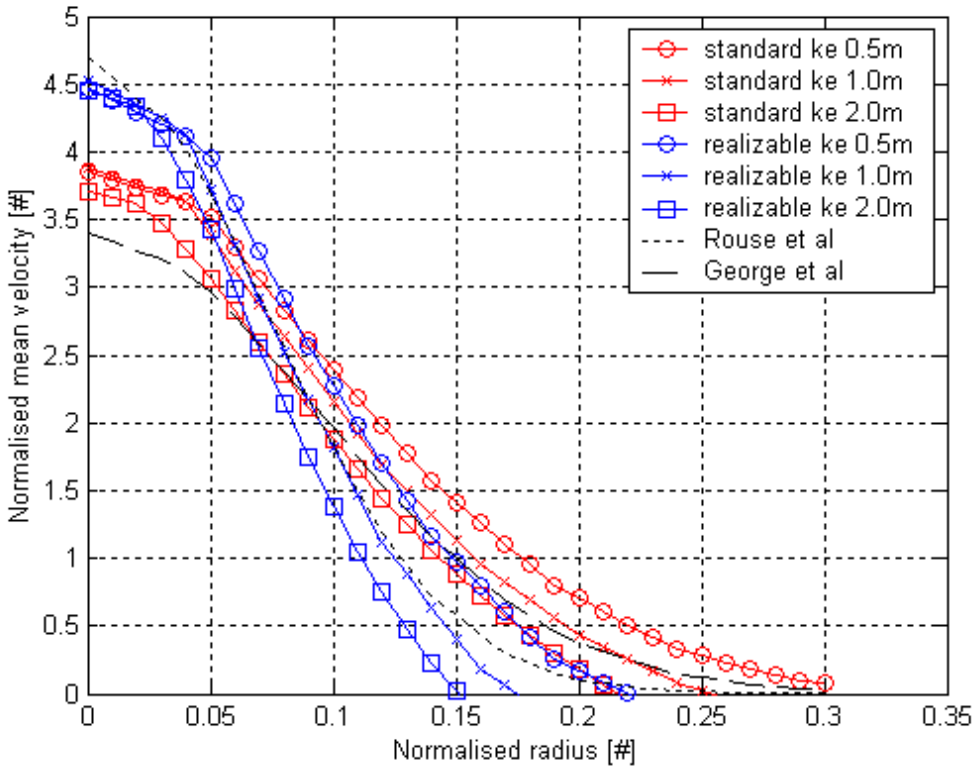

Figure B.4. Normalised mean axial velocity as a function of normalised radius, for several heights above the source.

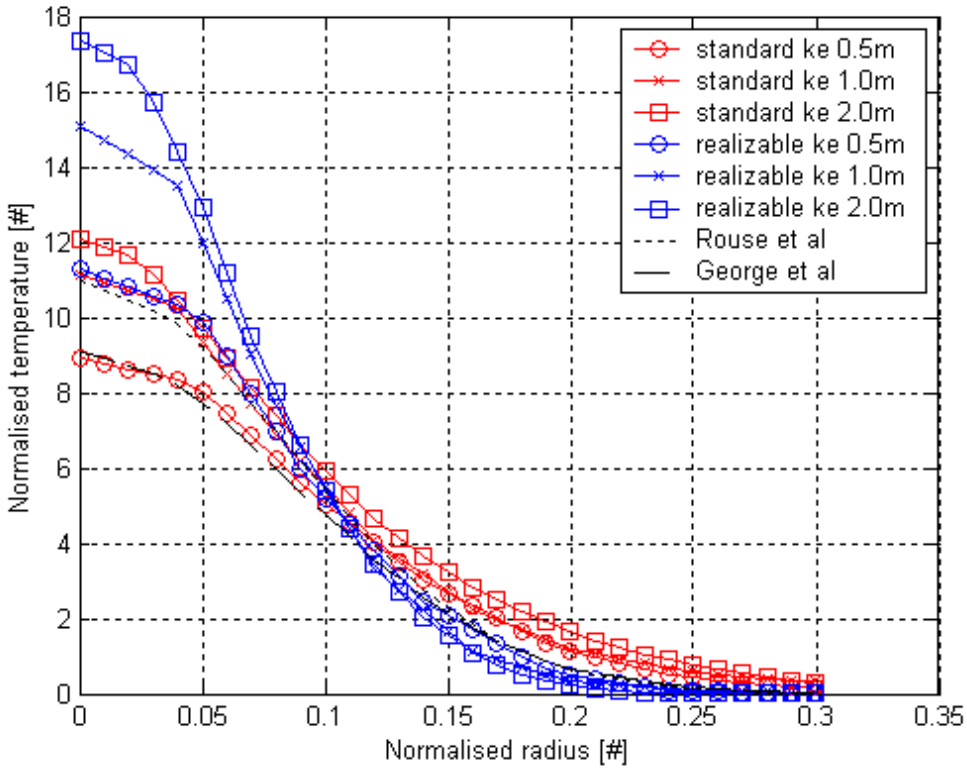

Figure B.5. Normalised temperature as a function of normalised radius, for several heights above the source.

B.4 CONCLUSION

A study has been carried out to ensure that Fluent can accurately predict temperature and velocity in a buoyant plume above a point heat source. Two turbulence models were evaluated: the standard and realisable k-ε models. Both compared very well to experimental data, though the realisable k-ε model appeared to over-predict centre-line temperature by as much as 30-40%. Consequently the standard k-ε model will be used in further simulations of buoyant plumes above fixed beds of fuel.

APPENDIX C: CRIB FLOW RESISTANCE

While developing the CFD sub-model of wood combustion in chapter 3, the wood-crib is modelled as a porous zone, with a velocity dependant pressure drop, which appears as a source in the momentum equation (Fluent, 2007):

$$S = -\left(\sum_{j=1}^{3} D_{ij} \mu v_j + \sum_{j=1}^{3} C_{ij} \tfrac{1}{2} \rho v_{mag} v_j \right) \tag{C.1}$$

for anisotropic media, which simplifies to:

$$S = -\left(\tfrac{1}{\alpha} \mu v + C_2 \tfrac{1}{2} \rho v_{mag} v \right) \tag{C.2}$$

for homogenous media. In both, the first term is viscous loss and dominates at low fluid flow rates, and second term is inertial loss and dominates at high fluid flow rates. Viscosity and density are properties of the fluid, but 1/α and C2 are properties of the medium and must be found from one of two methods. The first method is experimental, by collecting data for a pressure-flow characteristic of the form:

$$\Delta p = a v^2 + b v \tag{C.3}$$

Comparing with eqn (C.2), $C_2 = \dfrac{2a}{\rho \Delta x}$ and $\tfrac{1}{\alpha} = \dfrac{b}{\mu \Delta x}$. The second method uses the Ergun equation (Ergun, 1952):

$$\frac{\Delta p}{\Delta x} g = 150 \frac{(1-\varepsilon)^2}{\varepsilon^3} \frac{\mu v}{D^2} + 1.75 \frac{(1-\varepsilon)}{\varepsilon^3} \frac{\rho v^2}{D} \tag{C.4}$$

Comparing with eqn (2), $C_2 = \dfrac{3.5}{D} \dfrac{(1-\varepsilon)}{\varepsilon^3}$ and $\tfrac{1}{\alpha} = \dfrac{150}{D^2} \dfrac{(1-\varepsilon)^2}{\varepsilon^3}$.

The aim of this investigation is to find suitable values of viscous and inertial resistance coefficients, C2 and 1/α for different aspects and configurations of wood-crib.

C.1 APPARATUS & METHOD

Apparatus was a square section duct, side 100mm, length 700mm, with a blower and 300mm diffuser (Figure C.1). Inlet was equipped with an EDRA-6 vane anemometer (uncertainty on velocity measurements less than 5 m/s ±0.1m/s) and inlet and outlet equipped with pressure tappings on each of the four sides, connected to differential pressure transducer (uncertainty ±0.1Pa).

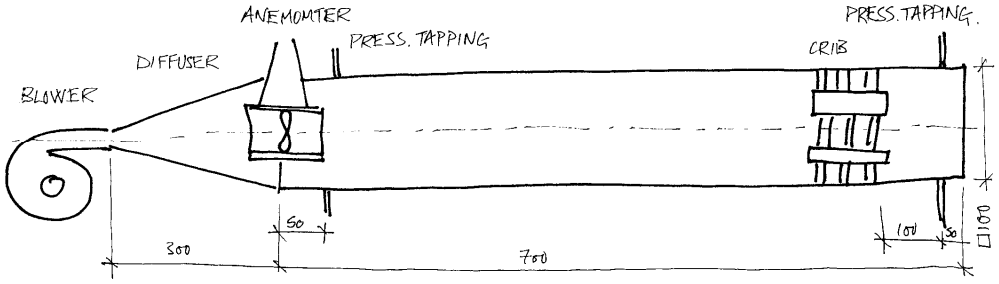

Figure C.1. Schematic of crib flow resistance apparatus.

Wood cribs were built with 100x20x20mm sawn blocks of pine as used in previous combustion tests, and positioned 100mm from outlet. Cribs all had 5 layers of wood, but different configurations had 2, 3 and 4 blocks per level, and one configuration with alternate layers of 2 and 3 blocks/layer. Each of the four configurations was tested with fluid entering from the front, side and bottom aspect to account for anisotropic construction (Figure C.2).

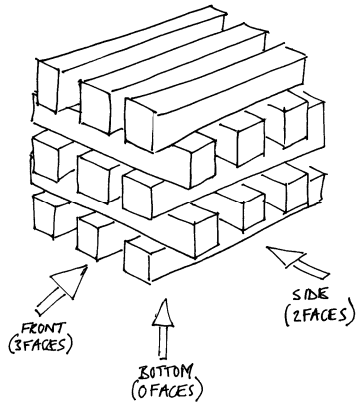

Figure C.2. Wood-crib (n=3), with the directions illustrated.

Method:

- Install wood-crib in the duct.
- Zero apparatus.
- Set fluid flow rate and take approximately 10 velocity readings and pressure readings. Randomly pair velocity and pressure readings for subsequent analysis.

- Repeat measurements with increasing fluid flow rate three times.
- Repeat measurements with decreasing fluid flow rate three times.
- Conduct linear regression of pressure, dp, against input variables, velocity, v, and velocity squared, v^2.

C.2 RESULTS

Table C.1. Recorded results for n=2 crib from the bottom.

Velocity [10x m/s]	Pressure differential [Pa]
39,36,40,40,38,37,36,41,34,37,35,41,36,41,39,39	22.0,24.0,22.0,22.0,19.0,24.0,23.0,21.0
28,26,27,23,28,25,24,24,27,26,28,24,29,24,23,22	12.1,12.2,12.3,13.0,12.4,10.8,13.9,12.7
19,20,20,23,18,17,18,18,19,20,20,17,21,21,21,17	6.4,6.4,7.4,7.3,6.6,7.3,6.7,6.6,6.4,6.0
10,11,12,9,10,11,9,9,12,10,10,11,11,9	1.9,2.1,2.1,2.3,2.1,2.3,2.0,1.8,2.3
9,6,9,7,7,8,7,8,8,9,9,7,8,8,7,9	1.4,1.5,1.3,1.2,1.3,1.2,1.5,1.5,1.4
17,14,15,16,14,14,18,17,14,16,14,13,17,19,17,16	4.3,4.5,4.2,4.3,4.4,3.4,4.1,3.8
24,21,24,24,21,24,25,20,20,26,24,24,24,25	9.7,8.8,9.9,9.4,9.3,9.2,9.7,9.8,9.3

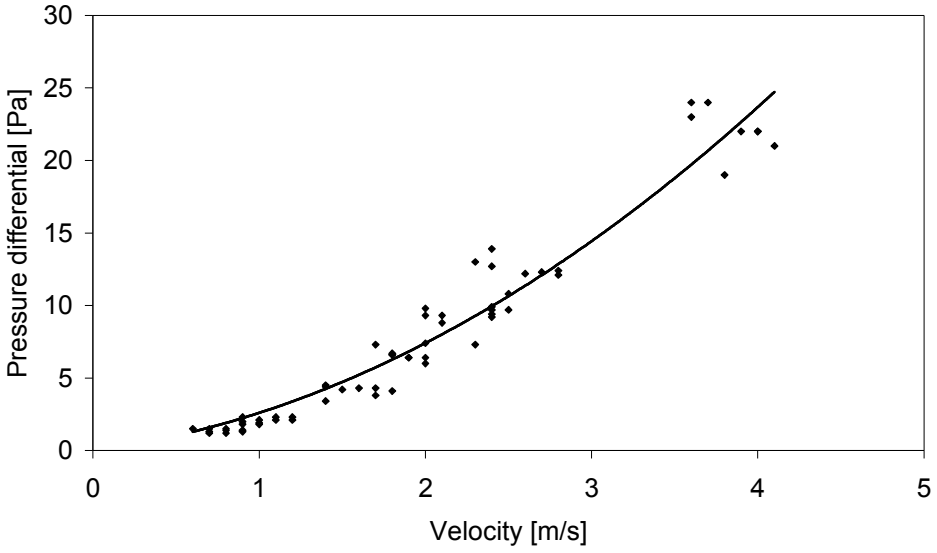

Figure C.3. Pressure-velocity characteristic and trend-line for results in Table C.1 $dp = av^2 + bv$, where $a = 1.1 \pm 0.2$ and $b = 1.5 \pm 0.6$.

Table C.2. Inertial and viscous flow resistance coefficients for wood cribs, from experiment and the Ergun equation.

	Inertia coefficient C2 [m-1]					Viscous coefficient 1/α [m-2]				
n	Btm	Front	Side	Mean	Ergun	Btm	Front	Side	Mean	Ergun
2	21	3	41	22±19	190	0.6	0.6	1.3	0.8±0.4	0.10
3	165	137	650	320±290	863	12	-5	-33	12	0.58
4	1282	373	477	710±500	7954	25	14	25	21±7	6.2
mix	53	115	313	160±140	400	5	2	8	5.0±3.0	0.24

C.3 DISCUSSION

Data showed that more densely packed cribs offer greater inertial and viscous resistance to flow. Front and side aspects of n=3 crib showed negative viscous friction coefficients (i.e. friction aids flow), so have been ignored. Large standard deviations in averaged data illustrate that the cribs are strongly anisotropic. Though in the correct order of magnitude, Ergun's equation consistently overestimates significance of inertial effects and underestimates significance of viscous effects. Possible justifications are:

- Ergun's equation assumes a packed bed of spheres, which have minimum specific area (surface area per unit solid volume). Blocks have larger area therefore larger skin friction and viscous losses.
- Ergun's equation assumes a packed bed of particles which are small w.r.t. the overall bed dimensions. Block are large, so end effects are significant.

A previous experimental investigation yielded comparable inertial loss coefficients for a packed bed of wood char with 20mm diameter (810±30 m^{-1}), which were in good agreement with the Ergun equation (840 m^{-1}), giving greater credence to present results.

In the velocity range of interest (up to 2m/s) the magnitudes of inertial and viscous losses are comparable, so neither can be ignored. However, the small velocities and tight spaces under natural convection conditions in the crib will result in low Reynold's numbers, suggesting that flow in the crib is laminar. Fluent recommends that inertial loss be ignored in this situation.

C.4 CONCLUSION

Experiemental values of viscous and inertial flow resistance coefficients have been found for small wood cribs with a variety of configurations. More densely packed cribs have a greater resistance to flow.

The highly anisotropic nature of the cribs was reflected in large variation of coefficients. Results are not in exact accordance with values from the literature, though the general trend and order of magnitude are preserved. Results can be taken forward to subsequent CFD studies.

APPENDIX D: FUEL CHARACTERISATION

In order to build an accurate model of wood combustion in Fluent 6.2, the fuel wood must be characterised. Values for basic combustion parameters were found by experimental methods, and have been compared to values found in literature.

D.1 FLOW RESISTANCE

In order to model a fixed bed of char as a porous region in Fluent 6.2, it is necessary to identify the resistance to flow presented by the char. Fluent 6.2 requires user defined coefficients for both viscous and inertial pressure losses, and this section details theoretical end experimental approaches to finding these coefficients.

Ergun (1952) separated the pressure loss of a flow through a packed bed into viscous and inertial pressure loss components:

$$\frac{\Delta P}{\Delta x} g = \frac{150 \mu U}{{D_p}^2} \frac{(1-\varepsilon)^2}{\varepsilon^3} + \frac{1.75 \rho U^2}{D_p} \frac{(1-\varepsilon)}{\varepsilon^3} \qquad \text{(D.1)}$$

where P is pressure, x the bed thickness, μ the fluid viscosity, U the superficial velocity, D_p the diameter of particles in the bed, ε the void fraction and ρ the fluid density. Comparing this equation with the formulation of the momentum equation in porous zones in FLUENT, one can identify viscous pressure loss coefficient, α, and inertial pressure loss coefficient, C_2:

$$\alpha = \frac{{D_p}^2}{150} \frac{\varepsilon^3}{(1-\varepsilon)^2} \text{ and } C_2 = \frac{3.5}{D_p} \frac{(1-\varepsilon)}{\varepsilon^3} \qquad \text{(D.2 a \& b)}$$

Meanwhile, given an experimentally derived pressure-flow curve for a packed bed:

$$\Delta P = aU^2 + bU \qquad \text{(D.3)}$$

the inertial pressure loss coefficient, C_2, can be found as follows (FLUENT, 2005):

$$a = C_2 \tfrac{1}{2} \rho \Delta x \qquad \text{(D.4)}$$

Method

A fan was used to pass a current of air though a duct containing a packed bed of char, while superficial velocity and pressure drop across the bed were measured (see figure D.1). Velocity was measured with an EDRA-6 vane anemometer (uncertainty on velocity measurements less than 5 m/s ±0.1m/s) and pressure differential with a differential pressure transducer (uncertainty ±0.1Pa). The char was held in place by gauze at the down-stream end and by a removable section of flow straighteners at the upstream end. A butterfly valve was used to vary the superficial velocity of the air current. For each bed thickness, Δx, the experiment was repeated three times, while for low-velocity data points (v<0.75m/s), an average of eight readings were taken to overcome the unsteady fluctuations of readings. Data was collected for three different values of char bed thickness.

For each of the three bed thicknesses, a linear regression was performed on the pressure-velocity data, to give an average value of the inertial flow resistance coefficient, C_2. The three values were then averaged to find mean inertial flow resistance coefficient, and the standard deviation used to estimate the uncertainty on this mean value.

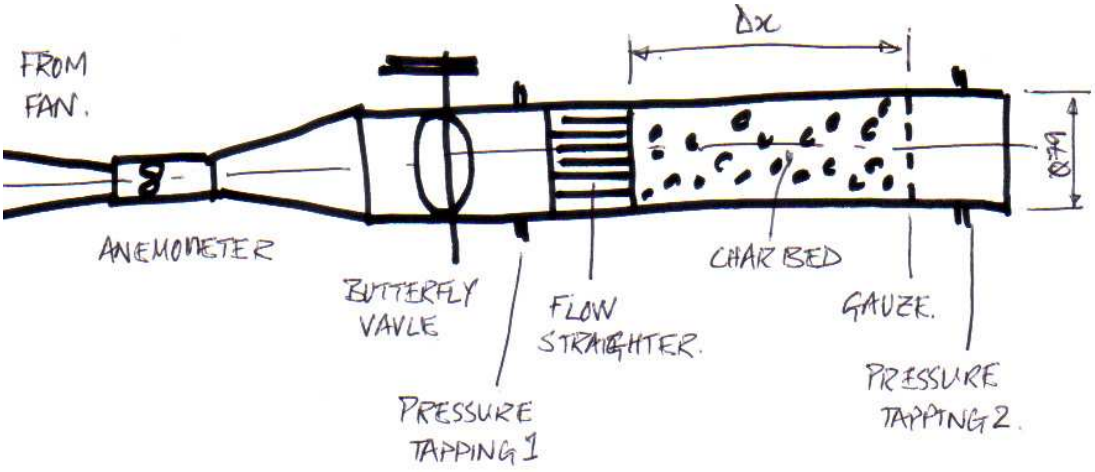

Figure D.1. Schematic of apparatus to measure the pressure-flow characteristic of a packed bed or char.

Results and Discussion

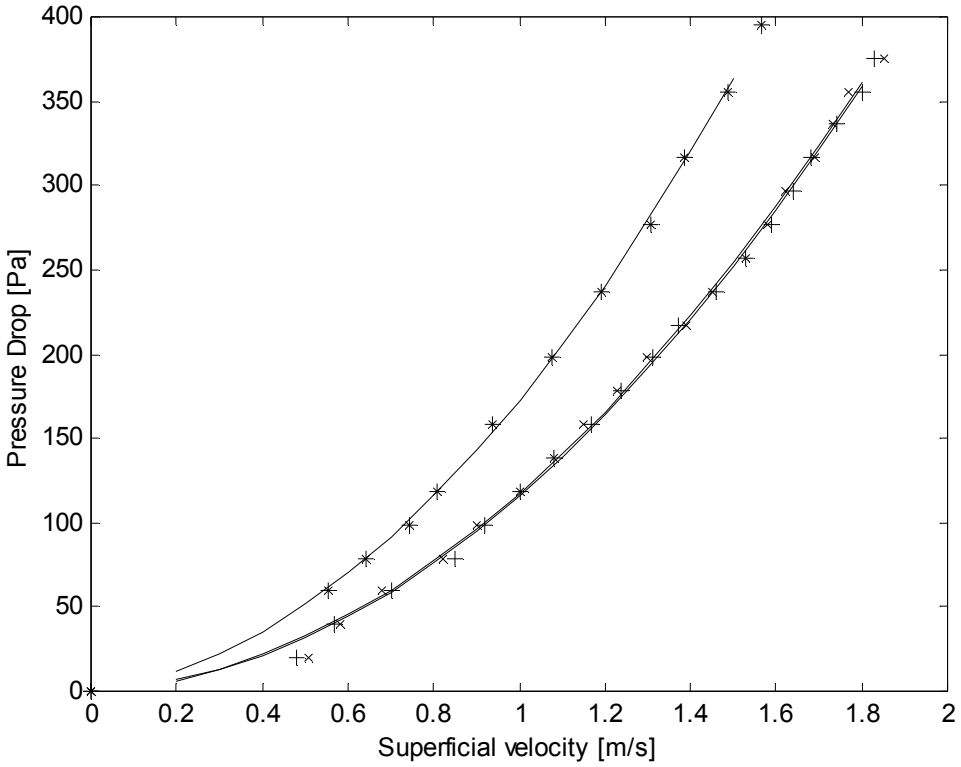

*Figure D.2. Pressure-flow curves for char beds: x, 0.20m thick; +, 0.24m thick; *, 0.26m thick.*

Results

The experimental investigation yielded coefficients a and b (defined in equation D.3) given in Table D.1 for three different char bed thicknesses. For each char bed thickness, the coefficient C2 was calculated using equation D.4, and the result tabulated in table D.1. The mean inertial flow resistance coefficient was calculated from these as 813 ± 33 m^{-1} for the inertial pressure loss coefficient, while the Ergun equation yields a value of 846 m^{-1}, under the assumption of 20mm diameter spherical char particles (i.e. the thickness of the sticks used to make the char), packed as a Cartesian grid. The Ergun equation therefore yields a perfectly reasonable approximation of the inertial pressure losses through the char bed. The viscous resistance term of the Ergun equation is small by comparison to the inertial term, and so can be neglected.

Table D.1. Experimentally derived values of inertial pressure loss coefficient for a packed bed of char.

Bed thickness [m]	Coefficient a [$Pa.s^2/m^2$]	Coefficient b [Pa.s/m]	Coefficient C_2 [m^{-1}]
0.20	104.14	13.329	848
0.24	104.87	10.87	713
0.26	139.83	32.625	878

D.2 PROXIMATE ANALYSIS

The model of wood combustion implemented in FLUENT's CFD code required user defined values for the moisture fraction and volatile fraction of the fuel wood. Any ash remaining after the char combustion would be chemically inert, and would tend to inhibit the diffusion of oxygen to the char surface. However, this effect has been ignored because of the unknown structure and thickness of the ash, and ash fraction is therefore not required as part of the proximate analysis.

Moisture fraction

Moisture fraction was found from eight samples, following BS1016:3, which requires the samples to be kept in a kiln at 105^{o}C until there is no further change of mass.

This procedure yielded a moisture fraction of 9.5 ± 0.6 % (wet basis). Ragland et al. (1991) give a value of 5-20 % for fuel wood, indicating that a moisture content of 10% is quite reasonable.

Volatile fraction

Volatile fraction was found from three samples, following BS1016:3, which requires the samples to be held in a silica crucible with a lid, and places in a kiln at 900^{o}C for seven minutes.

This procedure gives a volatile fraction of 74.6 ±0.4 %, leaving approximately 15% of the wood mass as char (wet basis). This value falls in the very middle of the 10-20% range given by Ragland et al. (1991), indicating that the present testing was acceptable.

D.3 CALORIFIC VALUES

The wood combustion model implemented in FLUENT's CFD code requires the calorific value of the fuel wood as well as the volatiles and char. The calorific value of the fuel wood and char were found using a IKA C5000 bomb calorimeter, using three samples for the fuel wood and char.

Results for the fuel wood give a lower heating value of 17.65 ± 0.19 MJ/kg. Given 10% moisture fraction (wet basis) and chemical composition of the dry fuel as $C_4H_6O_3$ (Drysdale, 2004 and Meyerriecks, 1998), this results in a higher heating value of 18.97 ± 0.19 MJ/kg. This is comparable to values found in literature for moist fuel wood (e.g. 19.77 MJ/kg in Meyerriecks, 1998; 19.58 MJ/kg in Friedl et al., 2005).

Results for the char gave a calorific value of 29.62 ± 0.6 MJ/kg, based on two samples (the third not having burned to completion). It is usually assumed that char consists of carbon and ash with no moisture content, however these samples had been kept at room temperature for several days before testing, and would have absorbed moisture during that time. Assuming a wet basis moisture content of 10% (comparable to fuel wood kept in identical conditions), this results in a moisture-free heating value of 29.85 ± 0.6 MJ/kg. This is slightly lower than values published in literature (e.g. 32.0 MJ/kg from Drysdale, 2004), but this represents less than 10% deviation, which is not unreasonable.

D.4 CONCLUSION

The fuel wood can be characterised by the following data:

Moisture fraction (wet basis):	10%
Volatile fraction (wet basis):	75%
Char and ash fraction (wet basis):	15%
Wood higher heating value:	19 MJ/kg
Char higher heating value:	30 MJ/kg
Char inertial flow resistance:	815 m^{-1}

All these values are consistent with values found in literature.

APPENDIX E: MOGOGO THERMAL PARAMETERS

E.1 INTRODUCTION

As part of an investigation into the efficiency of a wood burning stove from Eritrea, is was necessary to determine the thermal properties of a mogogo plate (an unfired earthen griddle plate used to cook large fermented pancakes). The thermal conductivity of the plate was to be found with the Lee's discs apparatus (Figure E.1), which consists of two discs sandwiching the sample, the top disc being heated, and temperature of the bottom disc being recorded.

The standard analysis of data from the apparatus was extended to give an estimate of the specific heat capacity of the specimen: a simple mathematical model (Figure E.2) was built to simulate the transient behaviour of the apparatus, where the thermal inertia of the bottom disc was assumed to include half of the thermal inertia of the specimen. This is similar (though not identical) to modifications of the Lee's disc technique described by Waliki et al. (2003).

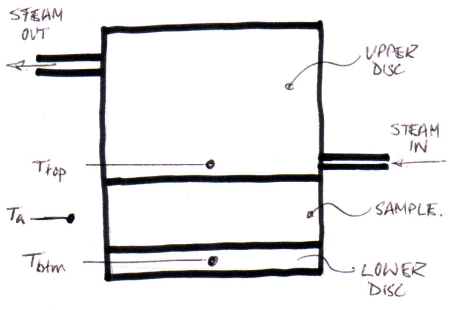

Figure E.1. Schematic of the Lee's disc apparatus.

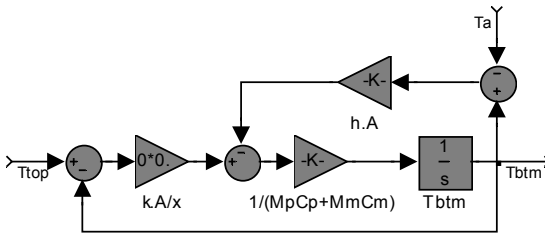

Figure E.2. Schematic of the simple mathematical model, as implemented in MATLAB.

E.2 METHOD & APPARATUS

The apparatus consists of two discs with the sample sandwiched between them (Figure E.1): the upper disc was feed with steam to heat it, while the lower disc acted as a target in order to determine the amount of heat moving through the sample. A thin layer of thermal paste was applied to either side of the sample to ensure that a good thermal contact with the discs. Three thermometers were used to take the temperatures of the top and bottom discs and the ambient air temperature. In all cases, temperatures were logged once per minute with uncertainty ± 1^{o}C.

The experimental method is divided into two parts: the first was to find the steady state temperature of the lower disc as it receives heat through the sample and loses heat to the surrounding air; the second part was to find the rate of heat loss at the steady state temperature from the first part.

To find the steady state temperature of the lower disc, the sample and layers of thermal paste were positioned between the discs. The top disc was heated with steam and the temperatures monitored until the transient was complete. The steady-state temperature of the lower disc, T_{∞}, was recorded. The procedure was repeated with a single layer of thermal paste but without the sample, to determine the thermal conductivity of the paste alone.

To find the rate of heat loss at the steady-state temperature, the sample was replaced with a thick piece of insulation. The lower disc was heated to a temperature far higher than T_{∞}, and allowed to cool under natural convection until it was in equilibrium with the ambient air.

The temperature decay rate of the bottom disc yielded the heat transfer coefficient between the disc and ambient air, the mass and specific heat capacity of the disc having been found previously. This heat transfer coefficient was then used in conjunction with the data from the first part of the experiment to give the thermal conductivity and specific heat capacity of the sample, which were the only remaining unknowns.

E.3 RESULTS & DISCUSSION

The simple model gives a very good approximation of the behaviour of the Lees' disc apparatus. The parameters derived from the results are:

Heat transfer coefficient (disc to ambient), h = 11 W/m^2/K

Mogogo plate specific heat, C_m = 900 J/kg/K

Mogogo plate thermal conductivity, λ_m = 0.41 W/m/K

The values of parameters for the mogogo plate compare reasonably with those for brick (taken from hypertextbook.com), which are specific heat capacity 810 J/kg/K and thermal conductivity 0.69 W/m/K. Errors may have been incurred since the mogogo plate did not cover the whole of the bottom disc, which left a small area open to ambient air, though the effect should have been small. This and other inaccuracies could be reduced by cutting another specimen of mogogo plate (a luxury not available due to shortage of material) and by repeating the experiment with a Perspex shield around the apparatus to give a more uniform heat transfer coefficient from the bottom disc to ambient.

E.4 CONCLUSION

The Lee's disc apparatus was used to investigate the thermal characteristics of a mogogo plate. Though the apparatus is typically used only to find the thermal conductivity of a specimen, a simple mathematical model was used to extend its use in order to give the specific heat capacity as well. The investigation yielded values of 0.41 W/m/K and 900 J/kg/K for the thermal conductivity and specific heat capacity of the mogogo plate. These values are comparable to values for brick, a similar material, found in the literature, and are therefore taken to be reasonable results.

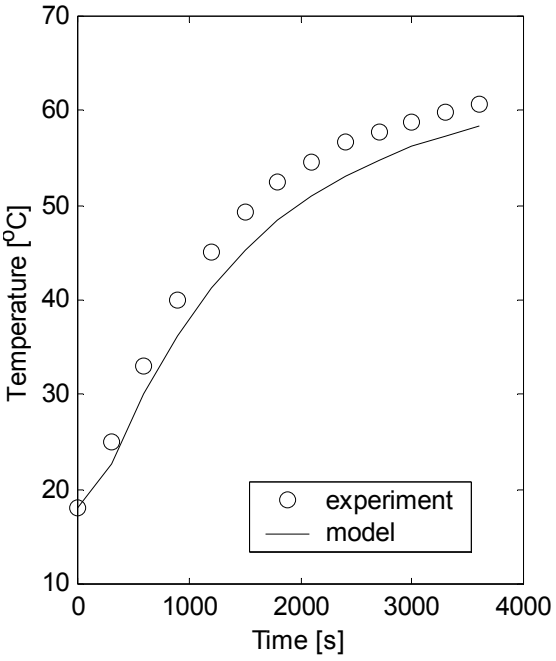

Figure E.3. Transient temperature profile of bottom plate.

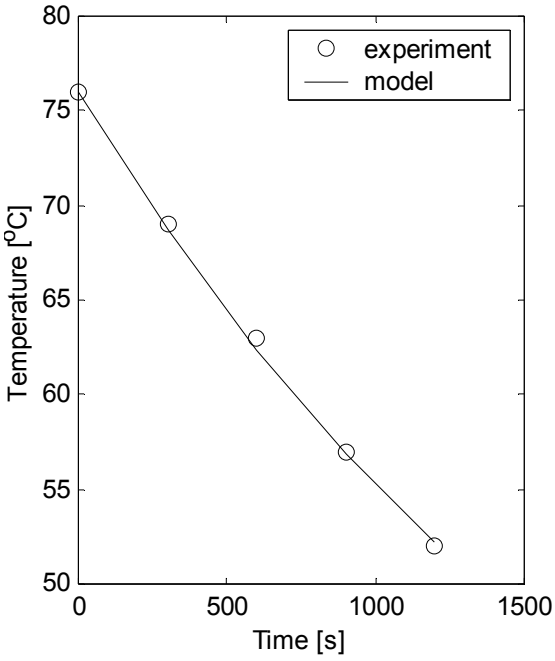

Figure E.4. Temperature decay with insulation instead of specimen.

APPENDIX F: MOGOGO PERFORMANCE ASSESSMENT

The aim of the work presented in this appendix was to evaluate the power required to cook ingera and to benchmark the classic mogogo in terms of performance and efficiency. van Buskirk (2004a, 2004b) reported mean efficiency of the classic mogogo to be approximately 10%. His measurements were taken in two sets of conditions: first in a test facility in the Energy Research and Training Centre (ERTC) in Asmara, and secondly in IDP camps near the border with Ethiopia. In both instances the method included the sensible and latent heat of water, and also included the harvesting of charcoal after the completion of the cooking cycle. Cooking cycles typically resulted in 30 ingera being baked. Ghebrehewit (2002) states that the classic mogogo is 6–8% efficient, though the paper describes the classic mogogo as "a three-stone open hearth", which seems like an unlikely description. Specific energy consumption is given as 9.4 MJ/kg of food. Assuming an average ingera is 0.3 kg and cooked in 4 minutes, this yields a 12 kW fire and 0.94 kW cooking requirement. Elsewhere in the same publication, the classic mogogo is described as being 8-10% efficient.

The objectives of the current work are to replicate the results of van Buskirk and Ghebrehewit, and estimate the power required to cook ingera. The work was executed in test facilities in the University of Nottingham, with the help of volunteers from the Eritrean diaspora. As such it can only hope to mimic conditions and materials found in Eritrea, and the results should be reviewed with caution.

F.1 APPARATUS & METHOD

The mogogo stove was constructed in laboratory test facilities at the University of Nottingham. Dimensions were taken from a survey of mogogo stoves in the Anseba and Makael regions of Eritrea in June 2004. The test mogogo was

constructed of a layer of refractory bricks to make the base, five further courses of refractory bricks to make the body (Figure F.1), and lined on the inside with a mixture of mud (common or garden) and straw as a binding agent. The stove body was furnished with a large fuel window at the front and a smaller ventilation window at the back. The mogogo plate (sourced from Asmara market) rested on the stove body, the join being sealed with more mud. A single thermocouple was located 2mm below the theoretical stagnation point below the mogogo plate. The mogogo was fired several times, and the plate repeatedly seasoned with cooking oil and beans before tests began.

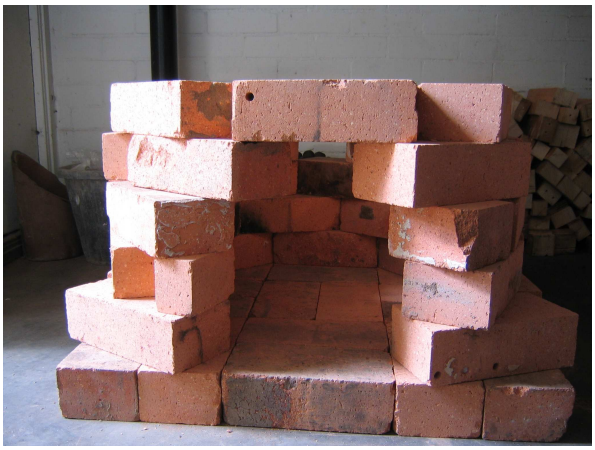

Figure F.1. Unlined mogogo body with large fuel window and small rear ventilation window.

Figure F.2. Cooking on the finished mogogo stove.

The test procedure was developed to minimise measurements while cooking so that a) it was unobtrusive to (Eritrean) operators unfamiliar with the test facility, and b) it was easier for the other operator to manage the test facility and cook at the same time. Operators were volunteers from the Eritrean community in Nottingham, except the author. The test method was:

1. Prepare and weigh the batter: approximately 1.5 kg of flour, 2.0 kg of water and 30g of yeast, stood in a warm place overnight.
2. Prepare and weigh extra cooking water to dilute the batter as required.
3. Prepare and weigh fuel in excess: kindling, sticks, rough and sawn wood, and charcoal.
4. Prepare safety equipment and ensure adequate ventilation.
5. Start timer and note ignition time, cooking start time and cooking end time.

6. Operator lights fire, preheats stove and carries out cooking preparations.
7. Operator bakes 10 ingera (note start and end time of cooking; Figure F.2).
8. Operator harvests charcoal (extinguished with sand).
9. Clean apparatus (using unmetered water).
10. Reweigh fuel, batter, cooking water and ingera and calculate the following according to equations (F.1) to (F.7): fire power; cooking power; efficiency; cooking cycle time (CCT); cooking cycle fuel (CCF); specific fuel consumption (SFC); specific energy consumption (SEC).

(F.1)

$$P_{fire} = \frac{\Delta m_{wood} - \Delta m_{char}}{t_{fire}}$$

$$P_{cook} = \frac{m_{water} c_{water} \Delta T + m_{flour} c_{flour} \Delta T + \Delta m_{water} h_{evap} + m_{flour} h_{gel}}{t_{cook}} \quad \text{(F.2)}$$

$$\eta = \frac{P_{cook} t_{cook}}{\Delta m_{wood} h_{wood} - \Delta m_{cchar} h_{char}} \quad \text{(F.3)}$$

$$CCT = t_{cook} / n_{ingera} \quad \text{(F.4)}$$

$$CCF = \Delta m_{fuel} / n_{ingera} \quad \text{(F.5)}$$

$$SFC = \Delta m_{wood} / \Delta m_{ingera} \quad \text{(F.6)}$$

$$SEC = \frac{\Delta m_{wood} h_{wood} - \Delta m_{char} h_{char}}{\Delta m_{ingera}} \quad \text{(F.7)}$$

F.2 RESULTS & DISCUSSION

Performance statistics for five operators are presented in Table F., with data for the classic and ERTC mogogos from van Buskirk (2004). Typical operators cook one ingera every three to four minutes, requiring 1 kW of cooking power, and 20 kW of fire power, rendering the stove approximately 5% efficient. The cooking power was typically dominated by sensible and latent heat of the water, while sensible heat of the flour and heat for the gelatinisation reaction typically accounted for 15%. The values of cooking power reported are comparable to the estimate of heat conducted through the cooking plate: assuming the top surface is at the temperature of boiling water (473 K), the bottom surface is at the flame temperature recorded by the stagnation temperature thermocouple (typically 850 K), dimensions from Figure F.3 and thermal conductivity 0.4 W/m/K from Appendix E, heat is conducted through the plate at approximately 1.5 kW. The

difference between the two values can be accounted for due to experimental error and losses of heat though the sides and rim of the mogogo plate.

Cooking style and experience account for the range of performance from one operator to another, though all operators exhibited very similar values of fuel per ingera.

The values of specific fuel consumption (kg fuel/kg food) and specific energy consumption (MJ/kg food) reported by van Buskirk for the classic mogogo are considerably lower than values for the current tests (10.0 MJ/kg rather than 17.0 MJ/kg). Even if the current results were scaled up to batches of 30 ingera rather than batches of 10, thereby amortising the fuel required for warm-up, the mean specific energy consumption would fall to 13.6 MJ/kg, still 30% higher than van Buskirk's data. This significant difference may be attributed to a combination of factors: the test mogogo in University of Nottingham facilities was a particularly inefficient design; the operators were inexperienced or out of practice when cooking over a fire; operators were profligate with fuel as they were not in an economically pressured setting, while operators in van Buskirks study were all residents of Internally Displaced Persons' camps (IDP camps, a.k.a. refugee camps) where resources were limited. These last two reasons are unlikely, as all operators in the present study were inefficient relative to van Buskirk's operators, including Abrehet, who was very experienced at cooking ingera on a wood burning stove.

Table F.1. Mogogo statistics as a function of operator.

	Sara K	Abrehet	HBS	Sara A	Sara S	Classic mogogo*	ERTC mogogo*
Fire power [kW]	26.0	16.4	23.5	16.0	14.5		
Cooking power [kW]	1.05	0.70	1.20	0.75	1.00		
Efficiency [%]	4.0	4.0	5.2	4.7	6.7	~10	~20
Cycle time [s/item]	240	190	225	230	240	~240	~240
Cycle fuel [kg/item]	0.35	0.33	0.31	0.35	0.32		
Sp. fuel cons. [kg/kg]	0.99	1.40	1.02	1.21	1.16	0.55	0.27
Sp. energy cons. [MJ/kg]	17.8	25.2	17.2	19.5	17.3	10.0	5.0

* data from van Buskirk (2004).

F.3 CONCLUSION

A mogogo test facility has been constructed in the University of Nottingham to evaluate the operating parameters of typical mogogo cooking operations. The stove was approximately 5% efficient, requiring 1.0 kW of heat to cook the food (hence 20 kW fire power). All operators displayed similarly performance. The performance of mogogo stoves reported by van Buskirk was significantly higher (typically 10% efficient), suggesting that the stove in the current investigiation did not conform to "best practice". Nonetheless, that data gathered is sufficient for the purpose, and the estimated cooking power of 1 kW is in agreement with the value of 0.94 kW suggested by Ghebrehewit.

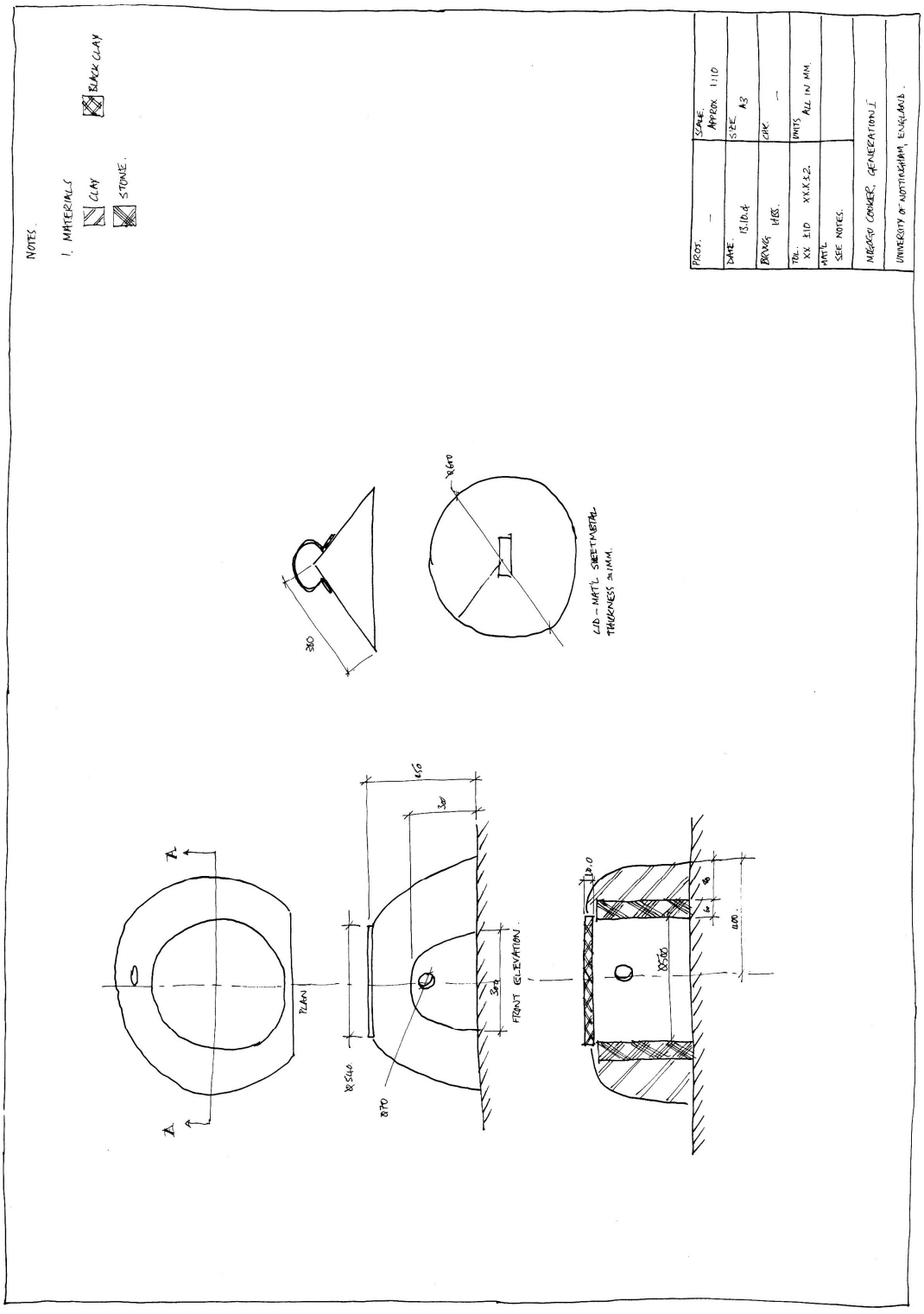

Figure F.3. Typical mogogo dimensions from unstructured survey of stoves in Anseba and Makael regions in June 2004.

APPENDIX G: ALGORITHM SCRIPTS

G.1 FUEL PYROLYSIS MODEL

prometheus21 is the coding of equations (3.9) to (3.23) as a UDF in Fluent. Thanks go to David Hargreaves for coding the user-defined memory allocation and retrieval.

```
/************************************************************************
       UDF that adds mass and heat to porous zone to simulate
       blowing, char combustion and devolatalisation.
************************************************************************/

#include "udf.h"

#define W      200.    // wood spacing frequency [1/m] (w=2*pi/l)
#define a      66.     // specific area per unit volume [m2/m3]
#define IFRC   200.    // inertial flow resistance coefficient [1/m]

#define PSI    3.      // lumpy limit [-]
#define v      0.1     // lumpiness solid fraction [-]

#define Tp     575.    // pyrolysis temperature [K]
#define Hc     30.0e6  // char calorific value [J/kg]
#define hm     0.1     // mass transfer coefficient [units]
#define k      0.05    // thermal conductivity of char [W/m/K]
#define RlnRr  0.0005  // char radius times log or char rad over virg rad [m]
#define Hv     2.5e6   // effective enthalpy of pyrolysis [J/kg]

#define UDM_MASS     0  // User-defined memory ID for mass source
#define UDM VOLS     1  // User-defined memory ID for volatiles source
#define UDM O2       2  // User-defined memory ID for oxygen source
#define UDM_CO2      3  // User-defined memory ID for carbon dioxide source
#define UDM_H2O      4  // User-defined memory ID for water vapour source
#define UDM_EN       5  // User-defined memory ID for energy source

#define PI2    6.28318 // 2 pi

/************************************************************************
       lumpy flow resistance
************************************************************************/

DEFINE PROFILE(virgin RESISTANCE,t,i)
       {
       real x[ND_ND];
       cell_t c;

       begin c loop(c,t)
              {F PROFILE(c,t,i) = IFRC;}
       end c loop(c,t)
       }
```

```
DEFINE PROFILE(virgin POROSITY,t,i) // or "void fraction"
        {
        real x[ND_ND];
        real p;
        cell t c;

        begin c loop(c,t)
                {
                C_CENTROID(x,c,t);
                if ( (1.0+cos(W*x[0]))*(1.0+cos(W*x[1]))>PSI )              //
fuel
                        {p = 0.85;}
                else                                                  // free air
                        {p = 1.0;}
                F_PROFILE(c,t,i) = p;
                }
        end c loop(c,t)
        }

/*************************************************************************
        sources for char combustion & pyrolysis
*************************************************************************/

DEFINE SOURCE(virgin MASS source,c,t,dS,eqn) //      Source      1      of      6
================================================
        {
        real x[ND_ND];
        real source;
        C CENTROID(x,c,t);
        if ( (1.0+cos(W*x[0]))*(1.0+cos(W*x[1]))>PSI & (C T(c,t)>Tp) )
        // hot fuel
                {

        source=12.0/32.0*a/v*sqrt(sqrt(pow(C U(c,t),2)+pow(C V(c,t),2))*5)*hm*C
 R(c,t)*C YI(c,t,1) + k*a*(C T(c,t)-Tp)/v/RlnRr/Hv;
                dS[eqn]= 0.;
                }
        else if ( (1.0+cos(W*x[0]))*(1.0+cos(W*x[1]))>PSI )                 //
cold fuel
                {

        source=12.0/32.0*a/v*hm*sqrt(sqrt(pow(C U(c,t),2)+pow(C V(c,t),2))*5)*C
_R(c,t)*C_YI(c,t,1);
                dS[eqn]= 0.;
                }
        else                                                                //
not fuel
                {source=dS[eqn]= 0.;}

        C_UDMI(c,t,UDM_MASS) = source;  // Store the source in UDM

        return source;
        }
DEFINE_SOURCE(virgin_VOLATILES_source,c,t,dS,eqn)    //    Source    2    of    6
=======================================
        {
        real x[ND ND];
        real source;
        C CENTROID(x,c,t);
        if ( (1.0+cos(W*x[0]))*(1.0+cos(W*x[1]))>PSI & (C_T(c,t)>Tp) )
        // hot fuel
                {
                source=75.0/85.0*k*a*(C T(c,t)-Tp)/v/RlnRr/Hv;
                dS[eqn]= 0.;
                }
        else                                                                //
not fuel
                {source=dS[eqn]= 0.;}

        C UDMI(c,t,UDM VOLS) = source;

        return source;
        }

DEFINE SOURCE(virgin OXYGEN source,c,t,dS,eqn)       //    Source    3    of    6
```

```
==============================================
        {
        real x[ND_ND];
        real source;
        C_CENTROID(x,c,t);
        if ( (1.0+cos(W*x[0]))*(1.0+cos(W*x[1]))>PSI )
        // any fuel
                {
                source=-
a/v*hm*sqrt(sqrt(pow(C_U(c,t),2)+pow(C_V(c,t),2))*5)*C_R(c,t)*C_YI(c,t,1);
                dS[eqn]=0.0;
                }
        else                                                            //
not fuel
                {source=dS[eqn]= 0.0;}

        C_UDMI(c,t,UDM_O2) = source;

        return source;
        }

DEFINE_SOURCE(virgin_CARBON_DIOXIDE_source,c,t,dS,eqn)      //  Source  4  of  6
=======================================
        {
        real x[ND ND];
        real source;
        C_CENTROID(x,c,t);
        if ( (1.0+cos(W*x[0]))*(1.0+cos(W*x[1]))>PSI )
        // any fuel
                {

        source=44.0/32.0*a/v*hm*sqrt(sqrt(pow(C_U(c,t),2)+pow(C_V(c,t),2))*5)*C
_R(c,t)*C_YI(c,t,1);
                dS[eqn]=0.0;
                }
        else                                                            //
not fuel
                {source=dS[eqn]= 0.0;}

        C_UDMI(c,t,UDM_CO2) = source;

        return source;
        }

DEFINE_SOURCE(virgin_WATER_VAPOUR_source,c,t,dS,eqn) //    Source    2    of    6
=======================================
        {
        real x[ND ND];
        real source;
        C_CENTROID(x,c,t);
        if ( (1.0+cos(W*x[0]))*(1.0+cos(W*x[1]))>PSI & (C_T(c,t)>Tp) )
        // hot fuel
                {
                source=10.0/85.0*k*a*(C T(c,t)-Tp)/v/RlnRr/Hv;
                dS[eqn]= 0.;
                }
        else                                                            //
not fuel
                {source=dS[eqn]= 0.;}

        C_UDMI(c,t,UDM_H2O) = source;

        return source;
        }
DEFINE SOURCE(virgin ENERGY source,c,t,dS,eqn)       //    Source    6    of    6
==============================================
        {
        real x[ND_ND];
        real source;
        C CENTROID(x,c,t);
        if ( (1.0+cos(W*x[0]))*(1.0+cos(W*x[1]))>PSI & (C T(c,t)>Tp) )
        // hot fuel
                {

        source=Hc*12.0/32.0*a/v*hm*sqrt(sqrt(pow(C U(c,t),2)+pow(C V(c,t),2))*5
)*C R(c,t)*C YI(c,t,1) - k*a*(C T(c,t)-Tp)/v/RlnRr;
```

```
                dS[eqn]= 0.;
                }
        else if ( (1.0+cos(W*x[0]))*(1.0+cos(W*x[1]))>PSI )                //
cold fuel
                {

        source=Hc*12.0/32.0*a/v*hm*sqrt(sqrt(pow(C U(c,t),2)+pow(C V(c,t),2))*5
)*C R(c,t)*C YI(c,t,1);
                dS[eqn]= 0.;
                }
        else                                                               //
not fuel
                {source=dS[eqn]= 0.;}

        C_UDMI(c,t,UDM_EN) = source;

        return source;
        }

DEFINE ON DEMAND(burnrate)
{
  Domain *domain = Get_Domain(1);

  FILE *dataFile;
  Thread *ct;
  cell_t c;
  real intMass, intVols, intO2, intCO2, intH2O, intEN;

  dataFile=fopen("hestia10integrals.dat","w");

  //


  intMass = intVols = intO2 = intCO2 = intH2O = intEN = 0.0;

  thread_loop_c(ct,domain)
    {
      begin_c_loop(c,ct)
        {
          real vol = C_VOLUME(c,ct)*PI2;
          intMass += C_UDMI(c,ct,UDM_MASS)*vol;
          intVols += C_UDMI(c,ct,UDM_VOLS)*vol;
          intO2 += C_UDMI(c,ct,UDM_O2)*vol;
          intCO2 += C_UDMI(c,ct,UDM_CO2)*vol;
          intH2O += C_UDMI(c,ct,UDM_H2O)*vol;
          intEN += C_UDMI(c,ct,UDM_EN)*vol;
        }
      end_c_loop(c,ct);
    }

  fprintf(dataFile,"%12.3e%12.3e%12.3e%12.3e%12.3e%12.3e\n",
          intMass, intVols, intO2, intCO2, intH2O, intEN);

  fclose(dataFile);

}


/*****************************************************************************
        end of UDF
*****************************************************************************/
```

G.2 GENETIC ALGORITHM

kronos10 is the coding of the genetic algorithm as a Matlab m-file:

```
clear
clc

% initialise parameters ============================================
disp('    ')
```

```
disp('Initialising...')
cd c:\fluent.inc\ntbin\ntx86
Nvertex=30;
Npop=10;
Ngen=50;
library.gene=[];
library.fitness=[];
fitnessLast=0;

% create genome ======================================================
genome=ceil(rand(Nvertex*2,Npop)*9);

% iterate thru generations ===========================================
for gen=1:Ngen
    disp('    ')
    disp('    ')
    disp(['Generation                                              ',num2str(gen),'
====================================='])

    % Form creatures & assess fitness ================================
    for creature = 1:Npop
        gene=genome(:,creature); % get gene form genome
        disp('    ')
        disp(['       Creature  ',num2str(creature),':  ',num2str(gene(1:20)'),'
...'])

        if gen>1 & creature==1
            fitness(creature)=max(fitness);
            disp(['          Creature copied from previous generation. Fitness:
',num2str(fitness(creature))])
        else
            hestia10callGambitAndFluent03
        end

        historyFitness(gen,creature)=fitness(creature);
        historyGene(gen,creature,:)=gene;
    end

    % record mean fitness and fittest creatures ======================
    meanFitness(gen)=mean(fitness);
    maxFitness(gen)=max(fitness);
    disp('    ')
    disp(['Mean fitness: ',num2str(meanFitness(gen))])
    for creature =1:Npop % record best creatures in library
        if fitness(creature)>meanFitness(gen)
            library.gene=cat(1,library.gene,genome(creature,:));
            library.fitness=cat(1,library.fitness,fitness(creature));
        end
    end % recording library
    disp('    Mating...')

    % Mating =========================================================
    wheel=0;
    for creature=1:Npop
        wheel(creature)=max(wheel)+fitness(creature);
    end
    for creature=1:Npop
        % selection...
        ball=rand*max(wheel);
        parent1=min(find(ball<wheel));
        parent2=parent1;
        while parent2==parent1
            ball=rand*max(wheel);
            parent2=min(find(ball<wheel));
        end

        % crossover...
        cut=round(rand*Nvertex*2);
        newgenome(:,creature)=[genome(1:cut,parent1);
genome(cut+1:Nvertex*2,parent2)];

        % and mutation
        mutations=[];
        for bit=1:Nvertex*2
            if rand<1/(Nvertex*2)
                newgenome(bit,creature)=ceil(rand*9);
```

```
                    mutations=[mutations bit];
                end
            end
            disp(['        creatures ',num2str(parent1), ' and ', num2str(parent2),
', with mutations at ', num2str(mutations)])
        end

        % carry best gene from last generagtion to next generation
        best=find(fitness==max(fitness));
        newgenome(:,1)=genome(:,best(1));

        disp('    Sons usurping fathers...')
        genome=newgenome;
        clear newgenome

        figure(1)
        subplot(3,1,2)
        colormap('gray')
        imagesc(genome')
        subplot(3,1,3)
        plot(1:gen,meanFitness,'k-');
        hold on
        plot(1:gen,maxFitness,'r-');
        hold off


    end
    save(['hestia10result',num2str(floor(now))])
    disp('    ')
    disp('end of kronos10 ========================================')
    % end of kronos10 ============================================
```

hestia10callGambitandFluent03 is the Matlab m-file which evaluated the fitness function for each creature:

```
    % initialise ======================================================================

    vsn=1e-12;
    Qt=5090;

    input=[
        1   0       0       0.2     0       0       0.2
        2   0       0       0.2     1       0       0.05
        3   0       0       0.2     2       0       0.05
        4   0       0       0.2     3       0       0.05
        5   1       0       0.05    0       0       0.2
        6   5       0       0.05    0       0       0.2
        7   6       0       0       0       0       0
        8   6       0       0       0       0       0
        9   6       0       0.2     0       0       0.2
        10  9       0       0.05    0       0       0.2
        11  10      0       0.05    0       0       0.2
        12  11      0       0.05    0       0       0.2
        13  12      0       0.05    0       0       0.2
        14  13      0       0.05    0       0       0.2
        15  14      -0.02   0.02    14      0       0.05
        16  15      -0.02   0.02    15      0       0.05
        17  16      -0.02   0.02    16      0       0.05
        18  9       0       0       0       0       0
        19  9       0       0       0       0       0
        20  0       0       0.1     0       0       0
        21  20      0.02    0.02    0       0       0
        22  20      0       0       0       0.25    0.25
        23  21      0       0       0       0.25    0.25
        24  22      -0.02   0.02    0       0.02    0.02
        25  21      0       0       24      0       0
        26  0       0       0       0       0       0
        27  0       0       0       0       0       0
        28  27      0       0       0       0       0
        29  0       0       0       28      0       0
        30  0       0       0       24      0       0];
```

```
trace=[27      28      29      30      24      25      23      22      24      22
       20      21      23      22      20      19      9       10      11      12
       13      14      15      16      17      18      7       4       3       2
       1       5       6       9       18      7       6       9       19      8
       6       8       27      26      29];

Xgene=gene(1:2:60);
Ygene=gene(2:2:60);
Xprec=input(:,1+1);
Xmin=input(:,2+1);
Xmax=input(:,3+1);
Yprec=input(:,4+1);
Ymin=input(:,5+1);
Ymax=input(:,6+1);

% create geometry ============================================================

for v=1:Nvertex
    switch v
    case {5}
        x(v)=Xgene(v)/9*(Xmax(v)-Xmin(v))+Xmin(v)+max(x(1:4));
        y(v)=min(y(2),Ygene(v)/9*(Ymax(v)-Ymin(v))+Ymin(v)+0);
    case {7}
        x(v)=x(6);
        y(v)=max(y(1:6))+0.02;
    case {17}
        x(v)=Xgene(v)/9*(Xmax(v)-Xmin(v))+Xmin(v)+x(Xprec(v));
        y(v)=max(y(9:16))+0.02;
    case {18}
        x(v)=x(9);
        y(v)=max(y(9:17));
    case {20}
        x(v)=max(x(14:17))+Xgene(v)/9*(Xmax(v)-Xmin(v))+Xmin(v);
        y(v)=0;
    case {24}
        x(v)=Xgene(v)/9*(Xmax(v)-Xmin(v))+Xmin(v)+x(Xprec(v));
        y(v)=max(y(1:23))+0.02;
    case {27}
        x(v)=x(1)/2;
        y(v)=0;
    case {28}
        x(v)=x(27);
        y(v)=min(y(1:3));
    otherwise
        if Xprec(v)==0
            x(v)=Xgene(v)/9*(Xmax(v)-Xmin(v))+Xmin(v)+0;
        else
            x(v)=Xgene(v)/9*(Xmax(v)-Xmin(v))+Xmin(v)+x(Xprec(v));
        end

        if Yprec(v)==0
            y(v)=Ygene(v)/9*(Ymax(v)-Ymin(v))+Ymin(v)+0;
        else
            y(v)=Ygene(v)/9*(Ymax(v)-Ymin(v))+Ymin(v)+y(Yprec(v));
        end
    end
end


% plot creature ==============================================================
subplot(3,1,1)
cla
for v=1:Nvertex
    text(x(v),y(v),num2str(v))
end
hold on
plot(x(trace),y(trace))
hold off
title(['Generation ',num2str(gen),'; Creature ',num2str(creature)])


% Write dimensions to file ===================================================
read=fopen('c:\fluent.inc\ntbin\ntx86\hestia10gambitReadMe.jou','r');
write=fopen('c:\fluent.inc\ntbin\ntx86\hestia10writtenJournal.jou','wt');
```

```
for line=1:110
    string=fgets(read);
    if sum(line==3:32)
        fprintf(write,'vertex create coordinates %-4.3f %-4.3f 0\n',[x(line-2)
y(line-2)]);
    else
        fprintf(write,string);
    end
end

fclose('all');


% call Gambit ========================================================
!gambit -id deleteMe -init hestia10WrittenJournal.jou
!del deleteMe.*

% call Fluent ========================================================
start=cputime;
!del hestia10integrals.dat
!fluent 2d  -i c:\fluent.inc\ntbin\ntx86\hestia10fluentJournal.jou
%!fluent 2d -g -i c:\fluent.inc\ntbin\ntx86\hestia10fluentJournal.jou

Nloop=30;
for loop=1:Nloop
    pause(10)
    if exist('hestia10integrals.dat','file')
        mogogoC=importdata('c:\fluent.inc\ntbin\ntx86\hestia10plateC.dat');
        mogogoC=mogogoC.data;

fuelSource=importdata('c:\fluent.inc\ntbin\ntx86\hestia10integrals.dat');

charSource=importdata('c:\fluent.inc\ntbin\ntx86\hestia10integralschar.dat');
        burnrate=fuelSource(1)+charSource(1);

        fit=interp1([-1e12 0 Qt 2*Qt 1e12],[vsn vsn Qt vsn vsn],-mogogoC(:,4));
        fitHeat=sum(fit)/size(fit,1);
        weight=interp1([0.0 0.8 1.0]*Qt,[0 0 1],fitHeat);
        fitness(creature)=fitHeat+weight/burnrate;

        disp(['        Creature fitness: ',num2str(fitness(creature))])
        break
    elseif loop==Nloop
        !taskkill /f /im fl6216s.exe
        fitness(creature)=1e-12;
        disp['                                Creature    aborted.    Fitness:
',num2str(fitness(creature))])
    end
end
dalay(gen,creature)=cputime-start;
% end of routine =====================================================
```

hestia10gambitReadMe.jou is modified for each creature to build a mesh:

```
/ Journal File for GAMBIT 2.1.6
/ File opened for write Thu Nov 15 12:09:16 2007.
vertex create coordinates 0.1 0.1 0
vertex create coordinates 0.1 0.13 0
vertex create coordinates 0.1 0.16 0
vertex create coordinates 0.1 0.2 0
vertex create coordinates 0.15 0.1 0
vertex create coordinates 0.2 0.1 0
vertex create coordinates 0.2 0.2 0
vertex create coordinates 0.2 0 0
vertex create coordinates 0.23 0.1 0
vertex create coordinates 0.26 0.1 0
vertex create coordinates 0.3 0.1 0
vertex create coordinates 0.33 0.1 0
vertex create coordinates 0.36 0.1 0
vertex create coordinates 0.4 0.1 0
vertex create coordinates 0.4 0.13 0
vertex create coordinates 0.4 0.16 0
vertex create coordinates 0.4 0.2 0
```

```
vertex create coordinates 0.23 0.2 0
vertex create coordinates 0.23 0 0
vertex create coordinates 0.42 0 0
vertex create coordinates 0.44 0 0
vertex create coordinates 0.42 0.25 0
vertex create coordinates 0.44 0.25 0
vertex create coordinates 0.4 0.3 0
vertex create coordinates 0.44 0.3 0
vertex create coordinates 0 0 0
vertex create coordinates 0.05 0 0
vertex create coordinates 0.05 0.1 0
vertex create coordinates 0 0.1 0
vertex create coordinates 0 0.3 0
edge create straight "vertex.26" "vertex.27" "vertex.8" "vertex.19" \
  "vertex.20" "vertex.21" "vertex.23" "vertex.25" "vertex.24" "vertex.30" \
  "vertex.29" "vertex.28"
edge create straight "vertex.26" "vertex.29"
edge create straight "vertex.27" "vertex.28"
edge create straight "vertex.20" "vertex.22" "vertex.24"
edge create straight "vertex.22" "vertex.23"
edge create straight "vertex.19" "vertex.9" "vertex.18" "vertex.17" \
  "vertex.16" "vertex.15" "vertex.14" "vertex.13" "vertex.12" "vertex.11" \
  "vertex.10"
edge create straight "vertex.8" "vertex.6" "vertex.7" "vertex.4" "vertex.3" \
  "vertex.2" "vertex.1" "vertex.5"
edge create straight "vertex.5" "vertex.6" "vertex.9" "vertex.10"
edge create straight "vertex.7" "vertex.18"
face create "char" wireframe "edge.11" "edge.13" "edge.1" "edge.12" real
face create "virgin" wireframe "edge.17" "edge.35" "edge.27" "edge.3" real
face create "window" wireframe "edge.18" "edge.37" "edge.28" "edge.35" real
face create "top" wireframe "edge.36" "edge.26" "edge.25" "edge.24" "edge.23" \
  "edge.22" "edge.21" "edge.20" "edge.19" "edge.18" real
face create "btm" wireframe "edge.28" "edge.34" "edge.33" "edge.32" "edge.31" \
  "edge.30" "edge.29" real
face create "lip" wireframe "edge.15" "edge.8" "edge.7" "edge.16" real
face create "plate" wireframe "edge.14" "edge.16" "edge.6" "edge.5" real
face create "freeair" wireframe "edge.2" "edge.27" "edge.34" "edge.33" \
  "edge.32" "edge.31" "edge.30" "edge.29" "edge.37" "edge.19" "edge.20" \
  "edge.21" "edge.22" "edge.23" "edge.24" "edge.25" "edge.26" "edge.36" \
  "edge.17" "edge.4" "edge.14" "edge.15" "edge.9" "edge.10" "edge.11" \
  "edge.13" real

sfunction create sourceedges "edge.27" "edge.17" "edge.35" "edge.36" \
  "edge.26" "edge.25" "edge.24" "edge.23" "edge.22" "edge.21" "edge.20" \
  "edge.19" "edge.18" "edge.28" "edge.34" "edge.33" "edge.32" "edge.31" \
  "edge.30" "edge.29" "edge.11" "edge.13" "edge.10" "edge.14" "edge.15" \
  startsize 0.005 growthrate 1.2 sizelimit 0.05 attachfaces "freeair" fixed
face mesh "freeair" triangle size 1

face mesh "virgin" "char" triangle size 0.005
face mesh "window" triangle size 0.005
sfunction create sourceedges "edge.36" "edge.26" "edge.25" "edge.24" \
  "edge.23" "edge.22" "edge.21" "edge.20" "edge.19" "edge.18" "edge.28" \
  "edge.29" "edge.30" "edge.31" "edge.32" "edge.33" "edge.34" startsize 0.005 \
  growthrate 2 sizelimit 0.05 attachfaces "top" "btm" fixed
face mesh "top" "btm" triangle size 1
sfunction create sourceedges "edge.15" "edge.14" startsize 0.005 growthrate 2 \
  sizelimit 0.05 attachfaces "lip" "plate" fixed
face mesh "lip" "plate" triangle size 1
solver select "FLUENT 5/6"
physics create "fuel_virgin" ctype "FLUID" face "virgin"
physics create "fuel_window" ctype "FLUID" face "window"
physics create "fuel_char" ctype "FLUID" face "char"
physics create "free air" ctype "FLUID" face "freeair"
physics create "stove top" ctype "SOLID" face "top"
physics create "stove btm" ctype "SOLID" face "btm"
physics create "plate" ctype "SOLID" face "plate"
physics create "stove_rim" ctype "SOLID" face "lip"
physics modify "plate" ctype label "stove_plate" face "plate"
physics create "centre-line" btype "AXIS" edge "edge.1" "edge.2" "edge.3" \
  "edge.4" "edge.5"
physics create "plate-top" btype "WALL" edge "edge.6"
physics modify "plate-top" btype label "stove-plate-top" edge "edge.6"
physics create "stove-lip-ext" btype "WALL" edge "edge.7" "edge.8"
physics create "ambient" btype "PRESSURE INLET" edge "edge.9"
physics create "floor" btype "WALL" edge "edge.10" "edge.12"
```

```
physics create "stove-top-edge" btype "WALL" edge "edge.36" "edge.26" \
  "edge.25" "edge.24" "edge.23" "edge.22" "edge.21" "edge.20" "edge.19" \
  "edge.18"
physics create "stove-btm-edge" btype "WALL" edge "edge.28" "edge.34" \
  "edge.33" "edge.32" "edge.31" "edge.30" "edge.29"
physics create "stove-plate-btm" btype "WALL" edge "edge.14"
physics create "stove-lip-int" btype "WALL" edge "edge.16" "edge.15"
physics create "remain" btype "INTERIOR" edge "edge.1" "edge.2" "edge.3" \
  "edge.4" "edge.5" "edge.6" "edge.7" "edge.8" "edge.9" "edge.10" "edge.11" \
  "edge.12" "edge.13" "edge.14" "edge.15" "edge.16" "edge.17" "edge.18" \
  "edge.19" "edge.20" "edge.21" "edge.22" "edge.23" "edge.24" "edge.25" \
  "edge.26" "edge.27" "edge.28" "edge.29" "edge.30" "edge.31" "edge.32" \
  "edge.33" "edge.34" "edge.35" "edge.36" "edge.37"
export fluent5 "hestia10WrittenMesh.msh" nozval
end force
```

hestia10fluentJournal.jou is executed with the mesh created by the modified gambit journal:

```
;
;       1. Import mesh & change directory --------------------------
chdir c:\fluent.inc\ntbin\ntx86
//file/read-case
        c:\fluent.inc\ntbin\ntx86\hestia10WrittenMesh.msh
;
;       2. Load prometheus -----------------------------------------
//define/user/user-defined-memory
        10
//define/user/comp/comp
        libudf
        yes
        c:\fluent.inc\ntbin\ntx86\prometheus21virgin_dmh.c
        c:\fluent.inc\ntbin\ntx86\prometheus21char dmh.c
        ; the next line is blank

        c:\fluent.inc\ntbin\ntx86\udf.h
        ; the next line is blank

//define/user/comp/load
        libudf
;
;       3. Define models -------------------------------------------
//define/models/axi
        yes
//define/models/energy
        yes
        no
        no
        no
        yes
//define/models/viscous/ke-standard
        yes
//define/models/radiation/discrete-ordinates
        yes
        2
        2
        1
        1
//define/models/species/species-transport
        yes
        wood-volatiles-air
//define/models/species/volumetric-reactions
        yes
//define/models/species/set-turb-chem-interaction
        no
        no
        yes
;
;       4. Define materials ----------------------------------------
//define/materials/change-create
        aluminum
        char
```

```
            yes
            2100
            yes
            constant
            1700
            yes
            constant
            100
            yes
            constant
            1000
            no
            no
            no
            yes
      //define/materials/change-create
            char
            mogogo
            yes
            2000
            yes
            constant
            900
            yes
            constant
            0.4
            yes
            constant
            0
            no
            no
            no
            no
      //define/materials/change-create
            wood-volatiles-air
            wood-volatiles-air
            no
            no
            no
            no
            no
            no
            no
            no
            yes
            wsggm-cell-based
            no
            no
            no
            no
      ;
      ;       5. Load BC's ------------------------------------------------
      //file/read-bc
            hestia10.bc
      ;
      ;       6. Adapt ----------------------------------------------------
      ;
      ;       7. Initialize -----------------------------------------------
      (cx-gui-do cx-activate-item "MenuBar*User-DefinedSubMenu*Memory...")
      (cx-gui-do                  cx-set-integer-entry                  "User-Defined
      Memory*Table1*IntegerEntry1(Number of User-Defined Memory Locations)" 10)
      (cx-gui-do cx-activate-item "User-Defined Memory*PanelButtons*PushButton1(OK)")
      //solve/initialize/initialize-flow
      //solve/patch
            fuel-virgin
            ; the next line is blank

            x-velocity
            yes
            0.1
      //solve/patch
            fuel-virgin
            ; the next line is blank

            temperature
            800
```

```
//solve/patch
        fuel-virgin
        ; the next line is blank

        species-0
        0.25
//solve/patch
        fuel-virgin
        ; the next line is blank

        species-2
        0.01
//solve/patch
        fuel-virgin
        ; the next line is blank

        species-3
        0.01
;
;       8. Iterate ------------------------------------------------
//solve/iterate
        1000
;
;       9. Re-adapt -----------------------------------------------
//adapt/set/cell-zones
        stove_rim
        stove_plate
        stove_btm
        stove top
        free air
        fuel window
        fuel_virgin
        ; the next line is blank

//adapt/mark-inout-rectangle
        yes
        no
        0
        1
        0
        1
//adapt/adapt-to-register
        0
        0
        100000
        yes
;
;       10. Re-iterate --------------------------------------------
//solve/iterate
        5000
;
;       11. Export ------------------------------------------------
//file/export/ascii
        c:\fluent.inc\ntbin\ntx86\hestia10plateC.dat
        stove-plate-top
        ; the next line is blank

        no
        no
        heat-flux
        q
        yes
        yes
//define/user/execute
        "burnrate::libudf"
//define/user/execute
        "charrate::libudf"
;
;       12. Exit --------------------------------------------------
(cx-gui-do cx-activate-item "MenuBar*FileMenu*Exit")
(cx-gui-do cx-activate-item "Warning*OK")
;
;       END OF JOURNAL --------------------------------------------
```